

SIZING AND OPTIMIZATION OF THE HORIZONTAL TAIL OF A JET
TRAINER

A THESIS SUBMITTED TO
THE GRADUATE SCHOOL OF NATURAL AND APPLIED SCIENCES
OF
MIDDLE EAST TECHNICAL UNIVERSITY

BY

SİNEM KARATOPRAK

IN PARTIAL FULFILLMENT OF THE REQUIREMENTS
FOR
THE DEGREE OF MASTER OF SCIENCE
IN
AEROSPACE ENGINEERING

SEPTEMBER 2019

Approval of the thesis:

**SIZING AND OPTIMIZATION OF THE HORIZONTAL TAIL OF A JET
TRAINER**

submitted by **SİNEM KARATOPRAK** in partial fulfillment of the requirements for
the degree of **Master of Science in Aerospace Engineering Department, Middle
East Technical University** by,

Prof. Dr. Halil Kalıpçılar
Dean, Graduate School of **Natural and Applied Sciences**

Prof. Dr. İsmail Hakkı Tuncer
Head of Department, **Aerospace Engineering**

Prof. Dr. Serkan Özgen
Supervisor, **Aerospace Engineering, METU**

Examining Committee Members:

Assoc. Prof. Dr. Utku Kanoğlu
Aerospace Engineering, METU

Prof. Dr. Serkan Özgen
Aerospace Engineering, METU

Prof. Dr. Nafiz Alemdaroğlu
School of Aviation, Atılım University

Assist. Prof. Dr. Mustafa Perçin
Aerospace Engineering, METU

Assist. Prof. Dr. Ali Türker Kutay
Aerospace Engineering, METU

Date: 10.09.2019

I hereby declare that all information in this document has been obtained and presented in accordance with academic rules and ethical conduct. I also declare that, as required by these rules and conduct, I have fully cited and referenced all material and results that are not original to this work.

Name, Surname: Sinem Karatoprak

Signature:

ABSTRACT

SIZING AND OPTIMIZATION OF THE HORIZONTAL TAIL OF A JET TRAINER

Karatoprak, Sinem
Master of Science, Aerospace Engineering
Supervisor: Prof. Dr. Serkan Özgen

September 2019, 104 pages

The sizing of the horizontal tail has a priority on the design phase. The horizontal tail provides a necessary longitudinal control and the sufficient static stability throughout the defined center-of-gravity (CG) range.

The jet trainer of this study is a control-configured vehicle (CCV). The control system has a significant role in shaping the aircraft with the usage of active control technology (ACT). ACT introduces the concept of relaxed static stability (RSS) by providing artificial stability.

The horizontal tail provides sufficient longitudinal static stability even at the most aft CG position. In order to determine whether an aircraft is stable, the determination of the static margin (SM) is one of methods. For a conventional aircraft, static margin is approximately 5 % in the subsonic regime. However, a large backward aerodynamic center (AC) shift occurs between subsonic to supersonic. This causes a large increase in static margin at supersonic flight regime which penalize the performance in terms of drag and weight. Therefore, the size of the horizontal tail is reduced by utilizing from RSS concept.

Some stability and control derivatives- such as $C_{m\alpha}$, $C_{m\delta}$, $C_{L\delta}$ -are needed to obtain during the evaluation of the control authority and stability of the aircraft. The evaluations are based on the defined certain parameters and force and moment equilibrium equations. Therefore, analyses based on Datcom and Computational Fluid Dynamics (CFD) were performed for six horizontal tails. C_M , C_L , and C_D aerodynamic coefficients of each horizontal tail were calculated at different AoAs throughout flight envelope.

Keywords: Design, Horizontal Tail, Longitudinal Stability, Relaxed Static Stability, Tail Sizing Diagram

ÖZ

JET EĞİTİM UÇAĞININ YATAY KUYRUK BOYUTLANDIRMASI VE OPTİMİZASYONU

Karatoprak, Sinem
Yüksek Lisans, Havacılık ve Uzay Mühendisliği
Tez Danışmanı: Prof. Dr. Serkan Özgen

Eylül 2019, 104 sayfa

Yatay kuyruk boyutlandırma, tasarım aşamasında, önceliğe sahiptir. Yatay kuyruk, gerekli boylamsal kontrolü ve yeterli boylamsal kararlılığı, tanımlanan ağırlık merkezi boyunca sağlar.

Çalışmalar boyunca kullanılan, jet eğitim uçağı, kontrol konfigüre edilen araçtır. Aktif kontrol teknolojinin kullanılmasıyla, kontrol sisteminin, uçağın şekillenmesinde çok önemli bir rolü vardır. Aktif kontrol teknoloji, sağladığı yapay kararlılık ile, gevşetilmiş statik kararlılık konseptini sunar.

Yatay kuyruk yeterli boylamsal kararlılığı, en arka ağırlık merkezinde dahi sağlar. Statik tolerans hesaplaması, bir uçağın statik olarak kararlı olduğuna karar vermek için bir yöntemdir. Klasik bir uçakta, sesaltı hızlarda, statik tolerans yaklaşık % 5'tir. Fakat sesaltı hızlardan sesüstü hızlara geçerken, aerodinamik merkez çok fazla arkaya doğru kayar. Bu da, sesüstü hızlarda, statik toleransın çok fazla artmasına neden olur. Yüksek statik tolerans, neden olduğu sürüklemadaki ve ağırlıktaki artış ile, uçağın performansını düşürür. Bu yüzden de, gevşetilmiş statik kararlılık konseptinden yararlanarak, yatay kuyruk boyutu küçültülür.

Yatay kuyruğun otoritesi ve uçağın kararlılığı değerlendirilirken, bazı kararlılık ve kontrol türevlerinin - $C_{m\alpha}$, $C_{m\delta}$, $C_{L\delta}$ - hesaplanması gerekir. Değerlendirmeler, tanımlanmış bazı parametreler ile kuvvet ve moment denklemlerine dayanır. Bu yüzden, 6 tane yatay kuyruk için, DATCOM ve Computational Fluid Dynamics (CFD) tabanlı analizler icra edildi. Her yatay kuyruk için C_M , C_L , ve C_D aerodinamik katsayıları, uçuş zarfı boyunca farklı hücum açılarında hesaplandı.

Anahtar Kelimeler: Tasarım, Yatay Kuyruk, Boylamsal Kararlılık, Gevşetilmiş Statik Kararlılık, Kuyruk Boyutlandırma Diyagramı

To my family...

ACKNOWLEDGEMENTS

I would like to express my gratitude to my supervisor Prof. Dr. Serkan Özgen, for giving me an opportunity to work with him, allowing me to benefit from his valuable comments and experiences and his endless patience throughout my study.

I would also like to thank Miray Şahin and Murat Canıbek for their support throughout the thesis stages. I wish to state my endless thanks to Ömer Kandemir for helping me in the computational fluid dynamics stages.

I also would like to express my thanks to my close friends Nihan Uzun, Simge Yılmaz, Övgü Ergüner and Evrim Türkmen for always being there for me with their continuous motivation.

I would like to express my deepest appreciation to my family, my mother Nermin Karatoprak, my father Halil Şimşat Karatoprak, my sister Şebnem Bildirici and Zeki Bildirici for their infinite support, patience and endless support.

TABLE OF CONTENTS

ABSTRACT	v
ÖZ	vii
ACKNOWLEDGEMENTS	x
TABLE OF CONTENTS	xi
LIST OF TABLES	xiii
LIST OF FIGURES	xiv
LIST OF SYMBOLS	xviii
CHAPTERS	
1. INTRODUCTION	1
1.1. Motivation of Thesis	1
1.2. Literature Review	1
1.3. Geometrical and Performance Specifications of the Aircraft.....	7
1.4. Specifications of the Analyzed Horizontal Tails.....	9
1.5. Conditions of Analyses	9
1.6. Scope of the Research	11
1.7. Content of the Thesis.....	11
2. THEORY	13
2.1. Longitudinal Static Stability.....	13
2.1.1. Longitudinal Stability of a Wing	14
2.1.2. Longitudinal Stability of a Wing – Tail Combination.....	17
2.1.3. Stick-Fixed Neutral Point and Static Margin.....	23
2.2. Take-Off Rotation	28

2.3. Nose-Down Recovery	32
2.4. Tipback Angle Requirement	37
3. RESULTS AND DISCUSSION	39
3.1. Determination of Neutral Point and Most Aft CG Position Regarding Longitudinal Static Stability	39
3.2. Determination of Most Aft CG Position Regarding Nose-Down Recovery Capability	45
3.3. Determination of Most Forward CG Position Regarding Take-Off Rotation	48
3.4. Determination of Aft CG Limit Regarding Tipback Angle Requirement	49
3.5. Horizontal Tail Sizing Diagram	49
4. METHODOLOGY	77
4.1. Computational Fluid Dynamics Method	77
4.2. DATCOM Method	79
5. CONCLUSION AND FUTURE WORK	81
5.1. Conclusion	81
5.2. Future Work	84
REFERENCES	85
APPENDICES	
A. Neutral Point Determination	87
B. Minimum Nose-Down Recovery Determination	99

LIST OF TABLES

TABLES

Table 1.1. Major Aircraft Specifications	8
Table 1.2. Major Performance Specifications.....	8
Table 1.3. Planform Parameters of Horizontal Tails - 1	9
Table 1.4. Planform Parameters of Horizontal Tails - 2	9
Table 1.5. The Analyzed Conditions for Longitudinal Stability.....	10
Table 1.6: The Analyzed Conditions for Nose-Down Recovery	10
Table 1.7: The Analyzed Conditions for Take-Off Rotation	11
Table 2.1. Typical Values for Wheel-Ground Friction Coefficient [10]	31
Table 3.1. The Neutral Points at 0.2, 0.9, and 1.2 Mach Numbers for Six Horizontal Tails.....	44
Table 3.2: The Most Aft CG Positions for $SM = +5\%$	44
Table 3.3: The Most Aft CG Positions for $SM = -7\%$	45
Table 3.4. The most aft CG positions regarding the minimum nose-down capability for all horizontal tails	47
Table 3.5. The Forward CG Positions Regarding Take-Off Rotation	49

LIST OF FIGURES

FIGURES

Figure 1.1. Generic Pitching Moment Variation with AoA for RSS Configurations [5]	7
Figure 2.1. Forces and moments acting on a cambered wing in flight [8]	14
Figure 2.2. Forces and moments acting on a wing combined with a horizontal tail [8]	18
Figure 2.3. Position of the stick-fixed neutral point relative to the center of gravity [8]	24
Figure 2.4. Stick-fixed neutral point of an aircraft [9]	27
Figure 2.5. The major forces and moments during take-off rotation[9]	29
Figure 2.6. Typical inertia coupling pitch angular acceleration due to stability-axis roll [5].....	34
Figure 2.7. Example of incremental pitching moment coefficient due to nonzero sideslip [5]	35
Figure 2.8. The developed methodology for high AoA nose-down pitch control [5]36	
Figure 2.9. The tipback angle of aircraft with tricycle landing gear [11].....	37
Figure 3.1. The variation of. C_m with AoA at 0.2 Mach for HT # 1	40
Figure 3.2. The variation of. C_m with AoA at 0.9 Mach for HT # 1	41
Figure 3.3: The variation of. C_m with AoA at 1.2 Mach for HT # 1	42
Figure 3.4: The variation of. C_m with AoA at 0.2 Mach for HT # 1	43
Figure 3.5. Nose-Down Recovery Characteristic for HT # 1 obtained from CFD....	46
Figure 3.6: Nose-Down Recovery Characteristic for HT # 1 obtained from DATCOM	47
Figure 3.7. Tail Sizing Diagram of HT#1 for Natural Stability at 0.2 Mach	51
Figure 3.8: Tail Sizing Diagram of HT#1 for Artificial Stability at 0.2 Mach.....	51
Figure 3.9: Tail Sizing Diagram of HT#2 for Natural Stability at 0.2 Mach	52

Figure 3.10: Tail Sizing Diagram of HT#2 for Artificial Stability at 0.2 Mach	52
Figure 3.11: Tail Sizing Diagram of HT#3 for Natural Stability at 0.2 Mach.....	53
Figure 3.12: Tail Sizing Diagram of HT#3 for Artificial Stability at 0.2 Mach	53
Figure 3.13: Tail Sizing Diagram of HT#4 for Natural Stability at 0.2 Mach.....	54
Figure 3.14: Tail Sizing Diagram of HT#4 for Artificial Stability at 0.2 Mach	54
Figure 3.15: Tail Sizing Diagram of HT#5 for Natural Stability at 0.2 Mach.....	55
Figure 3.16: Tail Sizing Diagram of HT#5 for Artificial Stability at 0.2 Mach	55
Figure 3.17: Tail Sizing Diagram of HT#6 for Natural Stability at 0.2 Mach.....	56
Figure 3.18: Tail Sizing Diagram of HT#6 for Artificial Stability at 0.2 Mach	56
Figure 3.19: Tail Sizing Diagram of HT#1 for Natural Stability at 0.9 Mach.....	57
Figure 3.20: Tail Sizing Diagram of HT#1 for Artificial Stability at 0.9 Mach	57
Figure 3.21: Tail Sizing Diagram of HT#2 for Natural Stability at 0.9 Mach.....	58
Figure 3.22: Tail Sizing Diagram of HT#2 for Artificial Stability at 0.9 Mach	58
Figure 3.23: Tail Sizing Diagram of HT#3 for Natural Stability at 0.9 Mach.....	59
Figure 3.24: Tail Sizing Diagram of HT#3 for Artificial Stability at 0.9 Mach	59
Figure 3.25: Tail Sizing Diagram of HT#4 for Natural Stability at 0.9 Mach.....	60
Figure 3.26: Tail Sizing Diagram of HT#4 for Artificial Stability at 0.9 Mach	60
Figure 3.27: Tail Sizing Diagram of HT#5 for Natural Stability at 0.9 Mach.....	61
Figure 3.28: Tail Sizing Diagram of HT#5 for Artificial Stability at 0.9 Mach	61
Figure 3.29: Tail Sizing Diagram of HT#6 for Natural Stability at 0.9 Mach.....	62
Figure 3.30: Tail Sizing Diagram of HT#6 for Artificial Stability at 0.9 Mach	62
Figure 3.31: Tail Sizing Diagram of HT#1 for Natural Stability at 1.2 Mach.....	63
Figure 3.32: Tail Sizing Diagram of HT#1 for Artificial Stability at 1.2 Mach	63
Figure 3.33: Tail Sizing Diagram of HT#2 for Natural Stability at 1.2 Mach.....	64
Figure 3.34: Tail Sizing Diagram of HT#2 for Artificial Stability at 1.2 Mach	64
Figure 3.35: Tail Sizing Diagram of HT#3 for Natural Stability at 1.2 Mach.....	65
Figure 3.36: Tail Sizing Diagram of HT#3 for Artificial Stability at 1.2 Mach	65
Figure 3.37: Tail Sizing Diagram of HT#4 for Natural Stability at 1.2 Mach.....	66
Figure 3.38: Tail Sizing Diagram of HT#4 for Artificial Stability at 1.2 Mach	66
Figure 3.39: Tail Sizing Diagram of HT#5 for Natural Stability at 1.2 Mach.....	67

Figure 3.40: Tail Sizing Diagram of HT#5 for Artificial Stability at 1.2 Mach.....	67
Figure 3.41: Tail Sizing Diagram of HT#6 for Natural Stability at 1.2 Mach	68
Figure 3.42: Tail Sizing Diagram of HT#6 for Artificial Stability at 1.2 Mach.....	68
Figure 3.43: Tail Sizing Diagram of HT#1 for Natural Stability at 0.2 Mach	69
Figure 3.44: Tail Sizing Diagram of HT#1 for Artificial Stability at 0.2 Mach.....	69
Figure 3.45: Tail Sizing Diagram of HT#2 for Natural Stability at 0.2 Mach	70
Figure 3.46: Tail Sizing Diagram of HT#2 for Artificial Stability at 0.2 Mach.....	70
Figure 3.47: Tail Sizing Diagram of HT#3 for Natural Stability at 0.2 Mach	71
Figure 3.48: Tail Sizing Diagram of HT#3 for Artificial Stability at 0.2 Mach.....	71
Figure 3.49: Tail Sizing Diagram of HT#4 for Natural Stability at 0.2 Mach	72
Figure 3.50: Tail Sizing Diagram of HT#4 for Artificial Stability at 0.2 Mach.....	72
Figure 3.51: Tail Sizing Diagram of HT#5 for Natural Stability at 0.2 Mach	73
Figure 3.52: Tail Sizing Diagram of HT#5 for Artificial Stability at 0.2 Mach.....	73
Figure 3.53: Tail Sizing Diagram of HT#6 for Natural Stability at 0.2 Mach	74
Figure 3.54: Tail Sizing Diagram of HT#6 for Artificial Stability at 0.2 Mach.....	74
Figure 4.1. The variation of. C_L with AoA at 0.3 Mach for results of wind tunnel test and CFD analyses	79
Figure A 1. The variation of. C_m with AoA at 0.2 Mach for HT # 1.....	87
Figure A 2. The variation of. C_m with AoA at 0.9 Mach for HT # 1.....	87
Figure A 3. The variation of. C_m with AoA at 1.2 Mach for HT # 1.....	88
Figure A 4. The variation of. C_m with AoA at 0.2 Mach for HT # 2.....	88
Figure A 5. The variation of. C_m with AoA at 0.9 Mach for HT # 2.....	89
Figure A 6. The variation of. C_m with AoA at 1.2 Mach for HT # 2.....	89
Figure A 7. The variation of. C_m with AoA at 0.2 Mach for HT # 3.....	90
Figure A 8. The variation of. C_m with AoA at 0.9 Mach for HT # 3.....	90
Figure A 9. The variation of. C_m with AoA at 1.2 Mach for HT # 3.....	91
Figure A 10. The variation of. C_m with AoA at 0.2 Mach for HT # 4.....	91
Figure A 11. The variation of. C_m with AoA at 0.9 Mach for HT # 4.....	92

Figure A 12. The variation of. C_m with AoA at 1.2 Mach for HT # 4	92
Figure A 13. The variation of. C_m with AoA at 0.2 Mach for HT # 5	93
Figure A 14. The variation of. C_m with AoA at 0.9 Mach for HT # 5	93
Figure A 15. The variation of. C_m with AoA at 1.2 Mach for HT # 5	94
Figure A 16. The variation of. C_m with AoA at 0.2 Mach for HT # 6	94
Figure A 17. The variation of. C_m with AoA at 0.9 Mach for HT # 6	95
Figure A 18. The variation of. C_m with AoA at 1.2 Mach for HT # 6	95
Figure A 19. The variation of. C_m with AoA at 0.2 Mach for HT # 1	96
Figure A 20. The variation of. C_m with AoA at 0.2 Mach for HT # 2	96
Figure A 21. The variation of. C_m with AoA at 0.2 Mach for HT # 3	97
Figure A 22. The variation of. C_m with AoA at 0.2 Mach for HT # 4	97
Figure A 23. The variation of. C_m with AoA at 0.2 Mach for HT # 5	98
Figure A 24. The variation of. C_m with AoA at 0.2 Mach for HT # 6	98
Figure B 1. Nose-Down Recovery Characteristic for HT # 1	99
Figure B 2. Nose-Down Recovery Characteristic for HT # 2	99
Figure B 3. Nose-Down Recovery Characteristic for HT # 3	100
Figure B 4. Nose-Down Recovery Characteristic for HT # 4	100
Figure B 5. Nose-Down Recovery Characteristic for HT # 5	101
Figure B 6. Nose-Down Recovery Characteristic for HT # 6	101
Figure B 7. Nose-Down Recovery Characteristic for HT # 1	102
Figure B 8. Nose-Down Recovery Characteristic for HT # 2	102
Figure B 9. Nose-Down Recovery Characteristic for HT # 3	103
Figure B 10. Nose-Down Recovery Characteristic for HT # 4	103
Figure B 11. Nose-Down Recovery Characteristic for HT # 5	104
Figure B 12. Nose-Down Recovery Characteristic for HT # 6	104

LIST OF SYMBOLS

SYMBOLS

AC	: aerodynamic center
ACT	: active control technology
AoA	: angle of attack
AoS	: angle of sideslip
AR	: aspect ratio
b	: wing span
b_{HT}	: horizontal tail span
\bar{c}	: mean wing aerodynamic chord
CFD	: computational fluid dynamics
CG	: center-of-gravity
C_{HT}	: horizontal tail volume coefficient
\bar{c}_{HT}	: mean horizontal tail aerodynamic chord
C_L	: lift coefficient
C_m	: pitch moment coefficient
$C_{m_{ac}}$: pitch moment coefficient about wing aerodynamic center
D	: aircraft drag
FWD	: forward
HT	: horizontal tail

l_{HT} : distance from center-of-gravity to quarter-chord of the horizontal tail
 L : total lift
 L_h : tail lift
 L_{wf} : wing-fuselage lift
 M_{CG} : pitch moment about center-of-gravity
 MAC : mean aerodynamic chord
 NP : neutral point
 \bar{q} : dynamic pressure
 \dot{q} : pitch angular acceleration
 R : reaction force
 RSS : relaxed static stability
 S : wing reference area
 S_{HT} : horizontal tail area
 S_{ref} : wing reference area
 T : thrust
 W : aircraft weight
 X_{AC} : location of wing aerodynamic center
 X_{AC_h} : location of horizontal tail aerodynamic center
 X_{cg} : location of center-of-gravity
 X_{mg} : distance defined in Figure 2.5
 X_{NP} : location of neutral point

- Z_{cg} : distance defined in Figure 2.5
- Z_D : distance defined in Figure 2.5
- Z_{mg} : distance defined in Figure 2.5
- Z_T : distance defined in Figure 2.5
- α : angle of attack
- α_{tb} : tipback angle
- Λ_{LE} : leading edge sweep angle
- μ : friction coefficient
- $\ddot{\theta}_{mg}$: angular acceleration about main landing gear

CHAPTER 1

INTRODUCTION

1.1. Motivation of Thesis

The horizontal tail sizing is one of the most significant stage of the preliminary design of the aircraft. The horizontal tail provides necessary level of static stability in pitch and the required level of longitudinal control. Meeting these substantial requirements results in a large size of horizontal tail. Large horizontal tail causes significant performance penalties in terms of aircraft weight and aerodynamic drag. To minimize these penalties, active control system is incorporated into the aircraft. The aircraft with active control system is called control-configured vehicle (CCV). The control system has a really predominant role in shaping the airframe. Active control technology provides an artificial stability to the aircraft. An aircraft with ACT is designed longitudinally unstable. This relaxation in static stability allows to decrease in the required size of the horizontal tail. A reduced horizontal tail causes decrease in aircraft weight and parasite drag. The result is improvement in performance and maneuverability of the aircraft due to reduction in trim drag and gross weight.

High degree level of performance and maneuverability is demanded from current modern aircrafts. Therefore, most of them utilizes from the concept of active control technology. They have smaller horizontal tails with improved performance and maneuver capabilities.

1.2. Literature Review

The longitudinal stability and controllability are very significant problems from the earliest days of aviation. Many of early aircrafts were not sufficiently stable in pitch,

unfortunately. Therefore, some of the early pioneers were dead during the testing of new form of control surface [1].

Sir George Cayley (1774-1857) studied on the problem of stability. He did a number of experiments by utilizing from a model glider with an adjustable tail and rudder [1].

Otto Lilienthal (1848-1896) performed various successful glides. He controlled the aircraft by changing the position of his body to produce necessary moments to balance aerodynamic moments. However, Lilienthal could spend only about five hours in actual flight during five years of experimenting [1].

Wilbur Wright (1867-1912) and Orville Wright (1871-1948) made the first sustained flight in a powered aircraft. Before flight, they had performed several experiments with gliders. The gliders and first powered aircraft had the horizontal tail ahead of the wings (canard configuration). The front part of the stabilizer was fixed. The fore and aft control of the aircraft could be provided by deflecting the rear part [1].

The Wright brothers became very successful in aviation owing to their patient experimental researches and their careful usage of scientific knowledge to the problems of flight. Other investigators were concurrently studying on the theories of the stability and control of aircraft.

The theory of stability and control was begun to study in modern sense by Frederick William Lanchester. Lanchester was both a theoretician and mechanical engineer. He had some flight experience with free-flying gliders. His free-flying gliders were inherently stable [2].

Lanchester had two published books, Aerodynamics in 1907 and Aerodnetics in 1908 containing his views and the results of his experiments. He even had conversation with

Wilbur Wright. However, it was not useful since Wilbur had no knowledge on inherent stability in flight.

Professor George Hartley Bryan put into the mathematical theory of the motion of an aircraft during flight its present form by considering the aircraft as a rigid body with 6 degrees of freedom in England in 1911. Bryan had only developed the longitudinal equations of aircraft motion, collaboration with W.E. Williams [2].

Bryan focused on aircraft stability and control at his book (Bryan, 1911). The equations of motion used in analysis and simulation of most advanced today's aircraft are identical with Bryan's equations.

Bryan computed the stability derivatives with the assumption that the force on airfoil is perpendicular to the airfoil chord that is quite accurate for supersonic aircraft with nearly unswept wing.

Bryan obtained solutions for the equations and came up with correct modes of longitudinal and lateral motions of the aircraft. Bryan examines previous stability and control theories at the end of Stability in Aviation.

The horizontal tail provides a sufficient level of static stability and the necessary longitudinal control in a conventional aircraft design [3].

The size of the horizontal tail must be determined according to the following requirements [3]:

- The horizontal tail must have sufficient control authority during take-off nose wheel liftoff at forward (FWD) center-of-gravity (CG) position with maximum take-off flaps.

- The horizontal tail must ensure necessary stability in pitch at aft CG position.
- The horizontal tail must have sufficient nose-down control authority at aft CG position during stall recovery.

The most important horizontal tail design requirement in terms of longitudinal control is the take-off rotation requirement.

The horizontal tail must have sufficient control authority to rotate the aircraft about the main gear and lift the nose with specified angular pitch acceleration at the most FWD CG position.

In static stability, the static moments acting on an aircraft are considered after it is slightly disturbed from equilibrium state by assuming that the linear accelerations are negligible and the static forces are in equilibrium. An aircraft is statically stable if the static moments prone to return the aircraft to its initial equilibrium state [1].

The flight control systems were primarily used to alleviate the pilot's workload and to increase handling beyond the standard purely obtained by aerodynamic alone until the 1970s. Stability augmentation in this form had a substantial role in the design of aircraft. Nevertheless, it was often considered as vital even in aircraft having a degree of inherent stability. As modern improvements in active control systems have been conducted, they have become reliable and versatile such that increasing levels of stability augmentation can be possible to use in aircraft design. Relaxed static stability (RSS) has become an arising design concept with this advance. This aspect of the control-configured vehicle (CCV) concept contains the use of active controls more than stability augmentation alone or a cure for some localized design defects. The principal idea related with RSS was to help the shaping of the aircraft to provide improvements in performance, efficiency and cost [4].

The concept of relaxed static stability provides a relaxation of the demand for inherent stability by keeping the aircraft controllable with electronic means. The natural longitudinal static stability was essential up to the late 1960s. It was considered difficult to fly an aircraft with inherently unstable in pitch [4].

When an aircraft has an unstable configuration, a nose-up disturbance increases the nose-up tendency. This nose-up tendency could be countered if sufficient upload on the tail was produced to restore equilibrium about the CG point. This is the main idea of relaxed static stability, an inherently unstable aircraft is artificially transformed to a stable aircraft by utilizing from the active control system containing rapid-response actuators without any pilot.

Large downloads are required for a conventional aircraft at subsonic and especially supersonic speeds for longitudinal trim. The lift loss because of trimming is generally equal to 10-15% of maximum lift. Inherent longitudinal static stability can be relaxed (by moving the CG backward) by utilizing from a high-authority feedback control system. This can lead to an important reduction in tail downloads which decrease the total drag and so increase maneuverability.

The full upward lift capability of the horizontal tail can be used for trimming purposes with the concept of artificial stability. In fact, the aft CG limit is determined by maximum lift produced on the horizontal tail to balance the unstable lift on the wing. Thus, the maximum positive and negative lift capability of the horizontal tail can be exploited throughout the operational CG range. This leads to drag and weight savings.

Artificial stability provides either an increase in the performance of an aircraft or a reduction in its size and weight for a specified performance which could cause a weight reduction.

The higher usable lift is created with relaxed static stability which allows a higher wing loading. Lower drag is generated from the smaller wing and horizontal tail. This means that less fuel is required to burn. The reductions in aircraft size and fuel load lead to decrease in the total weight of the aircraft which permits a smaller engine.

The application of the relaxed static stability (RSS) on the aircrafts can cause significant stability and control problems at high AoA. Figure 1.1 indicates a graph of pitch moment coefficient with respect to AoA for an unstable aircraft. The variation of C_m with α for neutral, full downward and full upward positions of pitch control surface are presented in the figure. There are two major problems indicated by the shaded regions. The problems of unintended longitudinal control loss and longitudinal departures exist at the lower angle-of-attack region because of insufficient aerodynamic nose-down control moment. A potential deep stall trimmability may not possible due to reduced effectiveness of control is another problem at high AoA region. Such problems are eliminated as long as adequate pitch-down control authority are provided throughout the whole angle of attack envelope. Therefore, a parameter is defined for the aircrafts having artificial static longitudinal stability. Parameter can be simply described as minimum aerodynamic pitch moment generated with the usage of entire pitch down control authority. Defining minimum pitching down moment is a design target and very crucial during the preliminary design phase [5].

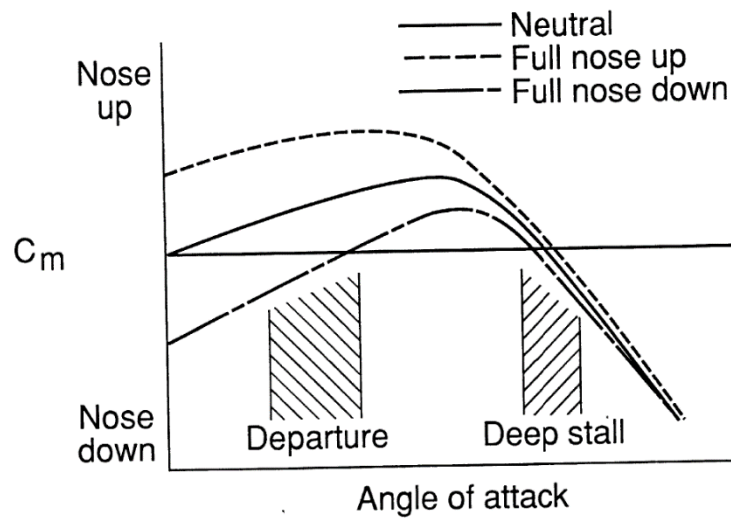


Figure 1.1. Generic Pitching Moment Variation with AoA for RSS Configurations [5]

1.3. Geometrical and Performance Specifications of the Aircraft

The aircraft is a conventional jet trainer with one engine. It has all-moving horizontal tail. It is developed in Turkish Aerospace Inc..

During this study, the analyses were done with the first configuration.

The major geometrical specifications of the jet trainer used during this study are tabulated in Table 1.1.

Table 1.1. Major Aircraft Specifications

Mean wing aerodynamic chord (\bar{c})	2.70	m
Wing reference area (S)	24	m ²
Wing span (b)	9.61	m
Pitching moment of inertia (I_{YY})	46162	kg.m ²
FWD CG Position	35	% of MAC
Aft CG Position	39	% of MAC
Distance defined in Figure 2.5 (X_{mg})	8.16	m
Location of wing-fuselage aerodynamic center ($X_{AC_{wf}}$)	7.62	m
Thrust (T)	69677	N
Distance defined in Figure 2.5 (Z_{cg})	2.10	m
Distance defined in Figure 2.5 (Z_{mg})	0	m
Distance defined in Figure 2.5 (Z_T)	1.85	m
Location of horizontal tail aerodynamic center (X_{AC_h})	11.85	m

The major performance specifications of the jet trainer are listed in Table 1.2.

Table 1.2. Major Performance Specifications

Service Ceiling	45000	ft
Sustained Turn (at 15 000 ft)	6.5 g	
Climb Rate	35000	fpm
Range	1400	nm
Maximum Speed	1.4	Mach
G limits	11.85	m

1.4. Specifications of the Analyzed Horizontal Tails

The analyses were conducted for six different horizontal tail areas. Parameters such as aspect ratio, sweep angle, taper ratio, etc. remain same during the analyses.

The parameters of each horizontal tail are given in Table 1.3 and Table 1.4. The geometries of horizontal tails taken from Pointwise program [6].

Table 1.3. Planform Parameters of Horizontal Tails - 1

	HT#1	HT#2	HT#3
Horizontal tail span (b_{HT})	5.04 m	5.23 m	5.58 m
Mean horizontal tail aerodynamic chord (\bar{c}_{HT})	1.59 m	1.65 m	1.76 m
Horizontal tail area (S_{HT})	7.26 m ²	7.80 m ²	8.89 m ²
AR	3.5	3.5	3.5
Leading edge sweep angle (Λ_{LE})	37°	37°	37°
Horizontal tail volume coefficient (C_{HT})	0.468	0.503	0.573

Table 1.4. Planform Parameters of Horizontal Tails - 2

	HT#4	HT#5	HT#6
Horizontal tail span (b_{HT})	5.91 m	6.22 m	6.52 m
Mean horizontal tail aerodynamic chord (\bar{c}_{HT})	1.87 m	1.97 m	2.06 m
Horizontal tail area (S_{HT})	9.98 m ²	11.06 m ²	12.15 m ²
AR	3.5	3.5	3.5
Leading edge sweep angle (Λ_{LE})	37	37	37
Horizontal tail volume coefficient (C_{HT})	0.64	0.713	0.783

1.5. Conditions of Analyses

The analyzed conditions are determined by considering the type of maneuver to avoid unnecessary analysis points.

DATCOM analyses were only performed at Mach 0.2 due to probable accuracy problems in transonic and supersonic regimes [7].

The longitudinal static stability characteristics were evaluated for subsonic, transonic and supersonic speeds. The analyzed conditions for longitudinal stability characteristics are tabulated in Table 1.5

Table 1.5. The Analyzed Conditions for Longitudinal Stability

Flap deflection	Non-Deflected
HT deflection	Non-Deflected
Speed (Mach)	0.2, 0.9, 1.2
Angle-of Attack (AoA)	0°, 3°, 9°, 15°, 20°, 25°
Angle-of-Sideslip (AoS)	0°

The nose-down recovery characteristic was evaluated only at subsonic speed. The analyzed conditions for nose-down recovery are tabulated in Table 1.6.

Table 1.6: The Analyzed Conditions for Nose-Down Recovery

Flap deflection	Non-Deflected
HT deflection	+30°
Speed (Mach)	0.2
Angle-of Attack (AoA)	25°
Angle-of-Sideslip (AoS)	0°

The take-off rotation characteristic was evaluated only at subsonic speed. The analyzed conditions for take-off rotation are tabulated in Table 1.7.

Table 1.7: The Analyzed Conditions for Take-Off Rotation

Flap deflection	25°
HT deflection	-30°
Speed (Mach)	0.2
Angle-of Attack (AoA)	0°
Angle-of-Sideslip (AoS)	0°

1.6. Scope of the Research

In the scope of this study, the effect of horizontal tail area on longitudinal stability and control is investigated. The horizontal tail of an aircraft is required to provide necessary longitudinal control and the sufficient static stability throughout the defined center-of-gravity (CG) range. Therefore, the horizontal tail must be sized in accordance with these considerations.

Several horizontal tails with different planform areas were analyzed with CFD and DATCOM [7].

Tail sizing diagrams known as an x-plots or scissor-plots for all of the horizontal tails are created to find the minimum required horizontal tail size over the defined center-of-gravity range. These diagrams show the forward and aft center-of-gravity limits against the non-dimensional horizontal tail volume. The minimum size of the horizontal tail size is determined throughout the required CG range by being choosing the smallest tail volume coefficient.

1.7. Content of the Thesis

The Thesis is composed of five chapters. Each of them is summarized as follows:

In Chapter 1 is an introductory part. Motivation of the study and literature review are explained briefly. The specifications of aircraft and analyzed horizontal tails as well as analyzed conditions are given.

Chapter 2 is a theory part. The theories of longitudinal static stability, take-off rotation and nose-down recovery are explained.

In Chapter 3, the results of analyses are presented. In addition, the results of analyses are discussed.

In Chapter 4, the methodologies used during the study are given and briefly explained.

In Chapter 5, conclusions about the study are given. Besides, the future works are stated.

CHAPTER 2

THEORY

2.1. Longitudinal Static Stability

Static equilibrium means that there is no acceleration of the aircraft. The sum of forces and moments acting on the aircraft are equal to zero during unaccelerated flight. In steady level flight, the lift must equal the weight, $L=W$, the thrust must equal the drag, $T=D$, and the side force on the aircraft must be zero which is often satisfied as a result of aircraft symmetry. In addition, the summation of the roll, pitch, and yaw moments about the center of gravity must all be zero during a statically equilibrium flight. Rolling and yawing moments are often zero due to aircraft symmetry while the pitching moment is usually zeroed with the application of control surfaces.

The static stability of an aircraft in an equilibrium is related with the response of the aircraft to a small disturbance from that equilibrium. If the aircraft in a statically equilibrium state returns to equilibrium after a small disturbance, the state is a stable equilibrium. However, if the aircraft diverges from equilibrium after slightly disturbed, the state is an unstable equilibrium. In addition, neutral stability is defined as a dividing line between stable equilibrium and unstable equilibrium.

Any disturbances in roll, pitch, or yaw must produce a restoring moment which returns the aircraft to the original equilibrium position for a statically stable aircraft. In the scope of the thesis, the longitudinal static stability will be only considered.

If an aircraft is statically stable in pitch, a negative (nose-down) pitching moment about center of gravity must be produced after a small increase in angle of attack to decrease the angle of attack. Conversely, a small decrease in angle of attack must

result in a positive (nose-up) pitching moment to increase the angle of attack. Therefore, it can be concluded that the pitching moment about center of gravity must change with angle of attack such that a restoring moment.

$$\frac{\partial C_{ac}}{\partial \alpha} \equiv C_{m,\alpha} < 0 \quad (2.1)$$

The derivative (2.1) is usually called the pitch stability derivative or pitch stiffness.

Each component of an aircraft has different effect on the longitudinal stability. In general, both the wing and fuselage provide a destabilizing nose-up moment when its angle of attack is increased. Therefore, a horizontal tail is usually used to provide a stabilizing nose-down moment. An aircraft with horizontal tail has a stable configuration. The horizontal tail is not a necessity for the stability of an aircraft [4].

2.1.1. Longitudinal Stability of a Wing

The longitudinal forces and moments on a cross section of a simple cambered wing are shown in Figure 2.1.

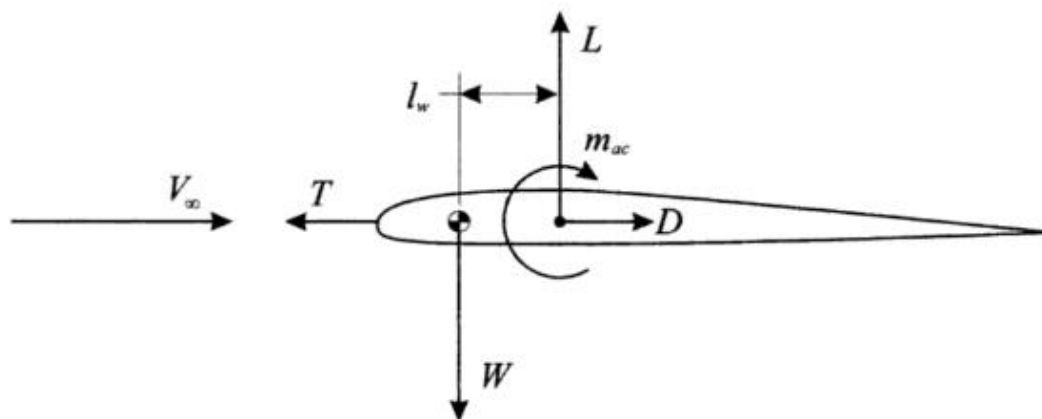


Figure 2.1. Forces and moments acting on a cambered wing in flight [8]

Wing is assumed as spanwisely symmetric. In addition, side force, rolling and yawing moments are assumed as zero. The aerodynamic forces on the wing are lift force, L , a drag force, D and the aerodynamic moment about the aerodynamic center on the wing is pitching moment throughout symmetric flight condition.

For the static equilibrium of the wing, the summation of forces in both the horizontal and vertical directions must be zero which requires that

$$T = D \quad (2.2)$$

and

$$L = W \quad (2.3)$$

Equilibrium also requires that the sum of the pitching moments about center of gravity, m , must be zero which yields

$$m = m_{ac} - l_w L \quad (2.4)$$

where l_w is the distance between aerodynamic center and the center of gravity.

After substituting the definitions of the lift and moment coefficients, the Eq. (2.4) can be expressed as

$$\frac{1}{2} \rho V_\infty^2 S_w \bar{c} C_m = \frac{1}{2} \rho V_\infty^2 S_w (\bar{c} C_{m_{ac}} - l_w C_L) \quad (2.5)$$

or

$$C_m = C_{m_{ac}} - \frac{l_w}{\bar{c}} C_L = 0 \quad (2.6)$$

The lift coefficient and moment coefficient about the aerodynamic center are fixed for a given weight and airspeed. The Eq. (2.6) can be rewritten as

$$l_w = \frac{C_{m_{ac}}}{C_L} \bar{c} \quad (2.7)$$

Since the moment coefficient about the aerodynamic center of a simple cambered wing is negative and the lift coefficient is positive, l_w must be less than zero for equilibrium. Therefore, the aerodynamic center must be forward of the center of gravity for static equilibrium.

The mathematical criterion for longitudinal stability is defined in Eq. (2.1). Inserting Eq. (2.6) into Eq. (2.1), the following expression is obtained;

$$\frac{\partial C_{m_{ac}}}{\partial \alpha} - \frac{l_w}{\bar{c}} \frac{\partial C_L}{\partial \alpha} < 0 \quad (2.8)$$

The aerodynamic center is a point on the wing where the pitching moment coefficient does not change with angle of attack,

$$\frac{\partial C_{m_{ac}}}{\partial \alpha} = 0 \quad (2.9)$$

Therefore, the longitudinal stability is obtained by satisfying the following expression

$$-\frac{l_w}{\bar{c}} \frac{\partial C_L}{\partial \alpha} < 0 \quad (2.10)$$

The variation of lift coefficient with respect to AOA is greater than zero before stall, l_w must be higher than zero for stability. Therefore, the aerodynamic center should be located at rearward of CG.

By utilizing from the trim requirement in Eq. (2.7), the distance l_w can be eliminated from the stability requirement in Eq. (2.10) which gives

$$-\frac{C_{m_{ac}}}{C_L} \frac{\partial C_L}{\partial \alpha} < 0 \quad (2.11)$$

This expression is the requirement for stable equilibrium of a wing without tail. Lift must meet the aircraft weight and the change in lift coefficient due to change in angle of attack. In addition, it must be greater than zero for any AOA below stall. Therefore, it can be concluded that a single wing without a tail always generates a nose-up pitching moment coefficient about aerodynamic center as long as stable equilibrium is provided.

A symmetric airfoil produces no moment about the aerodynamic center, and an airfoil having positive camber produces a negative pitching moment. Therefore, an airfoil must have a negative camber in order to generate a positive pitching moment. An airfoil having negative camber is very inefficient when producing positive lift. In addition, it has a low maximum lift coefficient. Therefore, the conventional aft tail is a better solution in aircraft design.

2.1.2. Longitudinal Stability of a Wing – Tail Combination

Equilibrium and static stability in pitch can be readily provided in an aircraft with aft horizontal tail.

Figure 2.2 indicates aerodynamic and gravitational forces as well as aerodynamic moments generated on a wing and a horizontal tail.

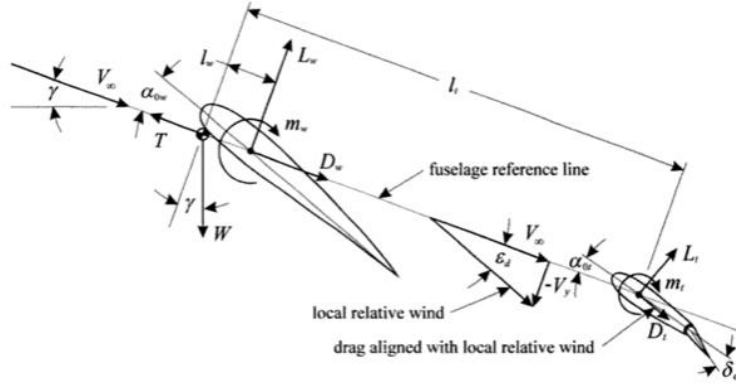


Figure 2.2. Forces and moments acting on a wing combined with a horizontal tail [8]

The angles of attack for the wing and tail are not always same; thus, the angle of attack for the aircraft can be defined with respect to a fuselage reference line. For a symmetric aircraft, the fuselage reference is chosen to be in the plane of symmetry.

Since static stability is always defined relative to an equilibrium state, the requirements for static equilibrium can be examined. The force balance for static equilibrium gives

$$T = D_w + D_h \cos \varepsilon_d + L_h \sin \varepsilon_d + W \sin \gamma \quad (2.12)$$

$$L = L_w + L_h \cos \varepsilon_d - D_h \sin \varepsilon_d = W \cos \gamma \quad (2.13)$$

where L is the total lift and ε_d is the angle between the local relative wind and the tail and freestream.

The pitching moment about CG position, m , must be zero at equilibrium,

$$m = m_w + m_h - l_w L_w - l_h L_h \cos \varepsilon_d + l_h D_h \sin \varepsilon_d = 0 \quad (2.14)$$

where m_w and m_h are the pitching moments of the wing and horizontal tail about aerodynamic centers of wing and tail, respectively. The l_w and l_h are defined as the distances between the CG and the AC of the wing and horizontal tail, respectively.

Downwash angle is generally small; therefore, small-angle approximation is mostly implemented $\cos \varepsilon_d \cong 1$ and $D_h \sin \varepsilon_d \ll L_h$. By utilizing from these approximations and dividing Eq. (2.15) by the wing area and freestream dynamic pressure, the following expressions are obtained

$$\frac{L}{\frac{1}{2} \rho V_\infty^2 S_w} = \frac{L_w}{\frac{1}{2} \rho V_\infty^2 S_w} + \frac{\frac{1}{2} \rho V_h^2 S_h}{\frac{1}{2} \rho V_\infty^2 S_w} \frac{L_h}{\frac{1}{2} \rho V_h^2 S_h} = \frac{W \cos \gamma}{\frac{1}{2} \rho V_\infty^2 S_w} \quad (2.15)$$

or

$$C_L = C_{L_w} + \frac{S_h}{S_w} \frac{\frac{1}{2} \rho V_h^2}{\frac{1}{2} \rho V_\infty^2} C_{L_h} = \frac{W \cos \gamma}{\frac{1}{2} \rho V_\infty^2 S_w} \quad (2.16)$$

$$\eta_h \equiv \frac{\frac{1}{2} \rho V_h^2}{\frac{1}{2} \rho V_\infty^2} \quad (2.17)$$

where C_{L_w} , C_{L_h} and C_{L_h} are lift coefficients for the wing and horizontal tail, each based on their planform area, respectively. C_L is total lift coefficient based on the area of wing. Dynamic pressure for horizontal tail may be less than or greater than the freestream dynamic pressure since on average over the horizontal tail span. The position of horizontal tail has a strong effect on the dynamic pressure on the horizontal tail. The dynamic pressure ratio is defined as horizontal tail efficiency.

The small-angle app. for ε_d to Eq. (2.14) is implemented and is divided by freestream dynamic pressure, the area of the main wing, and the mean chord length of the main wing in a manner similar that used to obtain Eq. (2.16):

$$\frac{M}{\frac{1}{2}\rho V_\infty^2 S_w \bar{c}_w} = \frac{M_w}{\frac{1}{2}\rho V_\infty^2 S_w \bar{c}_w} + \frac{S_h \bar{c}_h}{S_w \bar{c}_w} \eta_h \frac{M_h}{\frac{1}{2}\rho V_h^2 S_h \bar{c}_h} - \frac{l_w}{\bar{c}_w} \frac{L_w}{\frac{1}{2}\rho V_\infty^2 S_w \bar{c}_w} - \frac{S_h l_h}{S_w \bar{c}_w} \eta_h \frac{L_h}{\frac{1}{2}\rho V_h^2 S_h \bar{c}_h} = 0 \quad (2.18)$$

The Eq. (2.18) can be expressed by the definitions of the lift and moment coefficients:

$$C_m = C_{m_w} + \frac{S_h \bar{c}_h}{S_w \bar{c}_w} \eta_h C_{m_h} - \frac{l_w}{\bar{c}_w} C_{L_w} - \frac{S_h l_h}{S_w \bar{c}_w} \eta_h C_{L_h} = 0 \quad (2.19)$$

The lift coefficient of wing is assumed as a linear function of AOA for low AOA,

$$C_{L_w} = C_{L_{w,\alpha}} (\alpha + \alpha_{0w} - \alpha_{L0w}) \quad (2.20)$$

where $C_{L_{w,\alpha}}$ is the variation of wing lift with respect to AOA of aircraft as measured relative to specified reference line, α_{0w} is the angle between wing chord and specified reference line, and α_{L0w} is the zero-lift AOA of wing.

The vorticity trailing behind a lifting wing produces downwash in the region aft of wing for finite wings. The downwash causes an important effect on lift over a horizontal tail and should never be ignored during design of the horizontal tail. The downwash on the horizontal tail produced by the wing decreases the effective angle of attack of the horizontal tail. In addition, because the downwash changes with wing angle of attack, it decreases the effectiveness of the horizontal tail in stabilizing the aircraft. The downwash changes along the span of the horizontal tail. The planform shape of the wing and the presence of the fuselage affect the downwash. Computer simulations and/or wind tunnel tests are the only two ways to estimate accurately the interactions between the different surfaces of the aircraft.

Because the downwash angle at the horizontal tail is directly proportional with the wing lift. In addition, the downwash angle can be expressed as a linear function of the AOA,

$$\varepsilon_d = \varepsilon_{d0} + \varepsilon_{d,\alpha} \alpha \quad (2.21)$$

where ε_{d0} is the downwash angle for which the specified reference line is located at 0° AOA and $\varepsilon_{d,\alpha}$ is the variation of downwash with AOA.

For low AOA and elevator deflection as well as for the horizontal tail having a symmetric airfoil, the lift coefficient of horizontal tail by including the effect of downwash is expressed as

$$C_{L_h} = C_{L_{h,\alpha}} (\alpha + \alpha_{0h} - \varepsilon_d + \varepsilon_e \delta_e) = C_{L_{h,\alpha}} \left[(1 - \varepsilon_{d,\alpha}) \alpha + \alpha_{0h} - \varepsilon_{d0} + \varepsilon_e \delta_e \right] \quad (2.22)$$

where $C_{L_{h,\alpha}}$ is the lift slope of horizontal tail, α_{0h} is the angle between the horizontal tail and specified reference line, ε_e is the effectiveness of elevator, and δ_e is the deflection of elevator.

The pitching moment coefficient of horizontal tail can be expressed as a linear function of the elevator deflection when deflection of elevator is small. For the cases of horizontal tail having symmetric airfoil and for non-deflected elevator, it can be written $C_{m_{h,\delta_e}}$

$$C_{m_h} = C_{m_{h,\delta_e}} \delta_e \quad (2.23)$$

where $C_{m_{h,\delta_e}}$ is the variation of horizontal tail pitching moment coefficient with elevator deflection.

The derivative of the pitching moment coefficient for the complete aircraft with AOA must be negative for longitudinal stability. For a symmetric horizontal tail with low AOA and small deflection of elevator, the total pitching moment coefficient can be written by applying Eqs. (2.20), (2.22), (2.23) to Eq.(2.19). The following expression is derived

$$C_m = C_{m_w} + \frac{S_h \bar{c}_h}{S_w \bar{c}_w} \eta_h C_{m_h, \delta_e} \delta_e - \frac{l_w}{\bar{c}_w} C_{L_w, \alpha} (\alpha + \alpha_{0w} - \alpha_{L0w}) - \frac{S_h l_h}{S_w \bar{c}_w} \eta_h C_{L_h, \alpha} [(1 - \varepsilon_{d, \alpha}) \alpha + \alpha_{0h} - \varepsilon_{d0} + \varepsilon_e \delta_e] = 0 \quad (2.24)$$

For small variation in angle of attack, the aerodynamic center of the wing and horizontal tail are fixed points that do not change with angle of attack. Therefore, by differentiating Eq. (2.24) with respect to angle of attack, the longitudinal static stability of the wing-tail combination are obtained

$$C_{m, \alpha} \equiv \frac{\partial C_m}{\partial \alpha} = -\frac{l_w}{\bar{c}_w} C_{L_w, \alpha} - \frac{S_h l_h}{S_w \bar{c}_w} \eta_h C_{L_h, \alpha} (1 - \varepsilon_{d, \alpha}) < 0 \quad (2.25)$$

The variation in the downwash angle with respect to angle of attack is typically less than 1.0. Moreover, the lift slope, planform area, and mean aerodynamic chord length are always positive for both the wing and horizontal tail. The aerodynamic center of the horizontal tail is aft of the center of gravity ($l_h > 0$) due to the aft tail. As seen from Eq. (2.25), if the center of gravity is forward of the aerodynamic center of the wing ($l_w > 0$), the wing-horizontal tail combination will unconditionally stable.

If the center of gravity is located at aft of the aerodynamic center of the wing ($l_w < 0$), then the wing is destabilizing and the product of the horizontal tail length and the horizontal tail area, $S_h l_h$, must be sufficiently high so that the total pitching moment with respect to angle of attack is still negative. Therefore, it can be said that changing the size and/or length of the horizontal tail, the longitudinal stability of an aircraft can be controlled.

The second term in Eq. (2.25) indicates the contribution of the horizontal tail to the longitudinal stability of the aircraft. This term makes the major contribution to the overall longitudinal stability of the aircraft. This term is proportional to the product of the horizontal tail area and horizontal tail length, $S_h l_h$, divided by the product of the wing area and wing chord, $S_w \bar{c}_w$. Each of these products shows a characteristic volume associated with the aircraft. The product, $S_h l_h$, can be sometimes called the

tail volume. Increase in tail volume for an aft tail increase the longitudinal stability of the aircraft. The ratio, $S_h l_h / S_w \bar{c}_w$, is usually called the horizontal tail volume ratio.

$$V_h \equiv \frac{S_h l_h}{S_w \bar{c}_w} \quad (2.26)$$

The horizontal tail volume ratio can be easily varied by either varying the horizontal tail area or by varying its distance aft of the center of gravity. The magnitude of the horizontal tail volume ratio can be used to directly control the longitudinal stability of any aircraft with an aft horizontal tail. As seen from the Eq. (2.26), the horizontal tail volume ratio and the first term of the Eq. (2.25) are directly affected by the location of the CG and are, therefore, affected by the aircraft loading.

2.1.3. Stick-Fixed Neutral Point and Static Margin

A point about which the total pitching moment does not change with small variations in angle of attack exists on the aircraft. This is like the aerodynamic center of an airfoil or wing. The aircraft is longitudinally stable if the center of gravity is located at this point. Therefore, this point is commonly called as the stick-fixed neutral point. In other words, the stick-fixed neutral point is the aerodynamic center of the whole aircraft.

To locate the stick-fixed neutral point for the simplified wing-tail combination, the inequality obtained in Eq.(2.25) is replaced with the equality.

$$C_{m,\alpha} \equiv \frac{\partial C_m}{\partial \alpha} = -\frac{l_{wn}}{\bar{c}_w} C_{L_{w,\alpha}} - \frac{S_h l_{hn}}{S_w \bar{c}_w} \eta_h C_{L_{h,\alpha}} (1 - \epsilon_{d,\alpha}) = 0 \quad (2.27)$$

The variables l_{wn} and l_{hn} in Eq.(2.27) are replaced with l_w and l_h to represent a distance measured from aft of the neutral point. The distances measured aft of the neutral point, l_{wn} & l_{hn} can be written as $l_{wn} = l_w - l_{np}$ and $l_{hn} = l_h - l_{np}$. By utilizing this notation, Eq.(2.27) can be written as

$$C_{L,\alpha} \equiv \frac{\partial C_L}{\partial \alpha} = C_{L_w,\alpha} + \frac{S_h}{S_w} \eta_h C_{L_h,\alpha} (1 - \varepsilon_{d,\alpha}) \quad (2.31)$$

The denominator on the right-hand side of Eq.(2.29) is the lift slope of the wing-tail combination.

Therefore, by utilizing from Eq.(2.31), Eq.(2.29) can be rewritten as

$$\frac{l_{np}}{\bar{c}_w} = \left[\frac{l_w}{\bar{c}_w} C_{L_w,\alpha} + \frac{S_h l_h}{S_w \bar{c}_w} \eta_h C_{L_h,\alpha} (1 - \varepsilon_{d,\alpha}) \right] / C_{L,\alpha} \quad (2.32)$$

From Eq.(2.25), the longitudinal stability derivative for the wing-tail combination is

$$C_{m,\alpha} \equiv \frac{\partial C_m}{\partial \alpha} = -\frac{l_w}{\bar{c}_w} C_{L_w,\alpha} - \frac{S_h (l_h - l_{np})}{S_w \bar{c}_w} \eta_h C_{L_h,\alpha} (1 - \varepsilon_{d,\alpha}) \quad (2.33)$$

The numerator on the right-hand side of Eq.(2.32) is equal to the negative of the longitudinal stability derivative of the wing-tail combination. Thus,

$$\frac{l_{np}}{\bar{c}_w} = -\frac{C_{m,\alpha}}{C_{L,\alpha}} \quad (2.34)$$

The longitudinal stability derivative can be rewritten as

$$C_{m,\alpha} = -(l_{np}/\bar{c}_w) C_{L,\alpha} \quad (2.35)$$

The lift slope is positive for angles of attack below stall. An aircraft is longitudinally stable when the pitch stability derivative is a negative value. Therefore, as seen from Eq.(2.35), the center of gravity must be forward of the stick-fixed neutral point for a longitudinally stable aircraft.

The l_{np}/\bar{c}_w term is defined as the stick-fixed static margin. It is the distance that the center of the gravity is ahead of the stick-fixed neutral point, defined as a fraction of any chosen reference chord length. A static margin of at least 5 percent is generally a

rule of thumb for aircrafts to provide good handling qualities for pilot. The 5-percent-static-margin rule should be a rough initial estimation for aircrafts with traditional geometric proportions since the effects of longitudinal stability do not scale with wing chord. Wing chord appears in the ratio on the left-hand side of Eq.(2.34) since it is an arbitrarily chosen reference length to nondimensionalize the longitudinal stability derivative on the right-hand side. The aerodynamic pressure and shear forces acting on the aircraft can always be resolved into a lift force, a drag force, and an aerodynamic moment, all acting at center of gravity which are shown in Figure 2.4. m is used to show the aerodynamic pitching moment about center of gravity. If m_{np} represents the aerodynamic pitching moment with respect to neutral point, a summation of moments with respect to the neutral point is equal to

$$m_{np} = m + l_{np} (L \cos \alpha + D \sin \alpha) + h_{np} (L \sin \alpha - D \cos \alpha) \quad (2.36)$$

The vertical offset between the neutral point and the center of gravity is small and the drag is much less than the lift for a typical aircraft. Moreover, the angle of attack is small during normal flight operation. Therefore, by applying the traditional small-angle approximations, $h_{np} \sin \alpha \cong 0$, $h_{np} \cos \alpha \cong h_{np}$, $D \cong 0$, $L \cong L$, and $\cos \alpha \cong 1$, $\sin \alpha \cong \alpha$. By utilizing from these approximations in Eq.(2.36) and nondimensionalizing the result, the following expression is obtained:

$$C_{m_{np}} \cong C_m + \frac{l_{np}}{\bar{c}_w} C_L \quad (2.37)$$

Differentiating Eq.(2.37) with respect to angle of attack yields to

$$\frac{\partial C_{m_{np}}}{\partial \alpha} \cong \frac{\partial C_m}{\partial \alpha} + \frac{l_{np}}{\bar{c}_w} \frac{\partial C_L}{\partial \alpha} \quad (2.38)$$

The moment about the stick-fixed point does not vary with angle of attack since the stick-fixed neutral point is the aerodynamic center of the aircraft. Therefore, by using the approximations in this simplified model, the result in Eq.(2.38) can be simplified to the relation given in Eq.(2.35),

$$C_{m,\alpha} \cong -\left(l_{np}/\bar{c}_w\right)C_{L,\alpha} \quad (2.39)$$

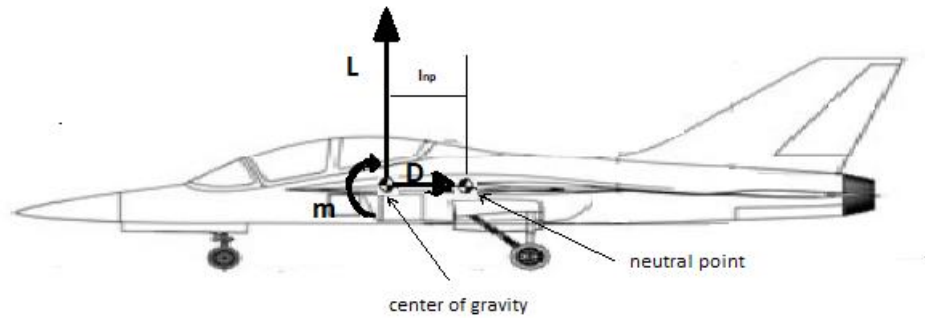


Figure 2.4. Stick-fixed neutral point of an aircraft [9]

Equation (2.39) shows how the center of the gravity affects the longitudinal stability of an aircraft. As the CG is moved forward, the aircraft becomes more stable.

The concept of the aerodynamic center is highly significant in the study of the longitudinal static stability. The stick-fixed neutral point is the aerodynamic center of the whole aircraft. The aerodynamic center of an airfoil section is the position on the chord line where the variation in pitching moment with respect to angle of attack is zero. The position of the aerodynamic center is almost independent of angle of attack. Thin airfoil theory estimates the aerodynamic center of an airfoil locates at the quarter chord over the subsonic regime. Experimental data also support this theory that show that the actual aerodynamic center of most airfoils is very close to the quarter chord at low Mach numbers and small angles of attack. The aerodynamic center goes towards rear from about quarter-chord to half-chord of the wing throughout acceleration to supersonic speed regime [4].

The aerodynamic center is traditionally defined as the point where the pitching moment is independent of angle of attack for a complete aircraft. Moreover, present

formulations for the pitch stability derivative ignores the change in position of aerodynamic center with respect to angle of attack. On the other hand, there may be no fixed point on the wing or complete aircraft where the pitching moment is independent of the angle of attack.

The aerodynamic center ($\bar{x}_{ac}, \bar{y}_{ac}$) is generally located to encounter two constraints [8].

- 1) The pitching moment about the aerodynamic center must be independent from small changes in angle of attack.

$$\frac{\partial C_{m_{ac}}}{\partial \alpha} \equiv 0 \quad (2.40)$$

- 2) The position of the aerodynamic center must be invariant to small changes in angle of attack.

$$\frac{\partial \bar{x}_{ac}}{\partial \alpha} \equiv 0, \quad \frac{\partial \bar{y}_{ac}}{\partial \alpha} \equiv 0 \quad (2.41)$$

2.2. Take-Off Rotation

The horizontal tail size required during the take-off rotation is a critical requirement which sizes the horizontal tail. Most of the aircrafts must be rotated about the main landing gear rotation point to be able to reach the required angle of attack for lift-off. During the take-off, aircrafts normally rotates at low speeds which are slightly higher than the stall speed. The low dynamic pressures at low speeds decrease the effectiveness of control surface. Therefore, a significant download on the horizontal tail is required for the necessary lift-off capability [10].

Figure 2.5 indicates the major forces and moments which act on the aircraft during the take-off rotation. The forces on the aircraft during the take-off rotation can be listed as wing lift, horizontal control surface lift, wing-body pitching moment, aircraft drag,

$$T - D - \mu R = \frac{W}{g} \dot{U} \quad (2.42)$$

$$L_{wf} + L_h + R = W \quad (2.43)$$

$$-W(X_{mg} - X_{cg}) + D(Z_D - Z_{mg}) - T(Z_T - Z_{mg}) + L_{wf}(X_{mg} - X_{ac_w}) + M_{ac_w} - L_h(X_{ac_h} - X_{mg}) + \frac{W}{g} \dot{U}(Z_{cg} - Z_{mg}) = I_{yy_{mg}} \ddot{\theta}_{mg} \quad (2.44)$$

The forces and moments in Eqns. 2.42 – 2.44 can be expressed as follows:

- The expression for the drag,

$$D = C_D \bar{q}_{rotate} S \quad (2.45)$$

where

C_D is the aircraft coefficient

\bar{q}_{rotate} is the dynamic pressure during the take-off rotation

$\ddot{\theta}_{mg}$ is the angular acceleration about the main landing gear rotation point in rad/sec²

- The expression for the wing-fuselage lift,

$$L_{wf} = C_{L_{wf}} \bar{q}_{rotate} S \quad (2.46)$$

where

$C_{L_{wf}}$ is the aircraft lift coefficient during the take-off rotation

- The expression for the horizontal tail lift,

$$L_h = C_{L_h} \bar{q}_{rotate} S \quad (2.47)$$

where

C_{L_h} is the horizontal tail lift coefficient during the take-off rotation. The horizontal tail lift coefficient is normally negative (download acting on the tail) to achieve the take-off rotation.

- The expression for the wing-fuselage pitching moment,

$$M_{ac_{w/f}} = C_{m_{ac_{w/f}}} \bar{q}_{rotate} S \quad (2.48)$$

where

$C_{m_{ac_{w/f}}}$ is the aircraft pitching moment coefficient about the wing-fuselage aerodynamic center in ground effect at the instant of take-off run. It is normally negative for a positively cambered wing. The aircraft pitching moment becomes more negative when the flaps are extended.

μ is the wheel-to-ground friction coefficient. The values of wheel-to-ground for different ground conditions are tabulated at Table 2.1.

Table 2.1. Typical Values for Wheel-Ground Friction Coefficient [10]

Wheel-Ground Friction Coefficient, μ	0.02	0.02	0.04	0.05	0.10	0.10-0.30
Type of Terrain	Concrete	Asphalt or Macadam	Hard Turf	Short grass	Long grass	Soft ground

The duration of take-off rotation does not exceed 1-3 seconds. Therefore, the angular acceleration about the main landing gear rotation point, $\ddot{\theta}_{mg}$, should be approximately taken between 10-12 deg/sec² for fighters in a preliminary design.

The aircraft rotation speed may be related with the stall speed in the take-off configuration during preliminary design.

$$V_{rotate} = V_R \geq 1.1V_{S_{takeoff}} \quad (2.49)$$

The most forward CG position for take-off rotation at the rotation speed can be solved from Eqns 2.42 – 2.44. The final result is summarized as:

$$X_{cg} = \frac{\left[I_{yy_{mg}} \ddot{\theta}_{mg} + WX_{mg} - D(Z_D - Z_{mg}) + T(Z_T - Z_{mg}) - L_{wf}(X_{mg} - X_{ac_{wf}}) - M_{ac_{wf}} \right.}{W} \left. + L_h(X_{ac_h} - X_{mg}) - \left\{ (T - D - \mu(W - L_{wf} - L_h))(Z_{cg} - Z_{mg}) \right\} \right] \quad (2.50)$$

2.3. Nose-Down Recovery

Maneuverable aircrafts can reach to high AOA because of low or negative static longitudinal stability. After the aircraft starts to pitch-up with the application of nose-up control, unstable or nose-up pitching moments also accompany to it. Pitch-down moment can be required for recovery in order to counter an unstable pitch-up moment.

A criterion for the required pitch-down moment during recovery is determined from some related simulation studies and practical fighter design. A pitching acceleration of 0.3 rad/sec is found to be sufficient by providing a margin for inertial coupling [2].

The magnitude of pitch-down control capability at high AOA is determined by five primary factors which are briefly explained below [5]:

Deep Stall: A deep stall trim is a very crucial characteristic for high maneuverable aircrafts. Adequate pitch-down cannot be provided by whole pitch-down control authority. Thus, the aircraft will not be recovered from high AoA (HiAoA).

High AoA Recovery: Rapid recovery from HiAoA conditions can be really significant capability during air combat. Therefore, necessary pitch down acceleration have to be ensured at high AOA.

Inertia Coupling: Inertia coupling can cause substantial nose-up moments which is given by the following expression:

$$M_{IC} = (I_Z - I_X) pr \quad (2.51)$$

Rolling about the velocity vector required to eliminate excessive sideslip at high AoA is an important contributor to this effect. The body-axis roll and yaw rates are expressed as $p = p_{stab} \cos \alpha$ and $r = r_{stab} \sin \alpha$. Substituting into Eq. 2.51 and simplifying gives:

$$M_{IC} = \frac{1}{2} (I_Z - I_X) p_{stab}^2 \sin 2\alpha \quad (2.52)$$

The moment expressed in terms of pitch angular acceleration is given as:

$$\dot{q}_{IC} = \frac{1}{2} \left(\frac{I_Z - I_X}{I_Y} \right) p_{stab}^2 \sin 2\alpha \quad (2.53)$$

For typical combat aircraft, $\left(\frac{I_Z - I_X}{I_Y} \right) \cong 1$, so:

$$\dot{q}_{IC} \cong 0.5 p_{stab}^2 \sin 2\alpha \quad (2.54)$$

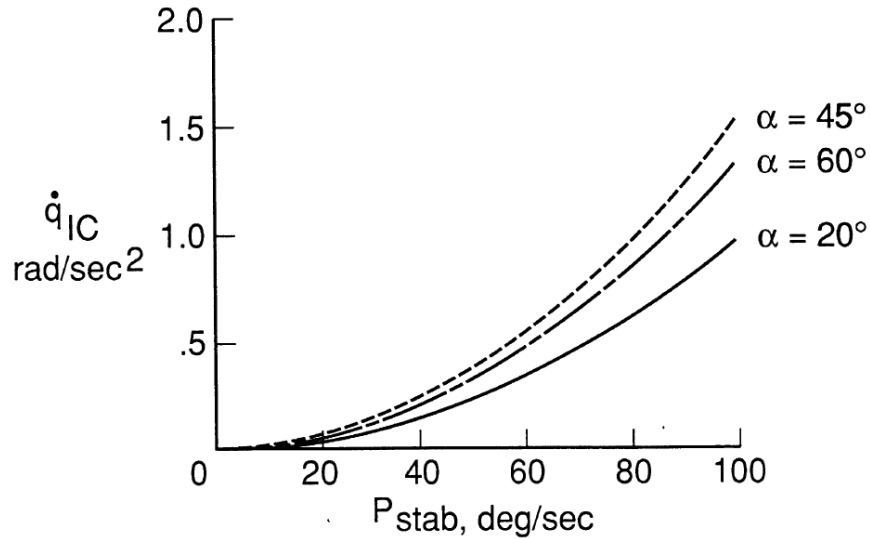


Figure 2.6. Typical inertia coupling pitch angular acceleration due to stability-axis roll [5]

By using Eq. 2.54, Figure 2.6 indicates the typical variation of \dot{q}_{IC} with respect to roll rate for three AOA. According to the consequences of studies, \dot{q}_{IC} takes its highest value at 45° AoA as well as high pitch-up accelerations may be produced at high roll rates as expected. Adequate pitch-down moment must be generated to overcome the undesirable pitch-up moments for artificial stability conditions.

Unintended motions in lateral or directional axis at high AOA like severe lateral oscillations, “wing rock” lead to significant additional nose-up inertia coupling moments. Therefore, having sufficient control authority for pitch down is very significant such that pitch-up moments because of intended high AoA roll maneuvers must be encountered.

Aerodynamic Coupling: Aerodynamic pitching moment can be significantly changed with the AOS at high AOA on some combat aircraft. This characteristic highly depends on aircraft geometry; however, large pitch-up moments because of AOS are common which are shown in Figure 2.7.

Kinematic Coupling: Excess rises in AOA can cause rolling with proverse AOS. The rate of variation of AOA because of kinematic coupling is expressed as:

$$\dot{\alpha}_{KC} = -(p \cos \alpha + r \sin \alpha) \tan \beta \quad (2.55)$$

If the sign of β is different from the sign of p and r , rolling due to proverse β , $\dot{\alpha}_{KC}$ becomes positive. Sufficient control for pitch-down may be needed in order to meet the α rise because of the kinematic coupling to eliminate the risk of pitch departure for RSS designs.

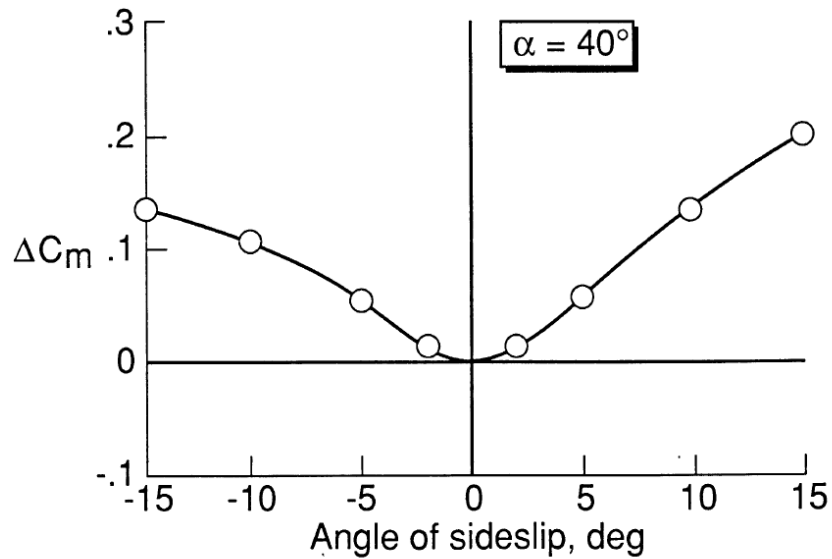


Figure 2.7. Example of incremental pitching moment coefficient due to nonzero sideslip [5]

High AOA pitch-down control authority for relaxed static stable fighters is very significant.

A methodology for pitch-down control authority are developed for artificially stable aircrafts by utilizing from some experiences on the high angles of attack aerodynamics and flight mechanics.

The developed methodology shown in Figure 2.8 is based on the following relationship:

$$C_m^* = \frac{I_y \dot{q}}{q S \bar{c}} = \left(\frac{\dot{q}}{q} \right) \left(\frac{I_y}{S \bar{c}} \right) \quad (2.56)$$

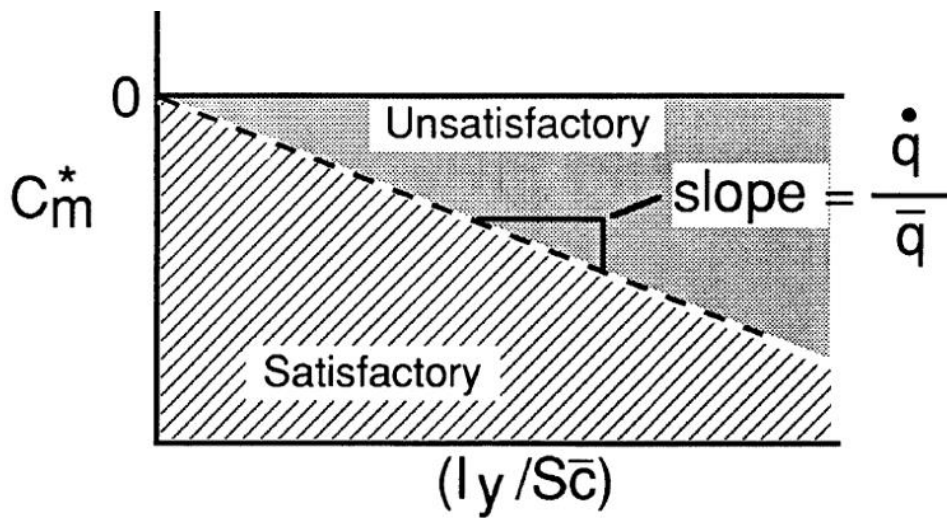


Figure 2.8. The developed methodology for high AoA nose-down pitch control [5]

The $\left(\frac{\dot{q}}{q} \right)$ term is the ratio of pitch acceleration and dynamic pressure. It shows control authority at the specified dynamic pressure. The $\left(\frac{I_y}{S \bar{c}} \right)$ term is affected from

the mass and aircraft geometry. Therefore, the variation of C_m^* with $\left(\frac{I_Y}{S\bar{c}}\right)$ is linear and have a slope equal to $\left(\frac{\dot{q}}{q}\right)$ as indicated in Figure 2.8. Aircrafts with value across the line has minimum pitch-down control authority while aircrafts having values above the line has less pitch-down control authority. In addition, aircrafts with values below the line will have greater pitch-down control authority.

Thus, the proper variation of C_m^* with $\left(\frac{I_Y}{S\bar{c}}\right)$ should be determined to achieve “satisfactory“ high AoA nose-down control capability.

2.4. Tipback Angle Requirement

Tipback angle is a requirement for an aircraft having a tricycle landing gear which can limit the aft CG of an aircraft. Tipback angle is defined as maximum pitch-up angle while horizontal tail touches the ground. The tipback angle should be greater than the take-off rotation angle in order to prevent the aircraft to tip back on its horizontal tail. The tipback angle of an aircraft with tricycle landing gear is shown in Figure 2.9.

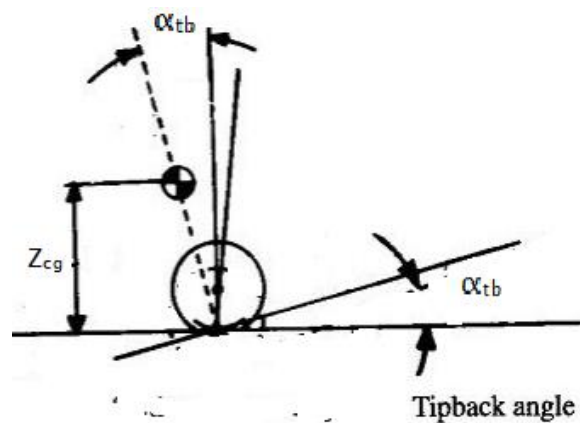


Figure 2.9. The tipback angle of aircraft with tricycle landing gear [11]

The take-off rotation angle is typically around $10^\circ - 15^\circ$. Thus, tipback angle should be $15^\circ - 20^\circ$.

The limit of CG position at tipback angle is calculated from Eq. (2.57).

$$X_{cg} = X_{mg} + \tan(\alpha_{tb}) \times Z_{cg} \quad (2.57)$$

CHAPTER 3

RESULTS AND DISCUSSION

3.1. Determination of Neutral Point and Most Aft CG Position Regarding Longitudinal Static Stability

The location of neutral point is determined by utilizing from the variation of pitching moment coefficient with respect to AoA. The CG position at which the slope of C_m vs α graph becomes zero is specified as neutral point.

Neutral points are determined from both CFD and Datcom analyses at specified airspeeds for each of six horizontal tails.

The neutral points of HT # 1 for Mach 0.2, 0.9 and 1.2 obtained from CFD analyses are presented below.

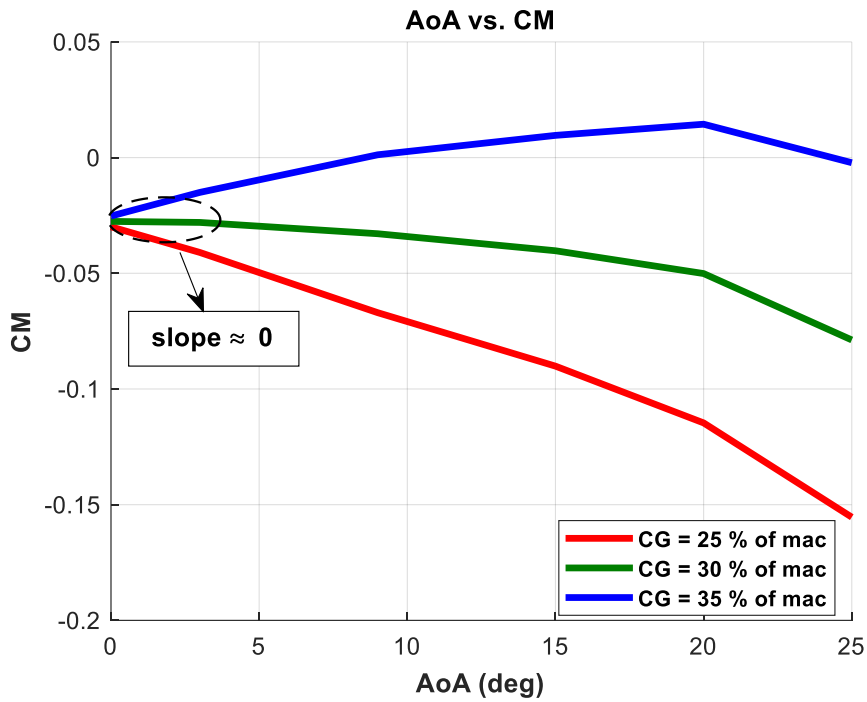


Figure 3.1. The variation of. C_m with AoA at 0.2 Mach for HT # 1

Figure 3.1 indicates the variation of C_m vs AoA for HT # 1 at 0.2 Mach over the analyzed AoA range. The slope of C_m with respect to AoA becomes zero approximately at 30 % of MAC. Therefore, according to the results of CFD analyses, the neutral point of HT # 1 for 0.2 Mach is approximately 30 % of MAC.

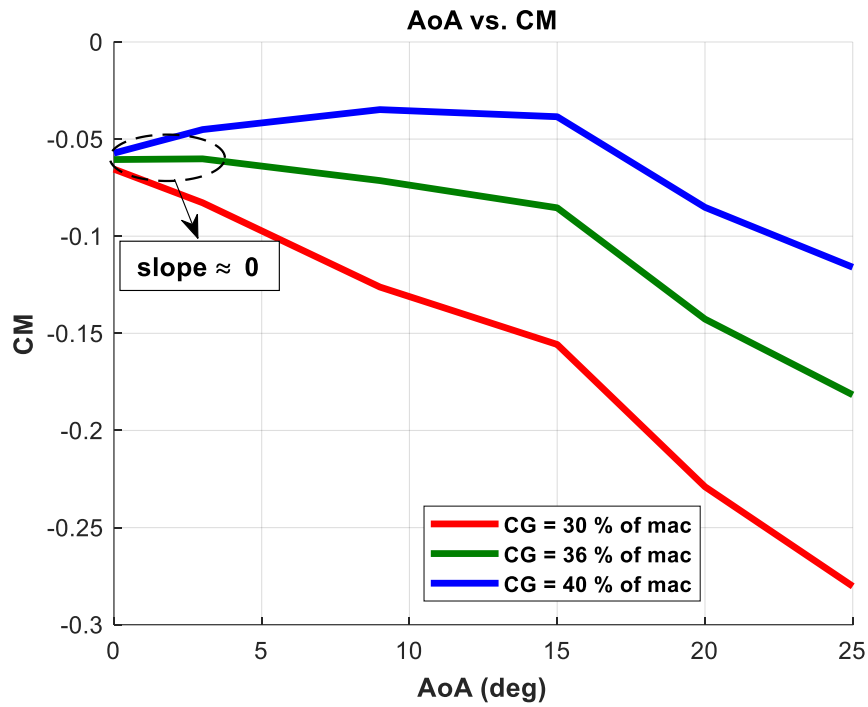


Figure 3.2. The variation of C_m with AoA at 0.9 Mach for HT # 1

The variation of C_m with respect to AoA for HT # 1 at 0.9 Mach is presented in Figure 3.2 over the analyzed AoA range. The slope of C_m vs α becomes zero approximately at 36 % of MAC, which is specified as the neutral point for 0.9 Mach according to the results of CFD analyses.

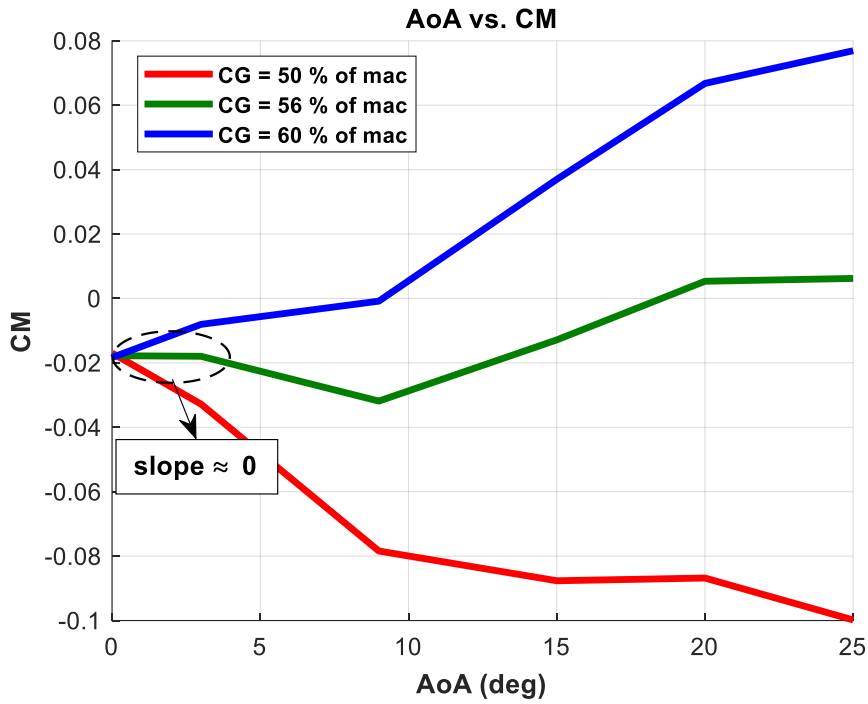


Figure 3.3: The variation of C_m with AoA at 1.2 Mach for HT # 1

Figure 3.3 illustrates the variation of C_m with AoA for HT # 1 at 1.2 Mach over the analyzed AoA range. The slope of C_m with respect to AoA becomes zero approximately at 56 % of MAC. Therefore, according to the results of CFD analyses, the neutral point of HT # 1 for 1.2 Mach is approximately 56 % of MAC.

The neutral points of HT # 1 for Mach 0.2 obtained from DATCOM analyses are presented below.

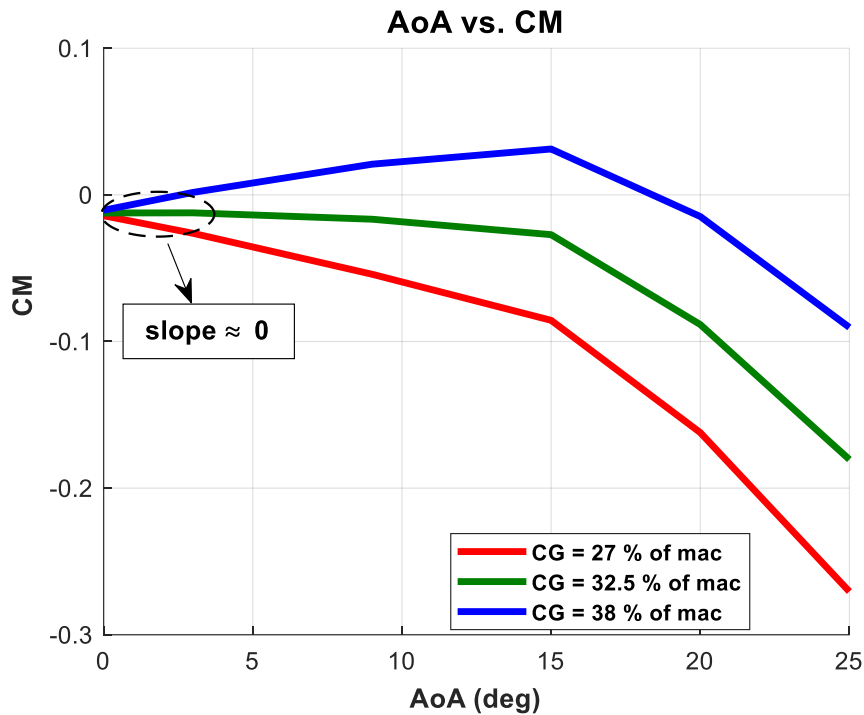


Figure 3.4: The variation of C_m with AoA at 0.2 Mach for HT # 1

Figure 3.4 shows the variation of C_m with AoA for HT # 1 at 0.2 Mach over the analyzed AoA range. The variation of C_m with respect to AoA becomes zero approximately at 32.5 % of MAC. Therefore, according to the results of DATCOM analyses, the neutral point of HT # 1 for 0.2 Mach is approximately 32.5 % of MAC.

The neutral points obtained from DATCOM and CFD Analyses are presented in Table 3.1 for six horizontal tails. The neutral points move towards back from HT # 1 to HT # 6 due to increase in the size of horizontal tail. The position of neutral point is directly affected from the horizontal tail size. As the size of the horizontal tail is increased, the

neutral point shifts backward. The neutral point also moves rearward from subsonic regime to supersonic regime.

Besides, as seen from Table 3.1, the sensitivities of DATCOM and CFD programs to the change of the horizontal tail size are quite different from each other. CFD Program is much more sensitive to change in horizontal tail.

Table 3.1. The Neutral Points at 0.2, 0.9, and 1.2 Mach Numbers for Six Horizontal Tails

Horizontal Tail Number	Subsonic Speed (0.2 Mach)		Transonic Speed (0.9 Mach)	Supersonic Speed (1.2 Mach)
	DATCOM	CFD	CFD	CFD
1	32.5	30	36	56
2	33	31	36.5	57.5
3	35	34	37.5	61
4	36	37	39	64
5	37	40	40	68
6	38	44	42	71

A static margin of at least +5 % is generally a rule of thumb for a conventional aircraft to provide good handling qualities for pilots as explained in Section 2.1.3[8].

The CG positions for +5 % static margin are calculated from CFD and DATCOM analyses. The aft CG for natural longitudinal stability condition are presented at below table.

Table 3.2: The Most Aft CG Positions for SM = +5%

Horizontal Tail Number	Subsonic Speed (0.2 Mach)		Transonic Speed (0.9 Mach)	Supersonic Speed (1.2 Mach)
	DATCOM	CFD	CFD	CFD
1	27.5	25.0	31.0	51.0
2	28.0	26.0	31.5	52.5
3	30.0	29.0	32.5	56.0
4	31.0	32.0	34.0	59.0
5	32.0	35.0	35.0	63.0
6	33.0	39.0	37.0	66.0

Relaxed static stability allows an aircraft to fly with a negative static margin. Therefore, the static margin can be decreased to a negative value by utilizing from the concept of relaxed static stability. The static margins can be typically between -7 and -10% for artificially stable aircrafts [12]. In this study, the negative static margin is determined as -7 %.

The aft CG positions for -7 % static margin are calculated from CFD and DATCOM analyses. The most aft CG for artificial longitudinal stability condition are presented at below table.

Table 3.3: The Most Aft CG Positions for SM = -7%

Horizontal Tail Number	Subsonic Speed (0.2 Mach)		Transonic Speed (0.9 Mach)	Supersonic Speed (1.2 Mach)
	DATCOM	CFD	CFD	CFD
1	39.5	37.0	43.0	63.0
2	40.0	38.0	43.5	64.5
3	42.0	41.0	44.5	68.0
4	43.0	44.0	46.0	71.0
5	44.0	47.0	47.0	75.0
6	45.0	51.0	49.0	78.0

When the values of Table 3.2 and Table 3.3 are compared with each other, it can be clearly seen that the limit of aft CG position can be moved significantly backward with the relaxation of longitudinal static stability. This provides an aircraft to fly at more rearward CG positions.

3.2. Determination of Most Aft CG Position Regarding Nose-Down Recovery Capability

The aft CG positions regarding nose-down recovery capability are computed for six horizontal tails by using the results of DATCOM and CFD analyses.

The values of \dot{q}/\bar{q} are calculated over a CG at Mach 0.2. The CG position where the slope of C_m^* versus $\left(\frac{I_y}{S\bar{c}}\right)$ neutral point is equal to zero is determined. This CG position is the most aft CG at which the required minimum nose down capability exists.

The plot of \dot{q}/\bar{q} vs. CG Position for HT # 1 obtained from CFD analyses is presented in Figure 3.5.

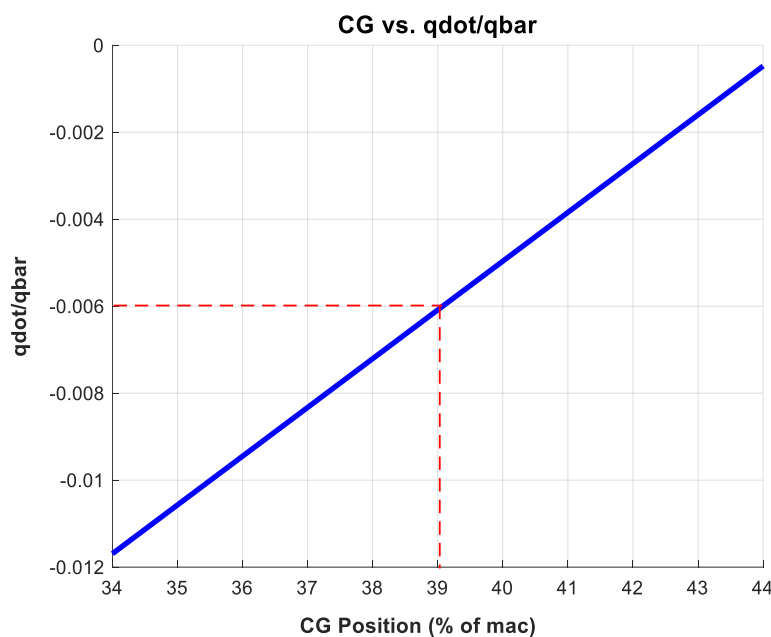


Figure 3.5. Nose-Down Recovery Characteristic for HT # 1 obtained from CFD

The value of \dot{q}/\bar{q} equal to -0.006 approximately at 39% of MAC which is the most aft CG position regarding minimum nose-down capability.

The variation of \dot{q}/\bar{q} with respect to CG Position for HT # 1 obtained from DATCOM analyses is presented in Figure 3.6.

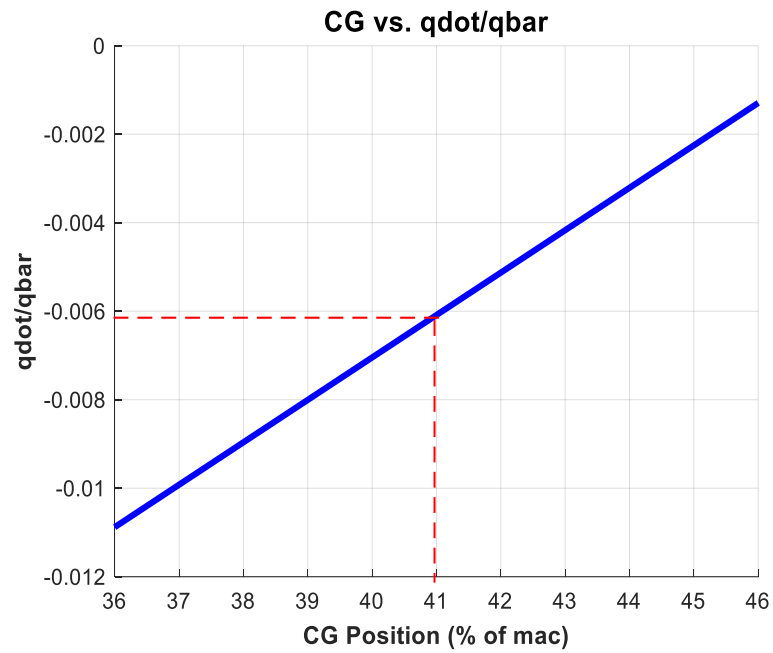


Figure 3.6: Nose-Down Recovery Characteristic for HT # 1 obtained from DATCOM

The value of \dot{q}/\bar{q} becomes -0.006 approximately at 41% of MAC which is the most aft CG position regarding minimum nose-down capability.

The aft CG positions for minimum nose-down capability are presented at Table 3.4 for six horizontal tails.

Table 3.4. The most aft CG positions regarding the minimum nose-down capability for all horizontal tails

Horizontal Tail Number	\dot{q}/\bar{q}	\dot{q} (rad/sec ²)[2]	CG Position (% of mac)	
			DATCOM	CFD
1			41	39.0
2			43	42.5
3			46.5	49.3
4	-0.006	-0.24	50	56.4
5			53	63.7
6			56.5	70.9

The aft CG position regarding minimum nose-down recovery shifts rearward from HT # 1 to HT # 6. This is surely because of increase in the size of horizontal tail. The CG position where the minimum nose down capability exists moves towards rear as the size of the horizontal tail is increased.

The sensitivities of DATCOM and CFD programs to the change of the horizontal tail size, as also mentioned at Section 3.1, are different. CFD is much more sensitive to change in horizontal tail.

3.3. Determination of Most Forward CG Position Regarding Take-Off Rotation

The forward CG positions are computed for six horizontal tails by using the results of DATCOM and CFD analyses.

Eq, 2.57 mentioned in Section 2.4 is solved by using the aircraft specifications listed in Table 1.1. Required CG positions are obtained such that they can be specified as the FWD CG limits.

DATCOM analyses are performed with/out ground effect. The ground effect does not cause any difference on the aerodynamic coefficient. Therefore, the ground effect is also included to CFD analyses.

The forward CG positions obtained from both CFD and DATCOM analyses are tabulated in Table 3.5.

Table 3.5. The Forward CG Positions Regarding Take-Off Rotation

Horizontal Tail Number	CG Position (% of MAC)	
	DATCOM Results	CFD Results
1	21	26.5
2	20	25
3	17.5	21.5
4	15.5	18
5	13	13.5
6	11	9

Table 3.5 illustrates that the limit of FWD CG position moves forward as the size of horizontal tail is increased from HT # 1 to HT # 6.

3.4. Determination of Aft CG Limit Regarding Tipback Angle Requirement

The aft CG limit regarding tipback angle requirement is computed for the aircraft by using the related geometric parameters. This aft CG limit does not change with the size of horizontal tail.

Eq, 2.57 mentioned in Section 2.2 is solved by using the aircraft specifications listed in Table 1.1. Tipback angle is taken as 15° . The most aft CG position of the aircraft without tipping back on the horizontal tail is approximately found as 66 % of MAC to.

3.5. Horizontal Tail Sizing Diagram

A tail sizing diagram are used to find the minimum required horizontal tail size for the aircraft to meet center-of-gravity requirements. This diagram is known as an x-plot or scissor-plot [13]. In this diagram, the forward and aft CG limits are plotted against the non-dimensional horizontal tail volume, which is proportional to the size and moment arm of the horizontal tail. To find the minimum tail size, the smallest value of tail volume is picked for which the distance between the forward and aft limits is equal to the required cg range.

The horizontal tail sizing diagrams for each of the horizontal tails are obtained for both natural and artificial stability conditions by utilizing from both CFD and Datcom based analyses. The diagrams are indicated in Figure 3.7 - Figure 3.54.

The solid blue lines illustrate take-off rotation and stability CG limits, respectively while the dash blue line shows the aft CG limit due to minimum nose-down control authority. The black line indicates the allowable CG range between the FWD and aft CG limits.

The limit of FWD CG position is determined from the required CG during take-off rotation while the aft CG limit is determined from the level of minimum required stability. The aft CG limit can be extended by utilizing from the concept of RSS. This causes extension of the allowable CG range which can be clearly seen from Figure 3.7 and Figure 3.8.

The tail sizing diagrams obtained from CFD and DATCOM analyses clearly show that the allowable CG range increases with increase in tail volume ratio (C_{HT}) for both natural and artificial stability conditions.

The tail sizing diagrams obtained from CFD results are presented below.

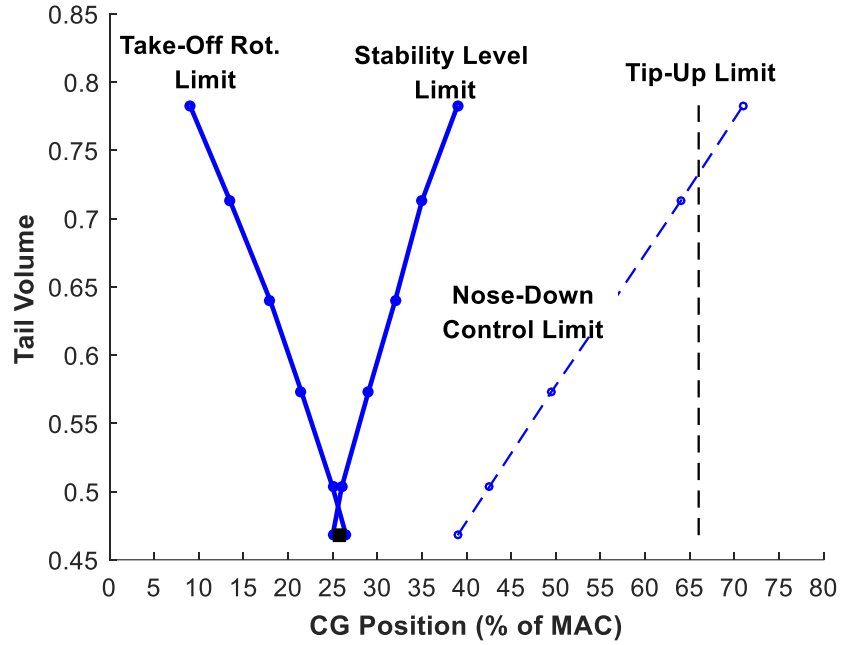


Figure 3.7. Tail Sizing Diagram of HT#1 for Natural Stability at 0.2 Mach

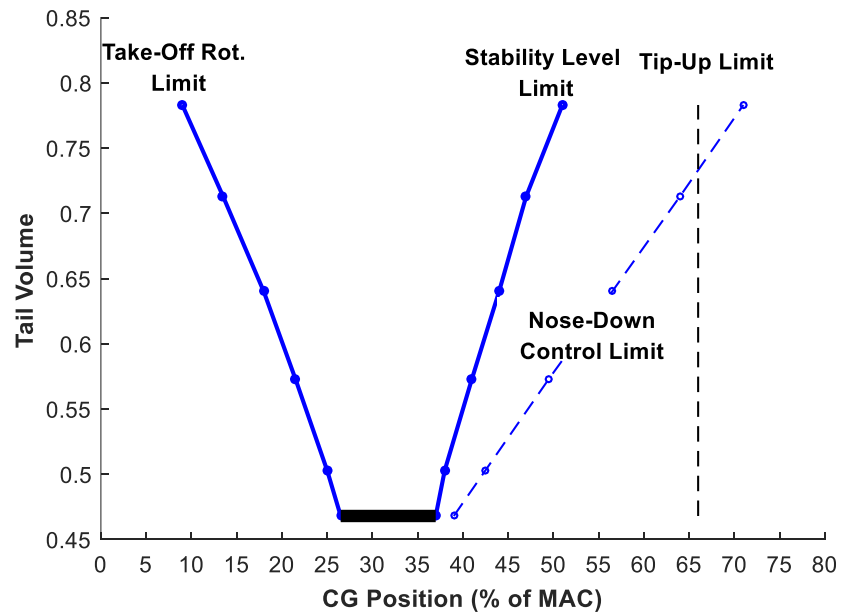


Figure 3.8: Tail Sizing Diagram of HT#1 for Artificial Stability at 0.2 Mach

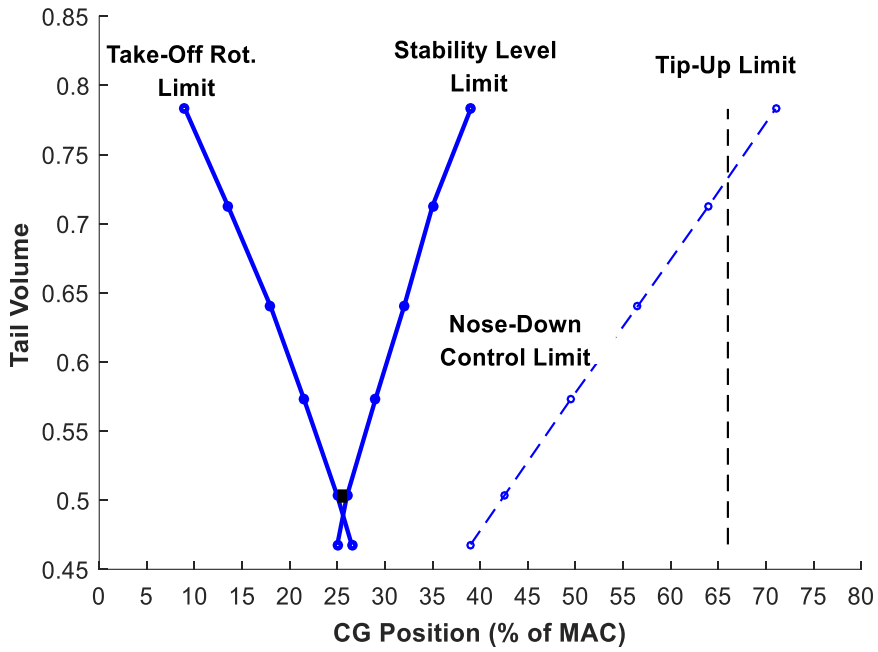


Figure 3.9: Tail Sizing Diagram of HT#2 for Natural Stability at 0.2 Mach

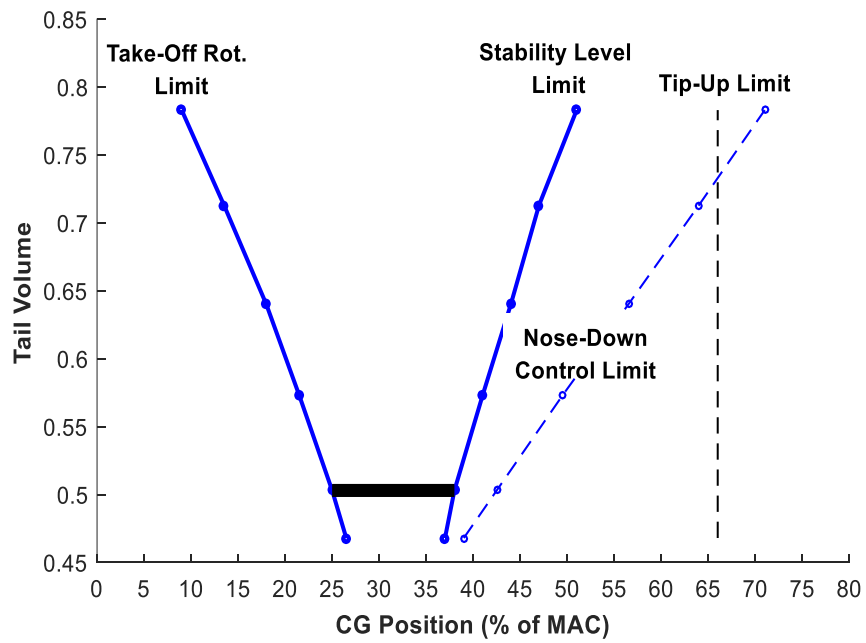


Figure 3.10: Tail Sizing Diagram of HT#2 for Artificial Stability at 0.2 Mach

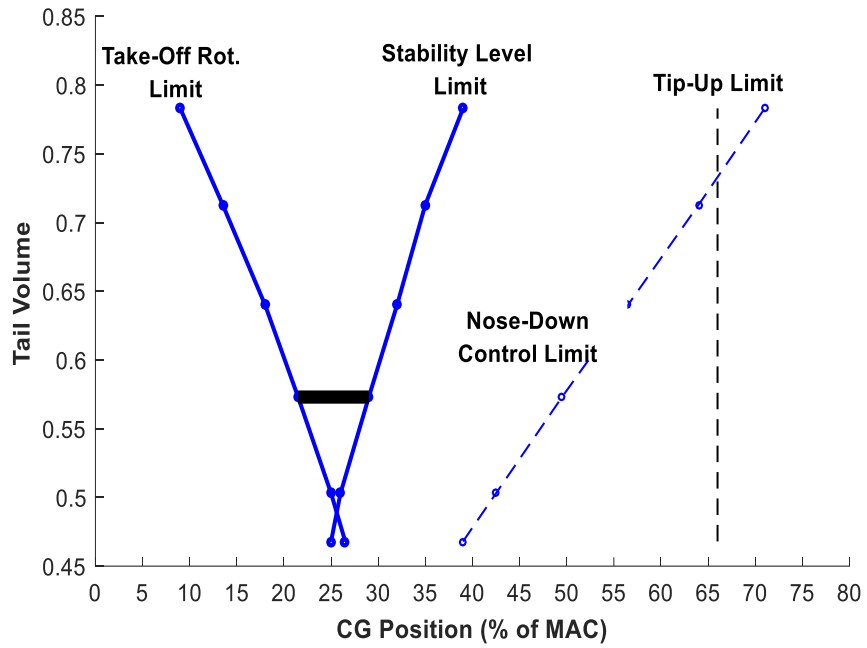


Figure 3.11: Tail Sizing Diagram of HT#3 for Natural Stability at 0.2 Mach

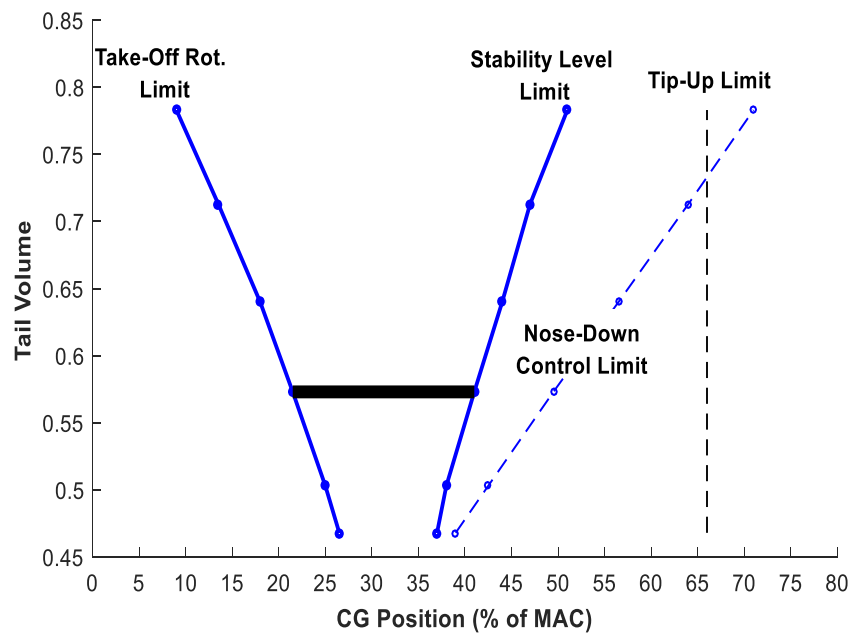


Figure 3.12: Tail Sizing Diagram of HT#3 for Artificial Stability at 0.2 Mach

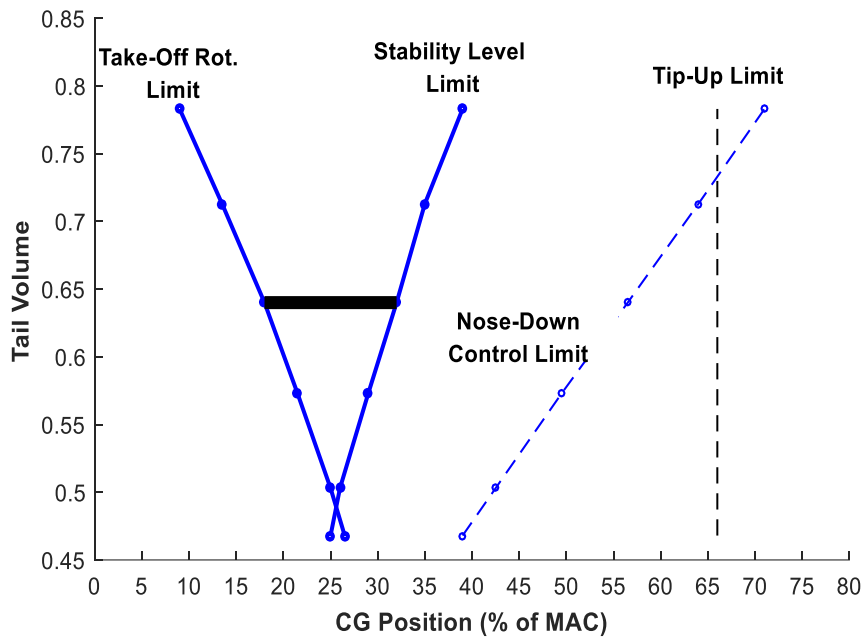


Figure 3.13: Tail Sizing Diagram of HT#4 for Natural Stability at 0.2 Mach

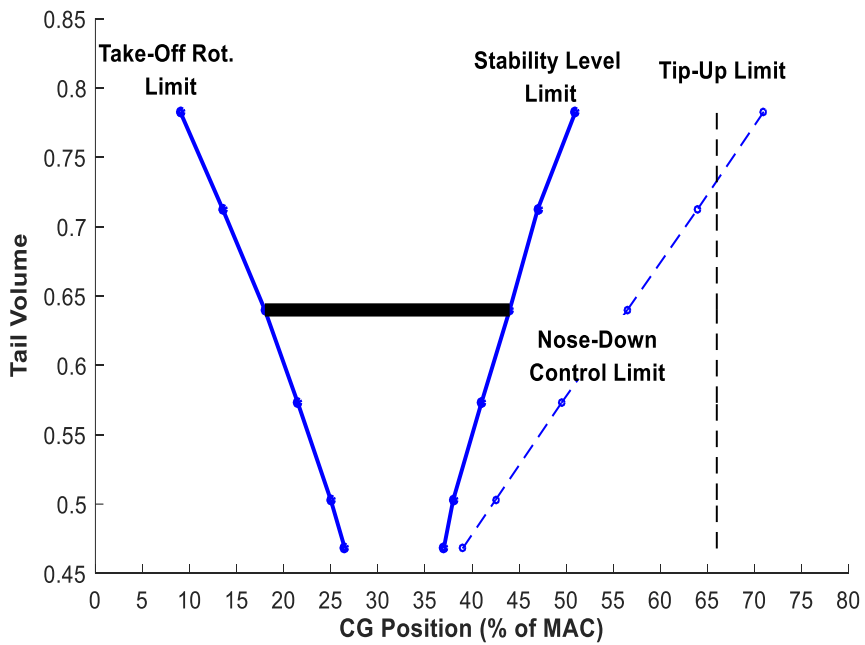


Figure 3.14: Tail Sizing Diagram of HT#4 for Artificial Stability at 0.2 Mach

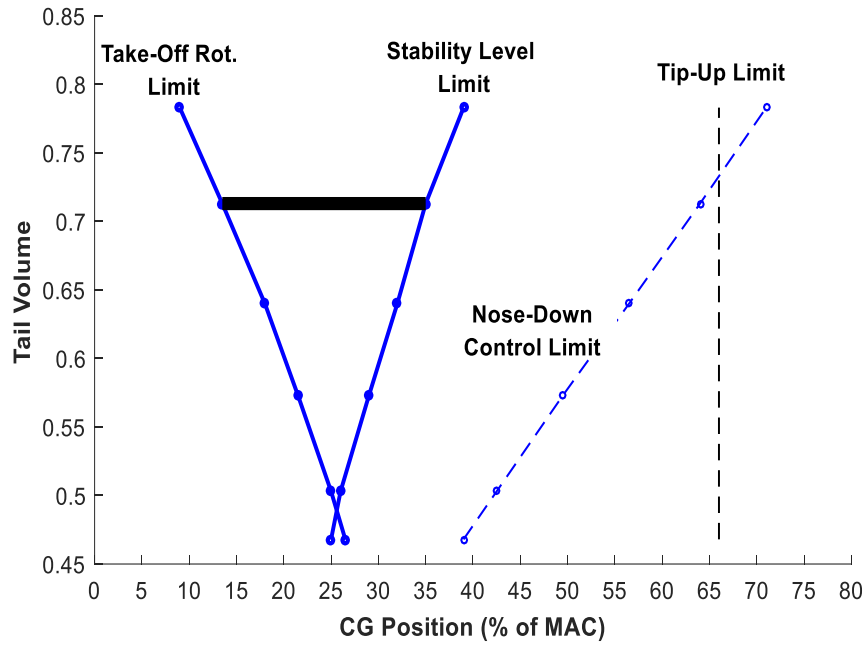


Figure 3.15: Tail Sizing Diagram of HT#5 for Natural Stability at 0.2 Mach

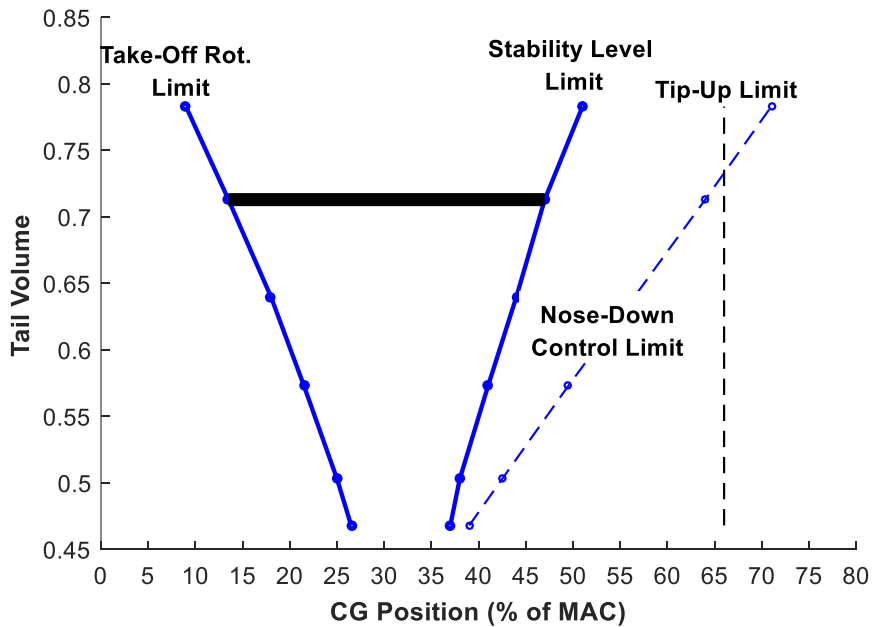


Figure 3.16: Tail Sizing Diagram of HT#5 for Artificial Stability at 0.2 Mach

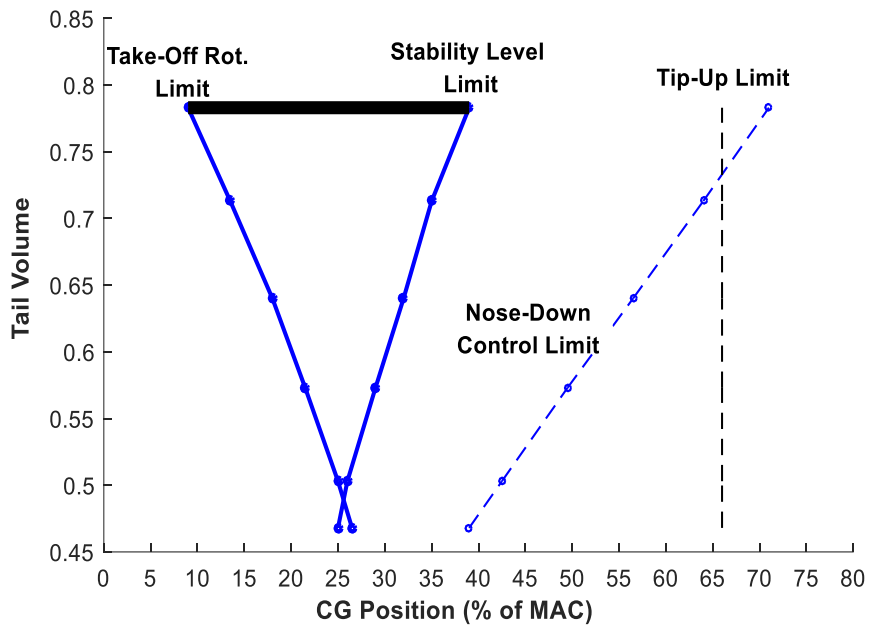


Figure 3.17: Tail Sizing Diagram of HT#6 for Natural Stability at 0.2 Mach

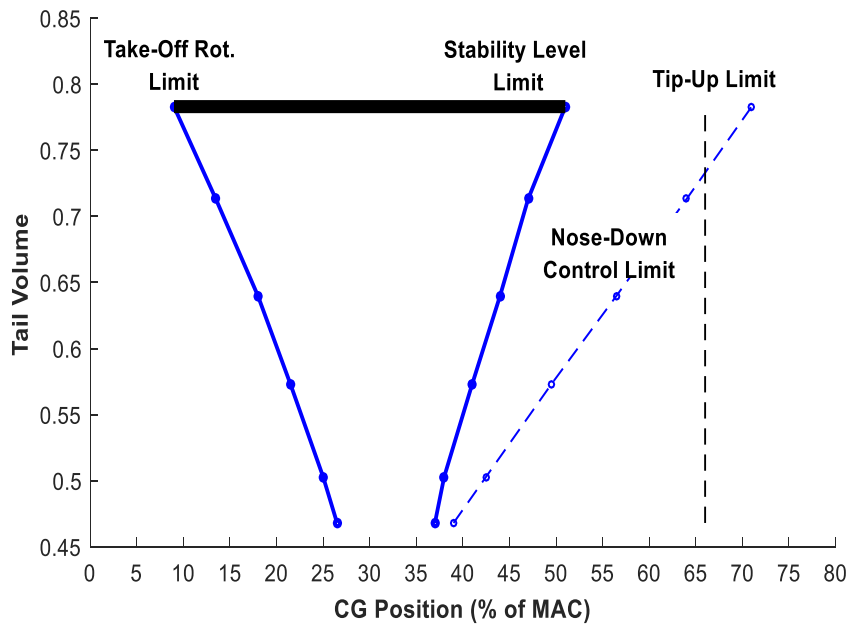


Figure 3.18: Tail Sizing Diagram of HT#6 for Artificial Stability at 0.2 Mach

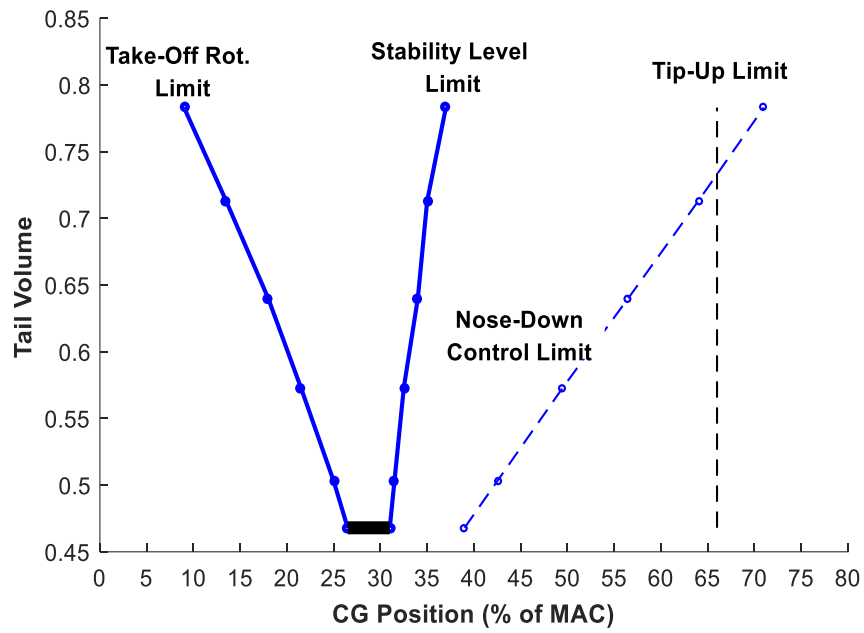


Figure 3.19: Tail Sizing Diagram of HT#1 for Natural Stability at 0.9 Mach

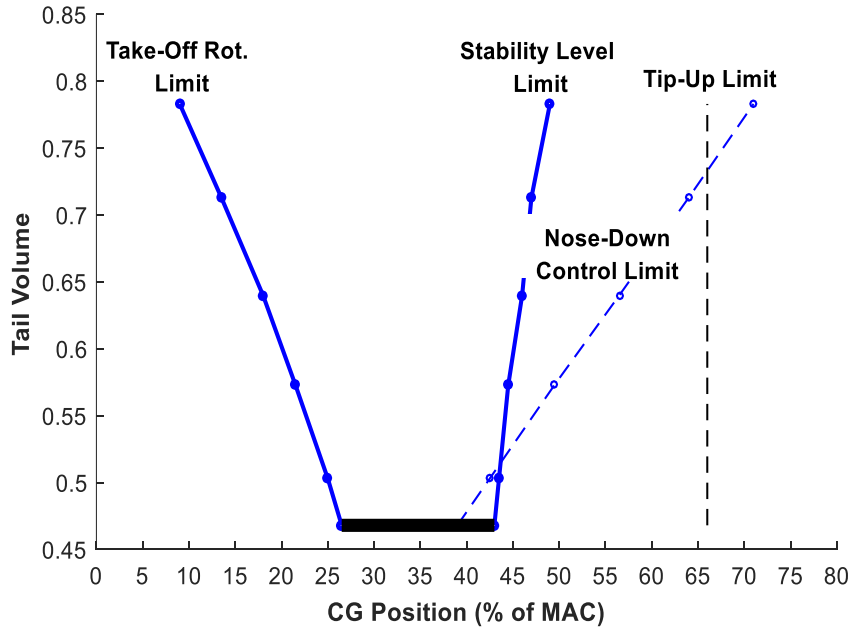


Figure 3.20: Tail Sizing Diagram of HT#1 for Artificial Stability at 0.9 Mach

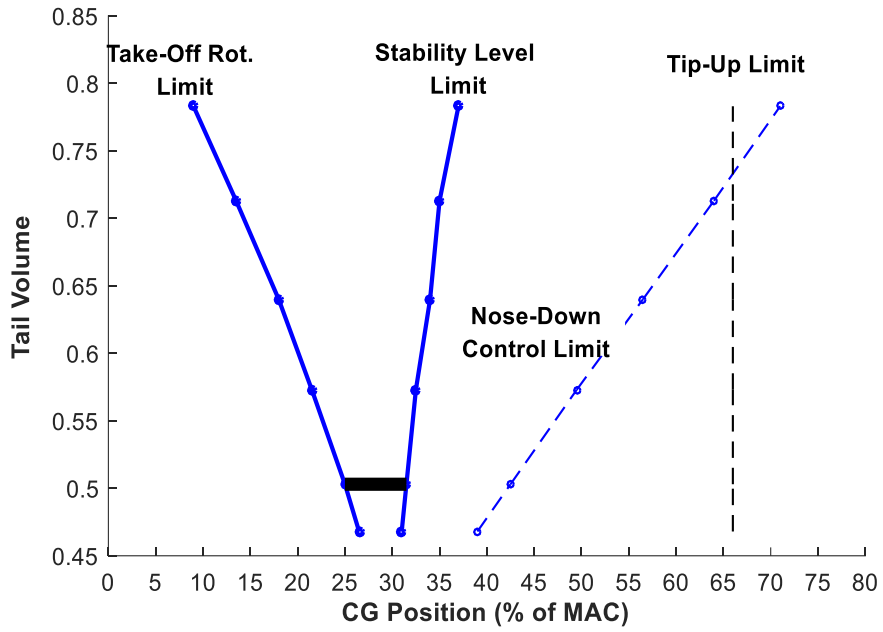


Figure 3.21: Tail Sizing Diagram of HT#2 for Natural Stability at 0.9 Mach

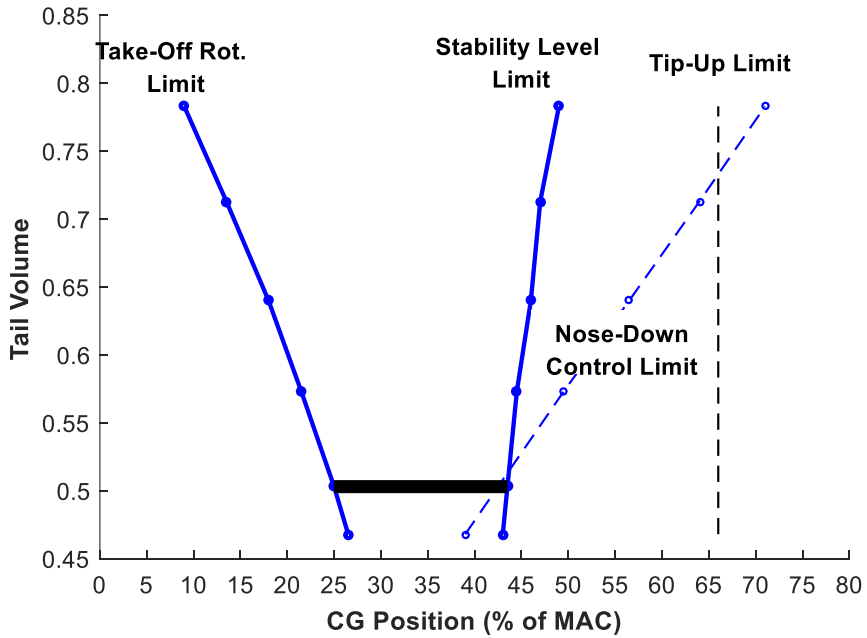


Figure 3.22: Tail Sizing Diagram of HT#2 for Artificial Stability at 0.9 Mach

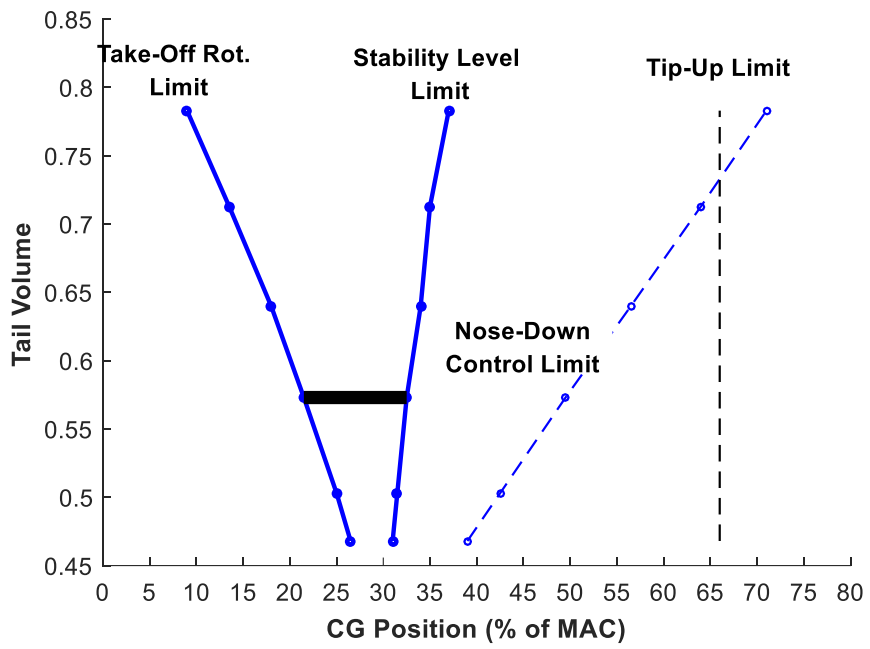


Figure 3.23: Tail Sizing Diagram of HT#3 for Natural Stability at 0.9 Mach

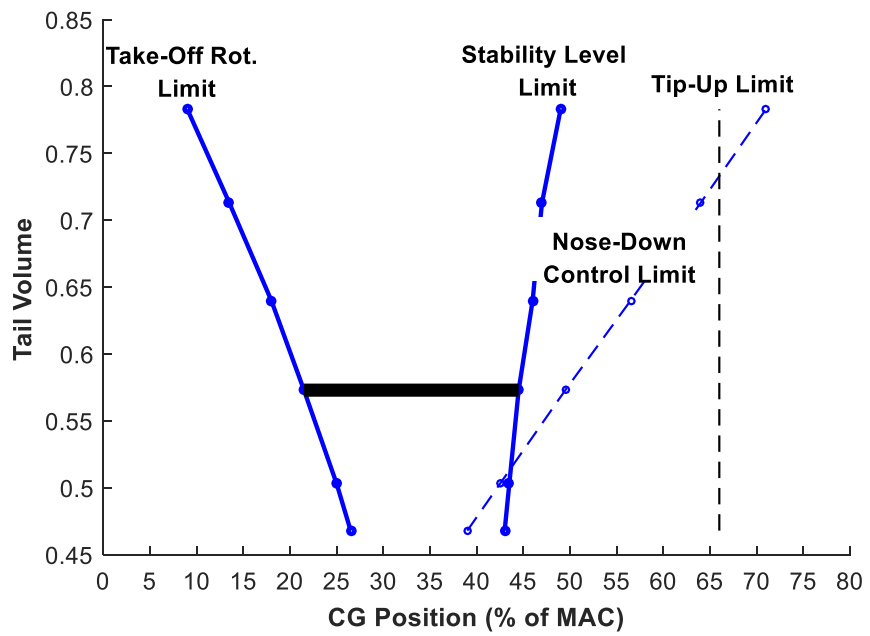


Figure 3.24: Tail Sizing Diagram of HT#3 for Artificial Stability at 0.9 Mach

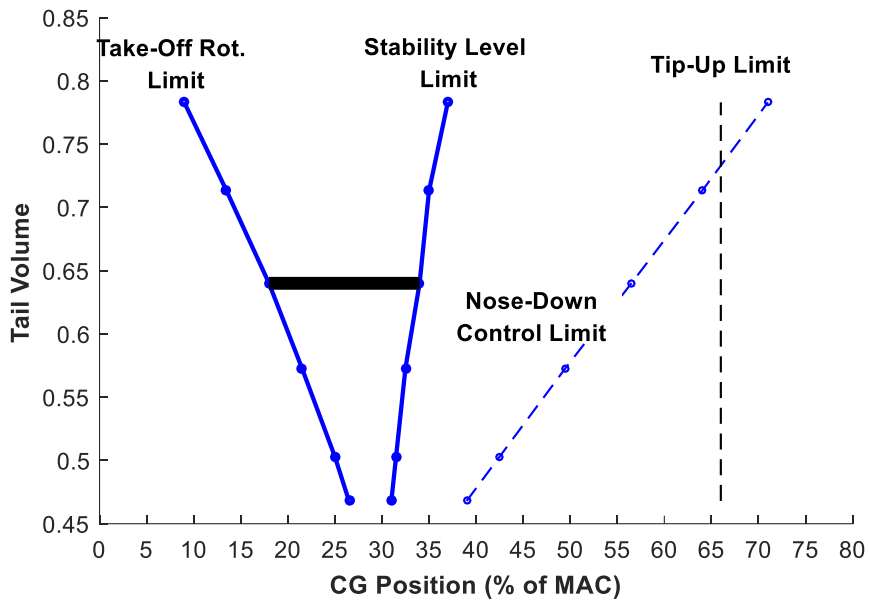


Figure 3.25: Tail Sizing Diagram of HT#4 for Natural Stability at 0.9 Mach

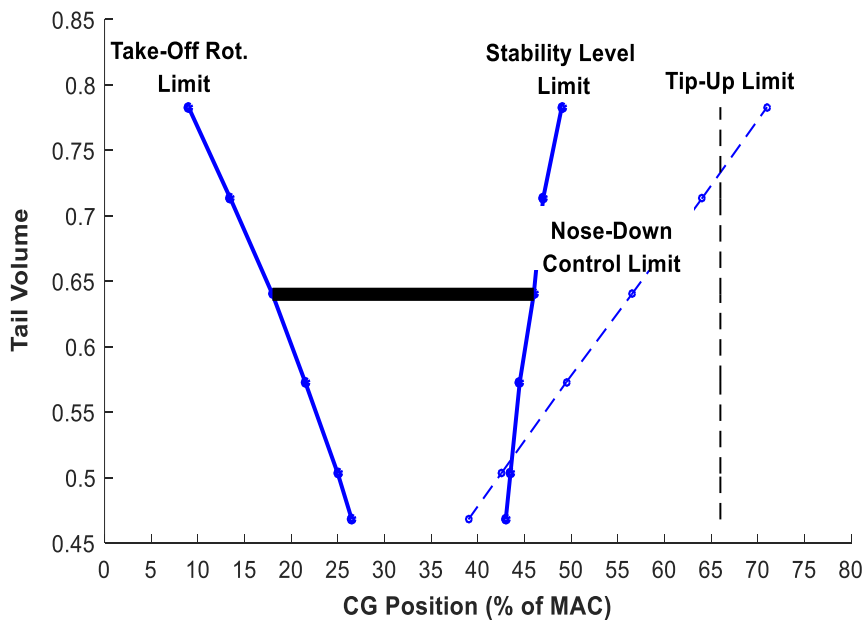


Figure 3.26: Tail Sizing Diagram of HT#4 for Artificial Stability at 0.9 Mach

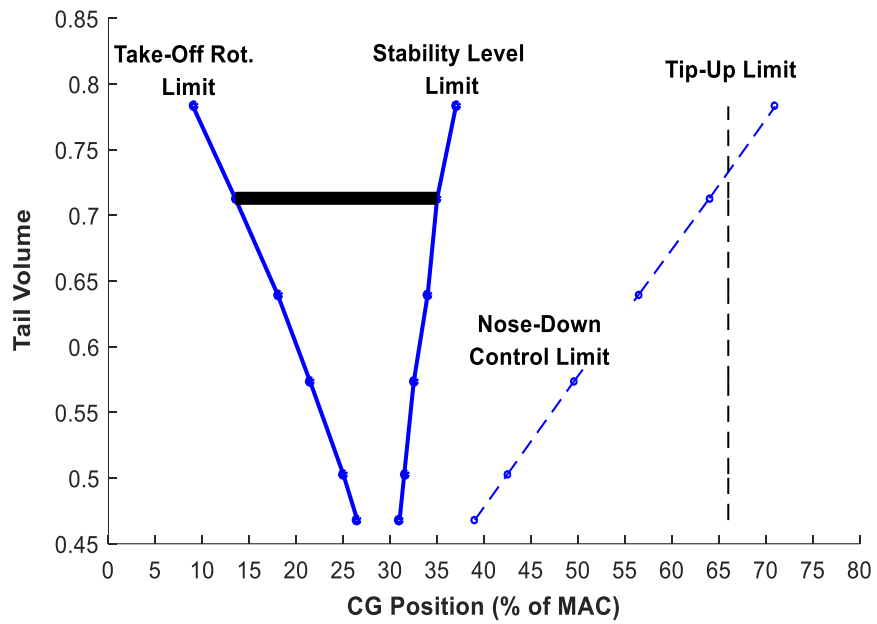


Figure 3.27: Tail Sizing Diagram of HT#5 for Natural Stability at 0.9 Mach

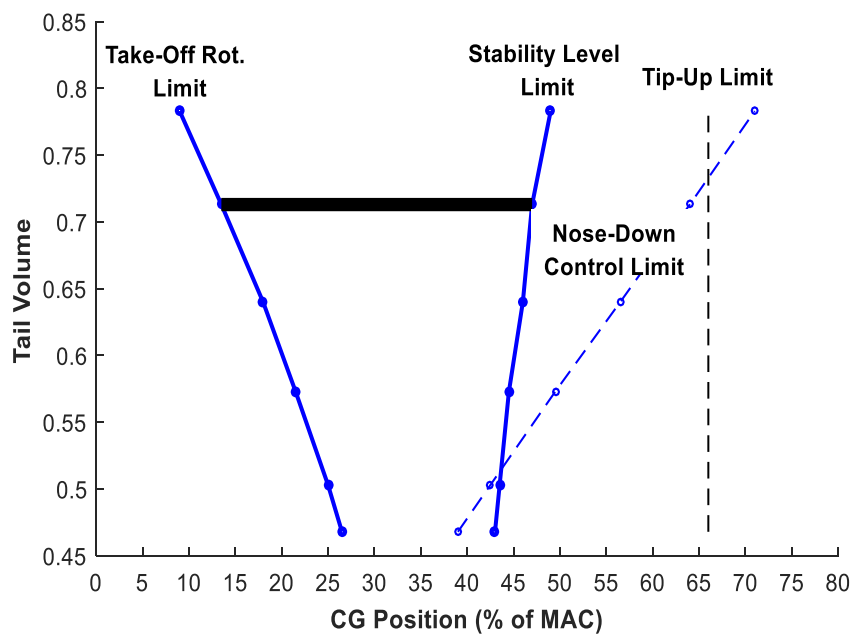


Figure 3.28: Tail Sizing Diagram of HT#5 for Artificial Stability at 0.9 Mach

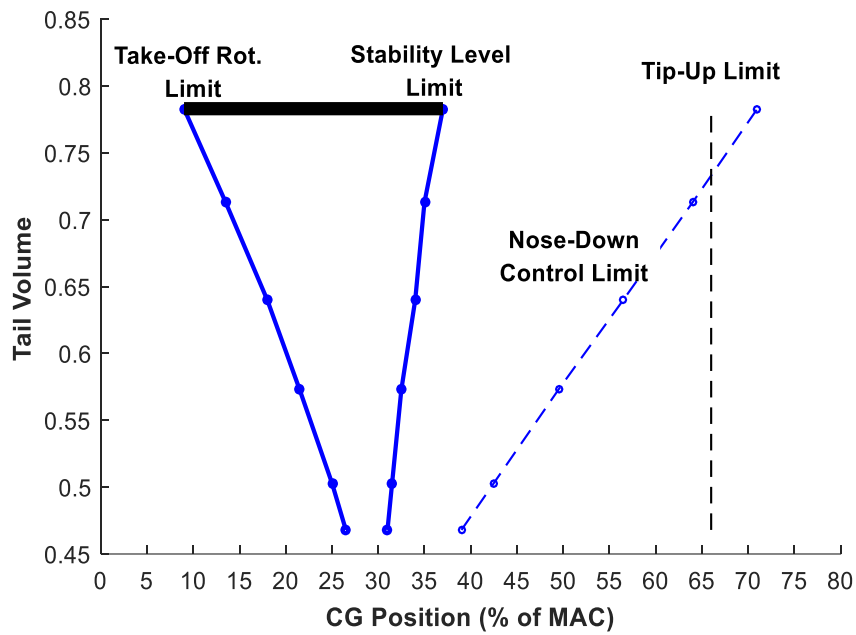


Figure 3.29: Tail Sizing Diagram of HT#6 for Natural Stability at 0.9 Mach

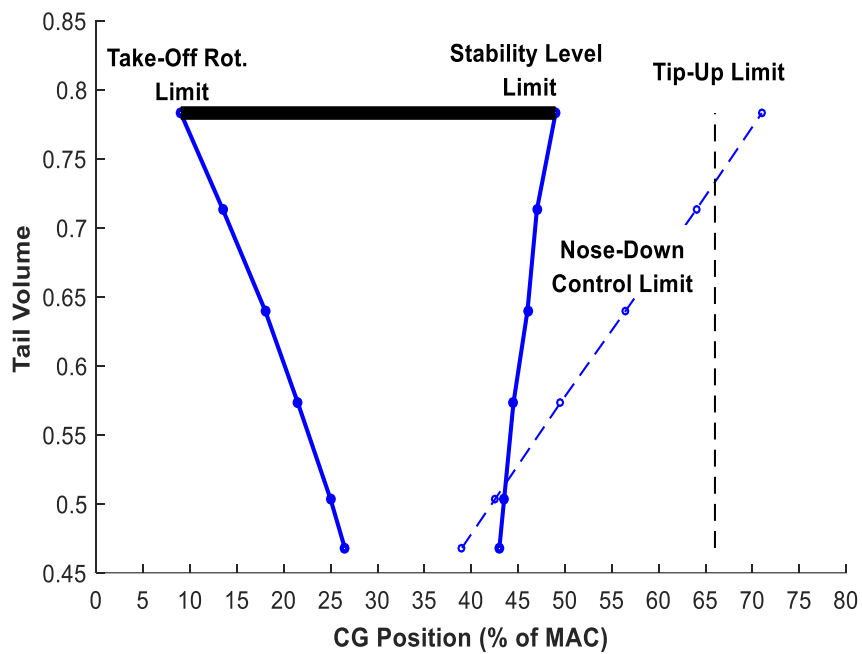


Figure 3.30: Tail Sizing Diagram of HT#6 for Artificial Stability at 0.9 Mach

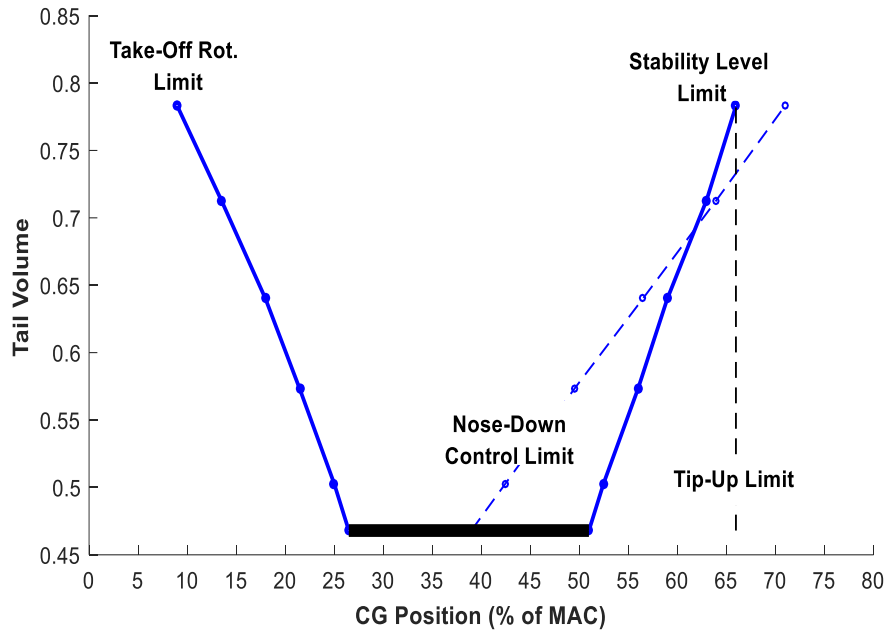


Figure 3.31: Tail Sizing Diagram of HT#1 for Natural Stability at 1.2 Mach

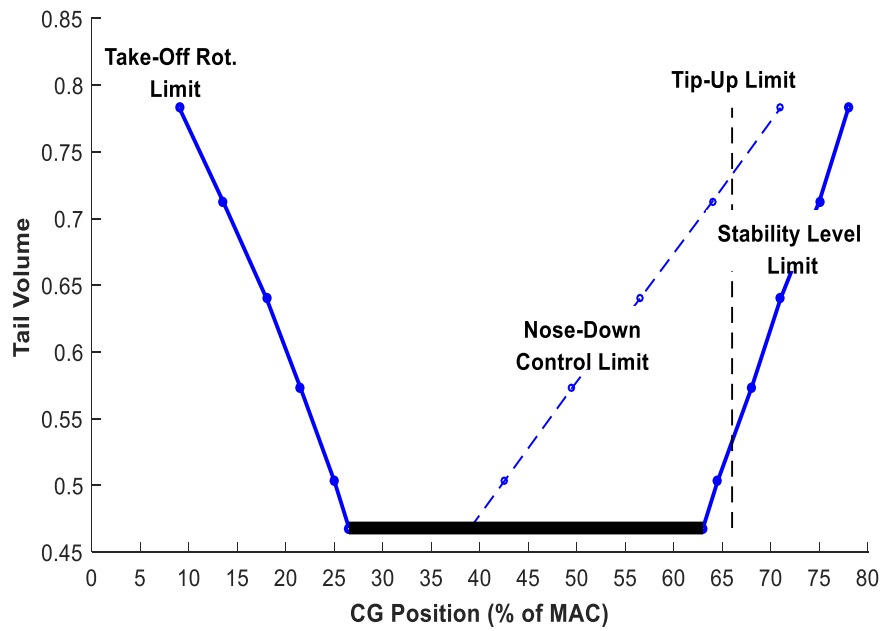


Figure 3.32: Tail Sizing Diagram of HT#1 for Artificial Stability at 1.2 Mach

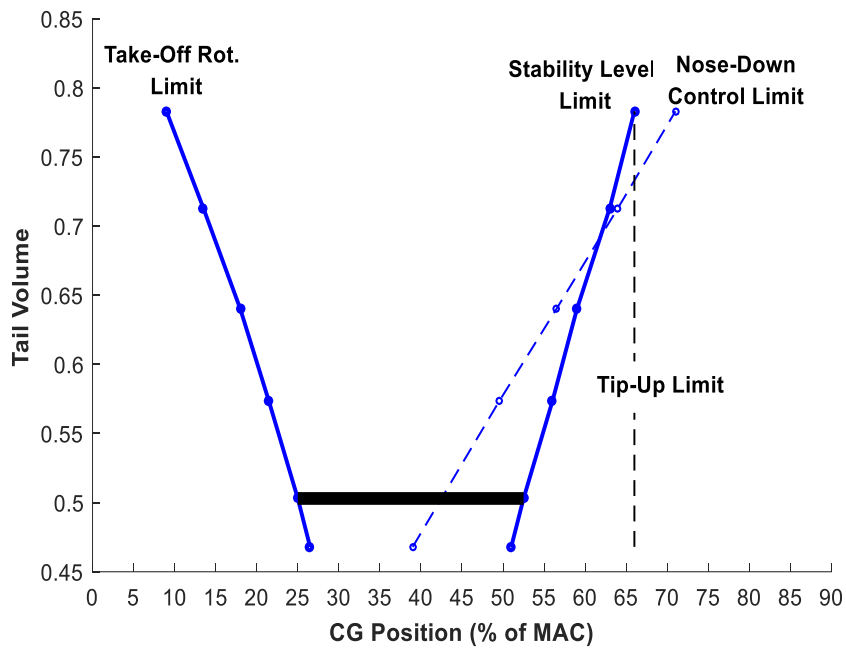


Figure 3.33: Tail Sizing Diagram of HT#2 for Natural Stability at 1.2 Mach

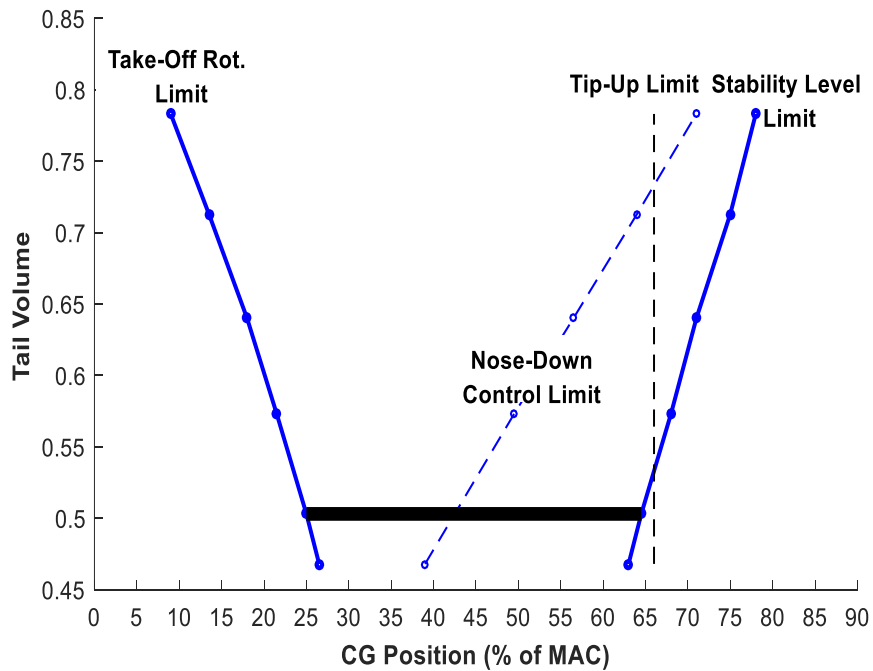


Figure 3.34: Tail Sizing Diagram of HT#2 for Artificial Stability at 1.2 Mach

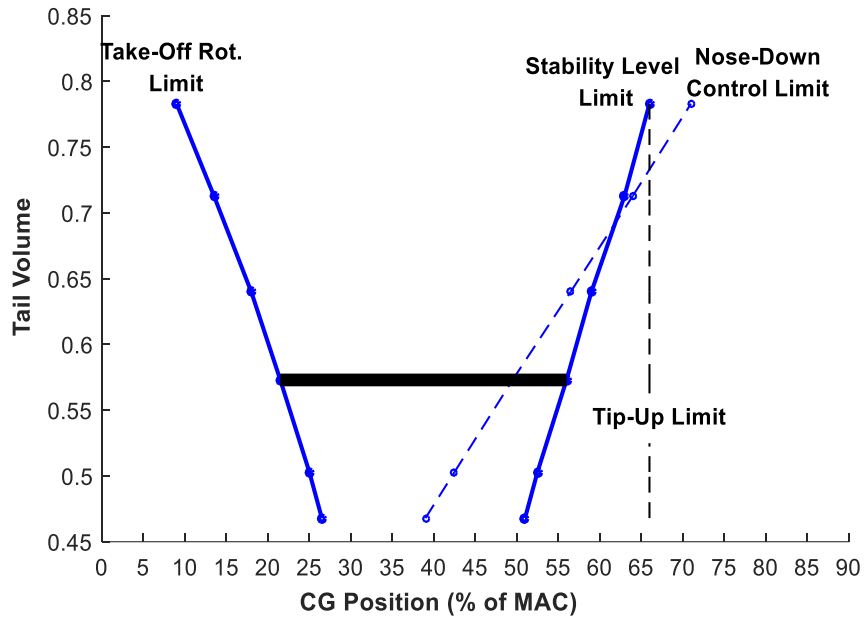


Figure 3.35: Tail Sizing Diagram of HT#3 for Natural Stability at 1.2 Mach

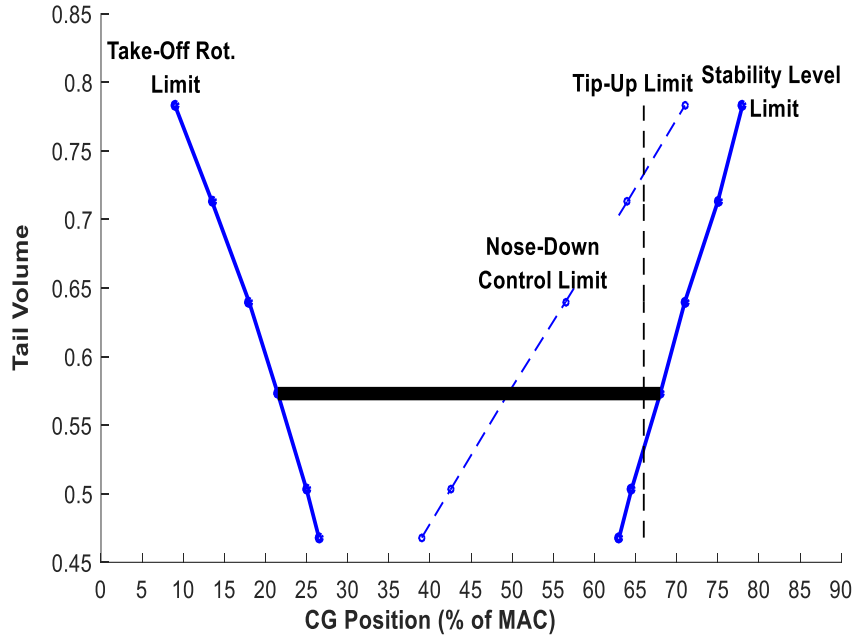


Figure 3.36: Tail Sizing Diagram of HT#3 for Artificial Stability at 1.2 Mach

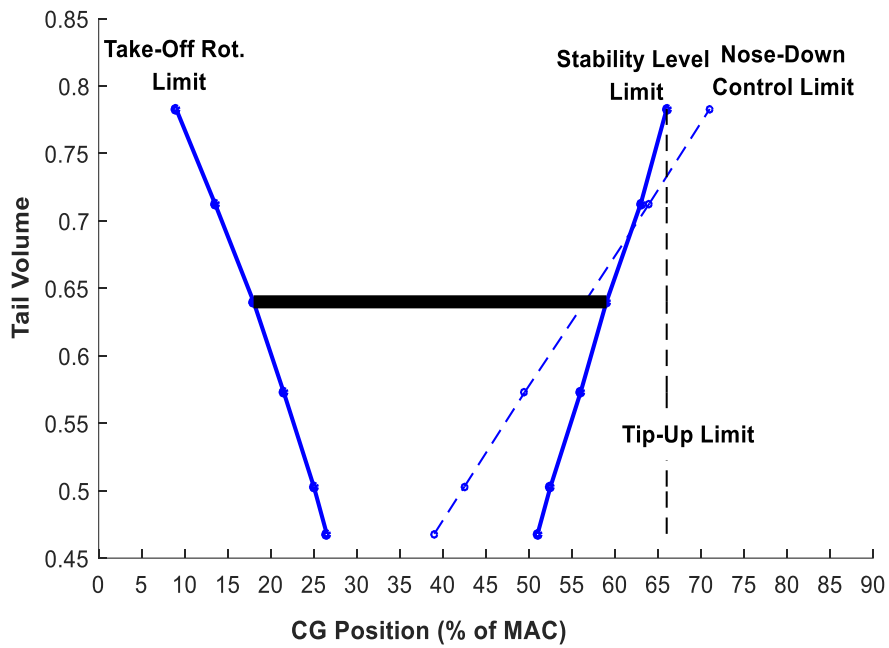


Figure 3.37: Tail Sizing Diagram of HT#4 for Natural Stability at 1.2 Mach

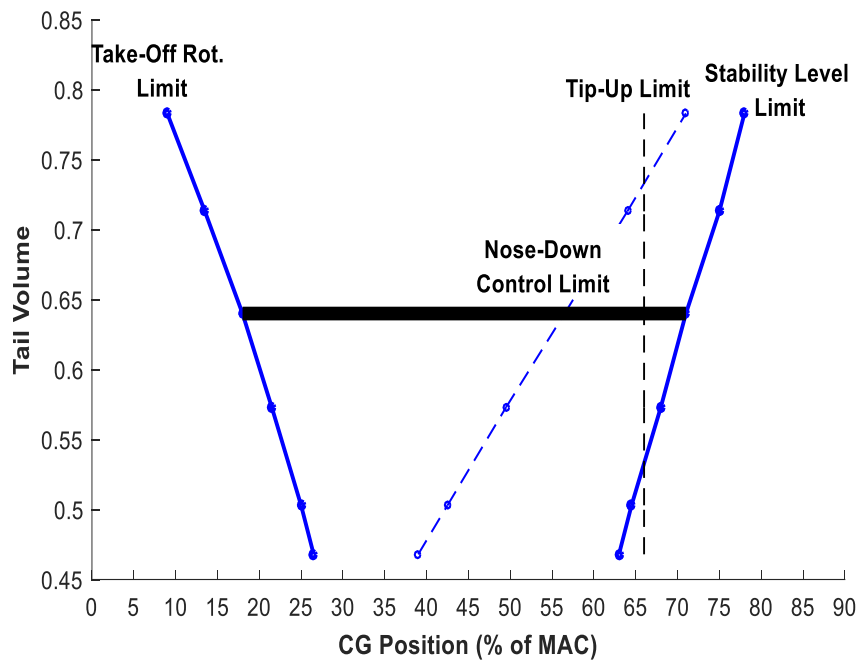


Figure 3.38: Tail Sizing Diagram of HT#4 for Artificial Stability at 1.2 Mach

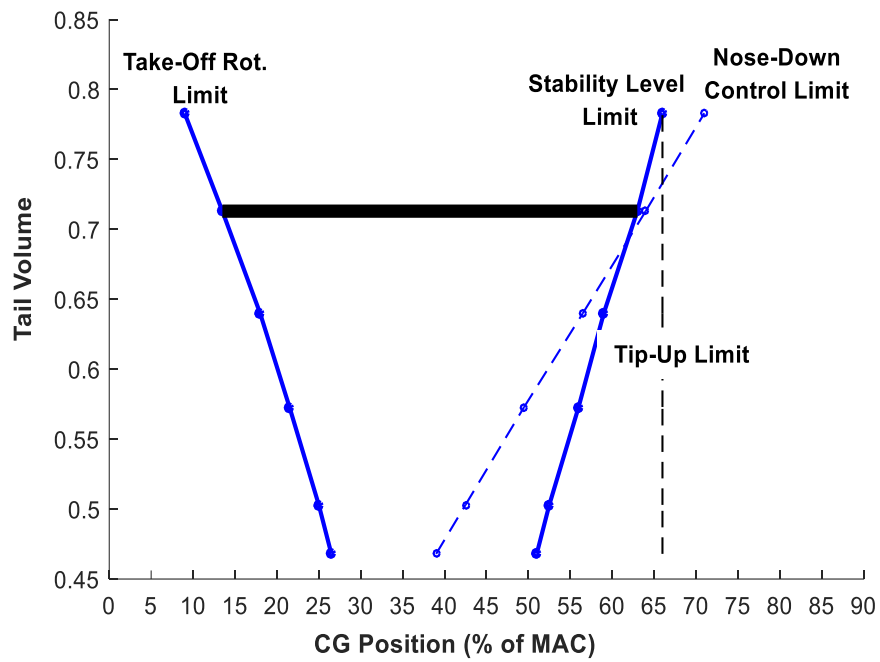


Figure 3.39: Tail Sizing Diagram of HT#5 for Natural Stability at 1.2 Mach

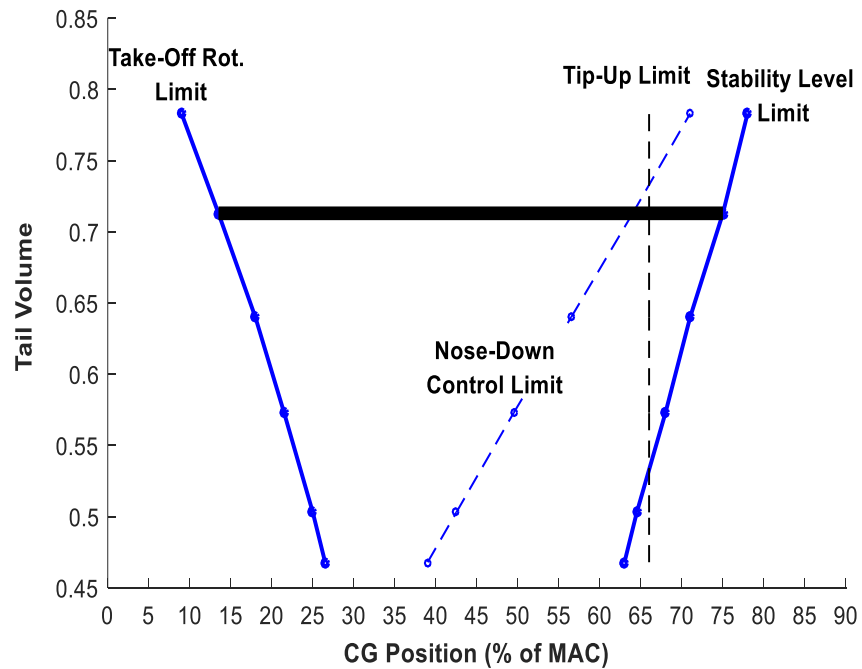


Figure 3.40: Tail Sizing Diagram of HT#5 for Artificial Stability at 1.2 Mach

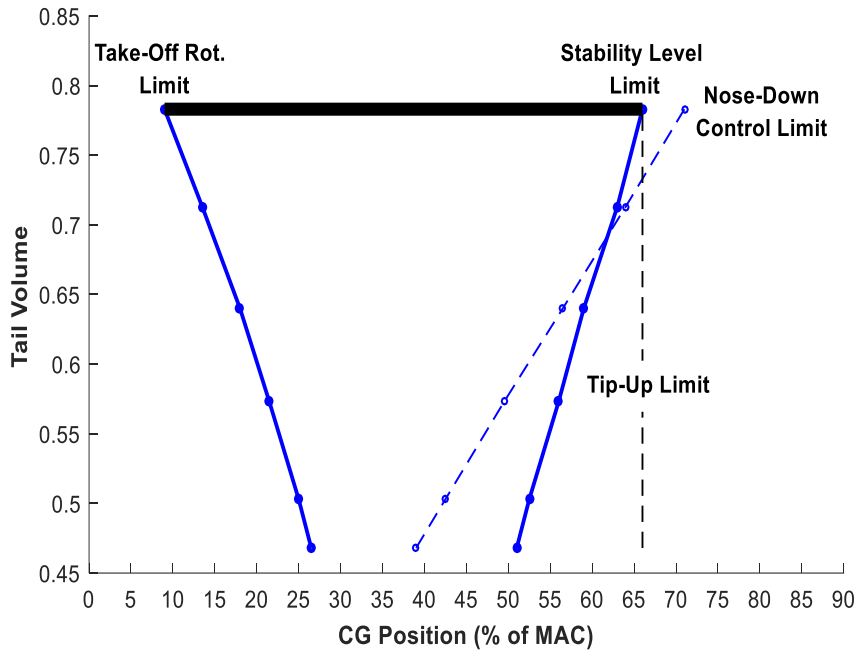


Figure 3.41: Tail Sizing Diagram of HT#6 for Natural Stability at 1.2 Mach

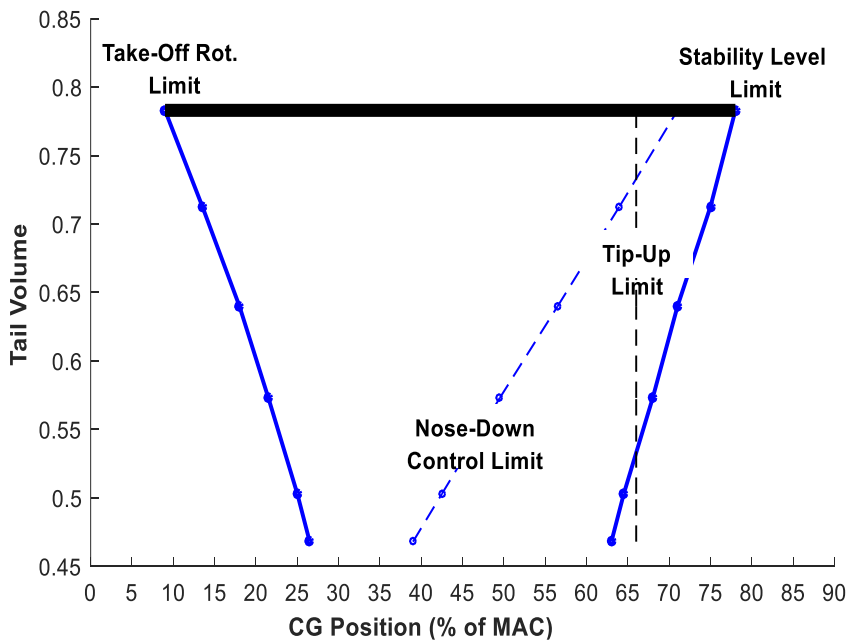


Figure 3.42: Tail Sizing Diagram of HT#6 for Artificial Stability at 1.2 Mach

The tail sizing diagrams obtained from Datcom results are presented below.

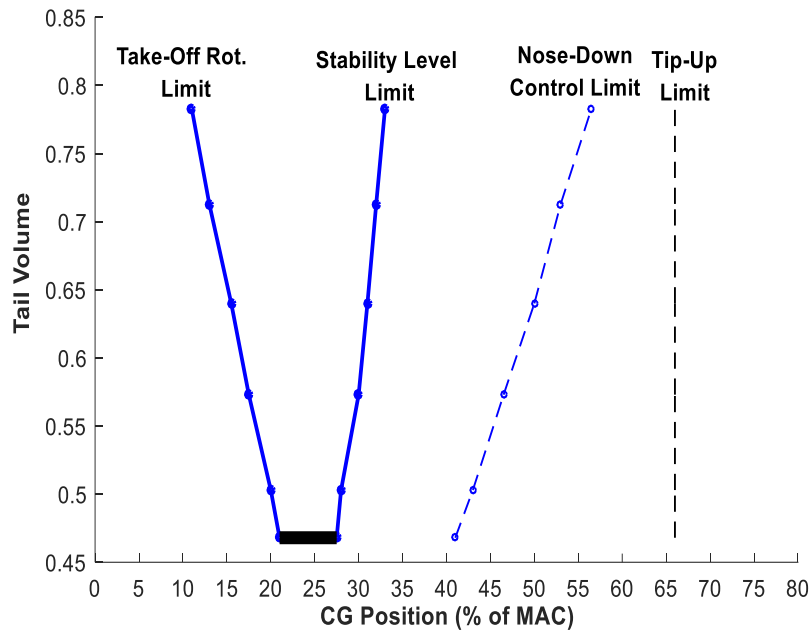


Figure 3.43: Tail Sizing Diagram of HT#1 for Natural Stability at 0.2 Mach

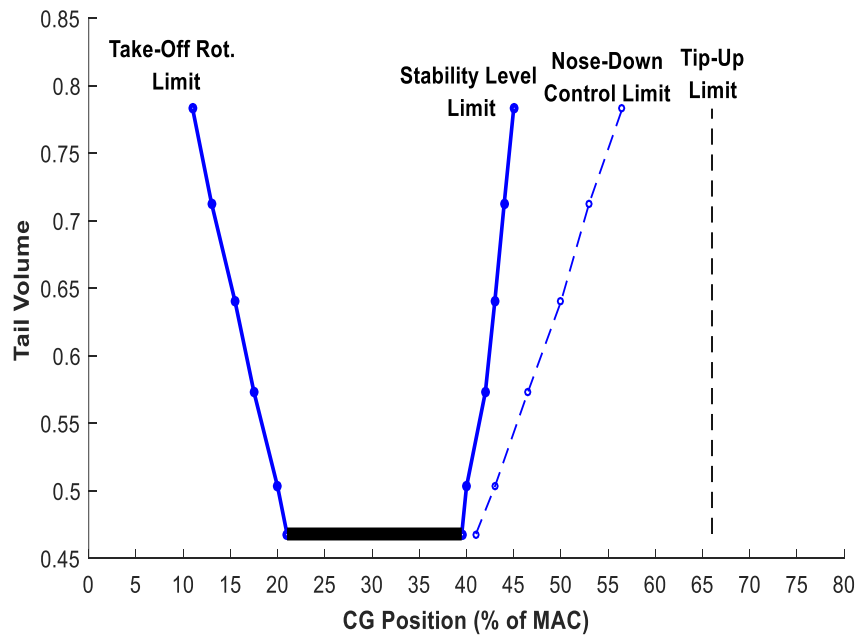


Figure 3.44: Tail Sizing Diagram of HT#1 for Artificial Stability at 0.2 Mach

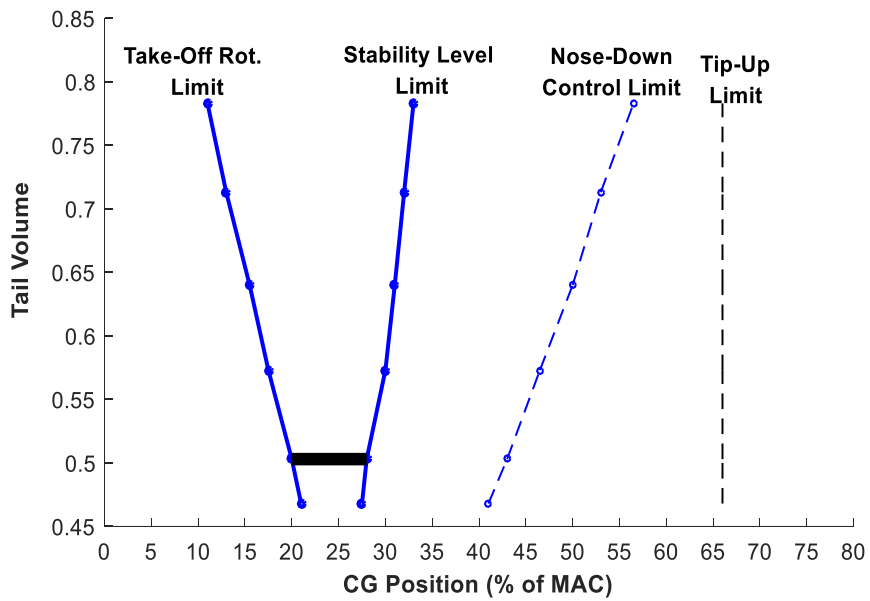


Figure 3.45: Tail Sizing Diagram of HT#2 for Natural Stability at 0.2 Mach

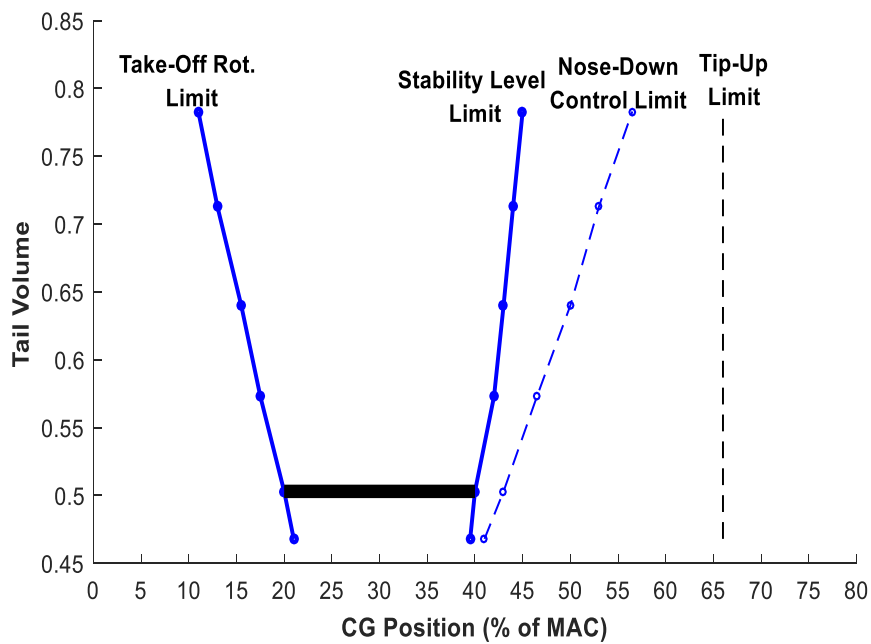


Figure 3.46: Tail Sizing Diagram of HT#2 for Artificial Stability at 0.2 Mach

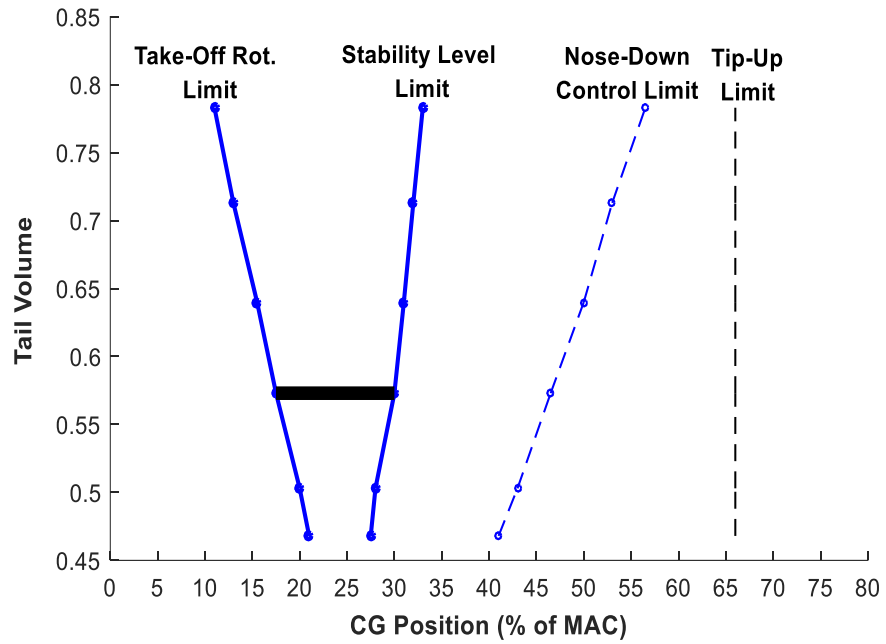


Figure 3.47: Tail Sizing Diagram of HT#3 for Natural Stability at 0.2 Mach

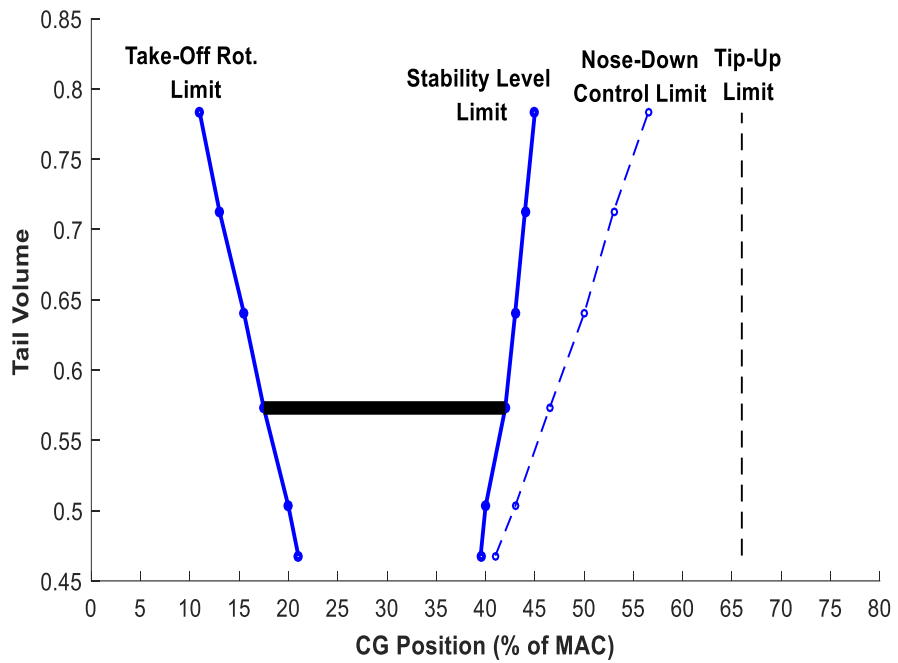


Figure 3.48: Tail Sizing Diagram of HT#3 for Artificial Stability at 0.2 Mach

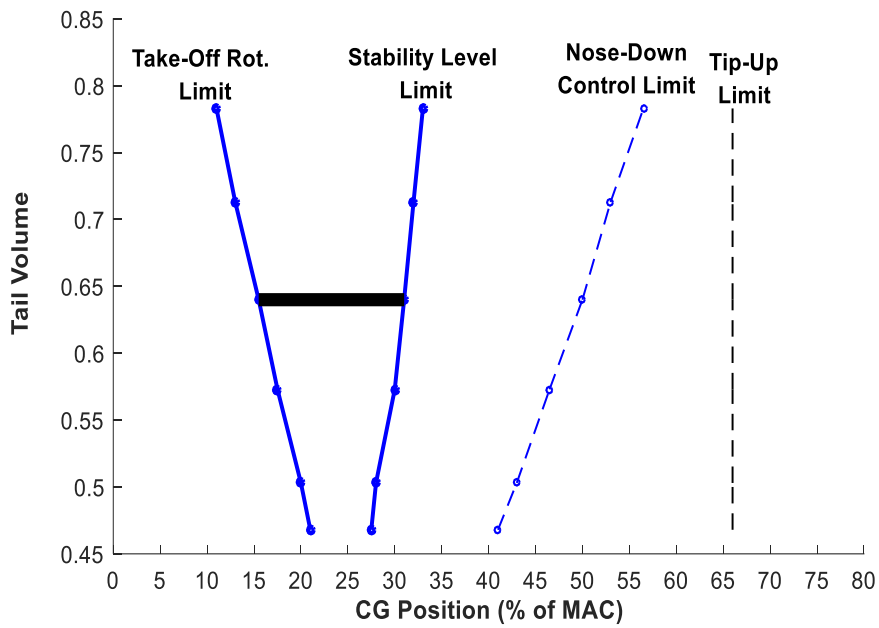


Figure 3.49: Tail Sizing Diagram of HT#4 for Natural Stability at 0.2 Mach

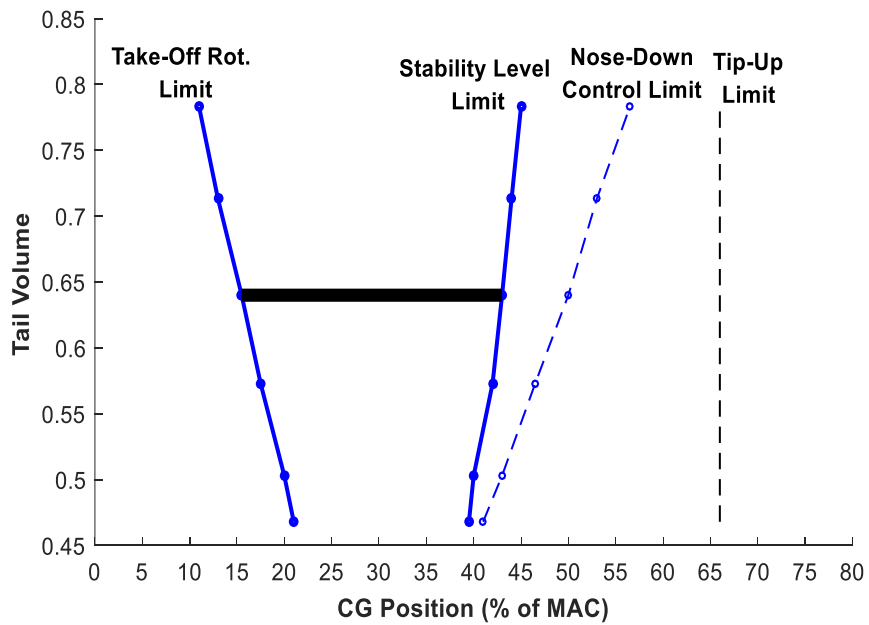


Figure 3.50: Tail Sizing Diagram of HT#4 for Artificial Stability at 0.2 Mach

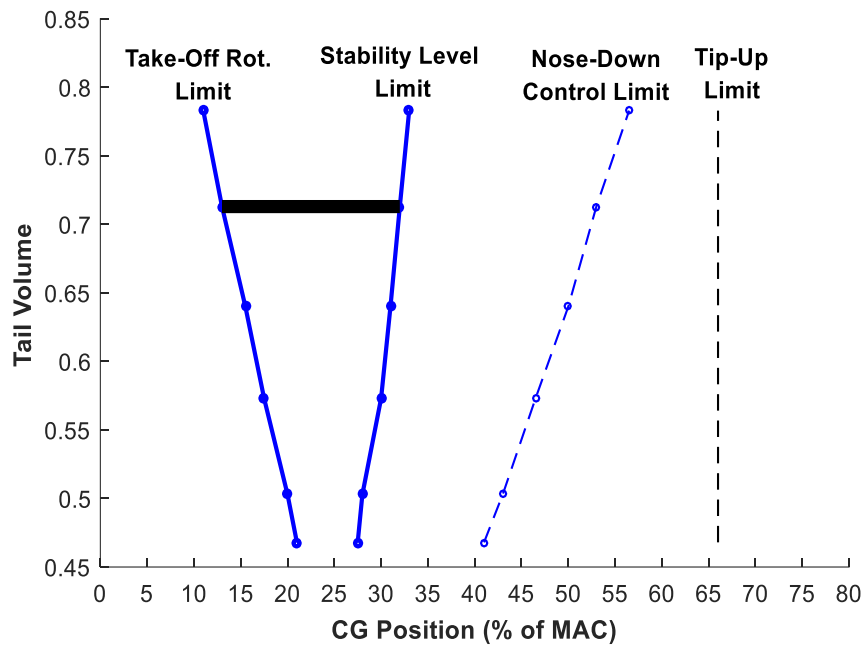


Figure 3.51: Tail Sizing Diagram of HT#5 for Natural Stability at 0.2 Mach

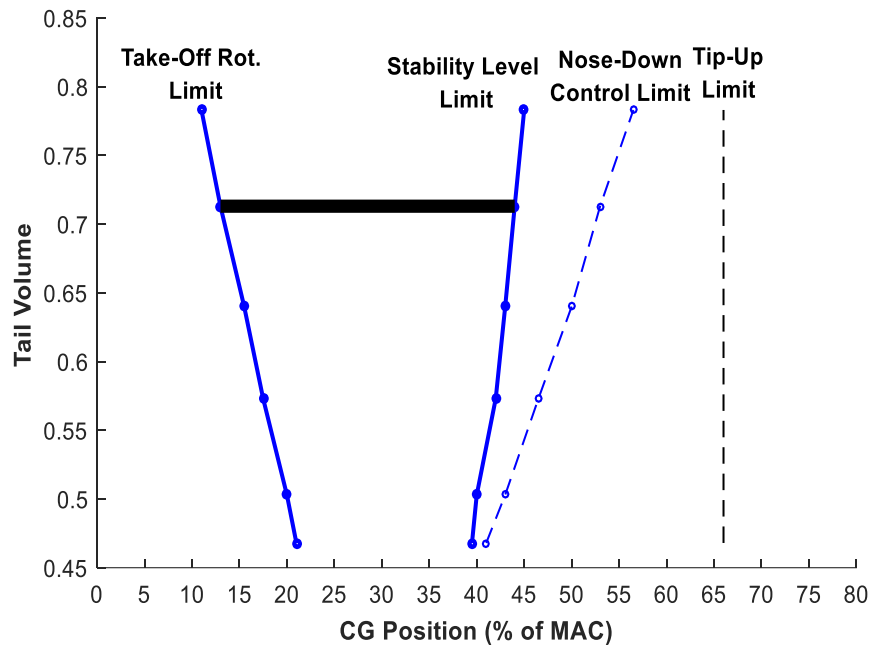


Figure 3.52: Tail Sizing Diagram of HT#5 for Artificial Stability at 0.2 Mach

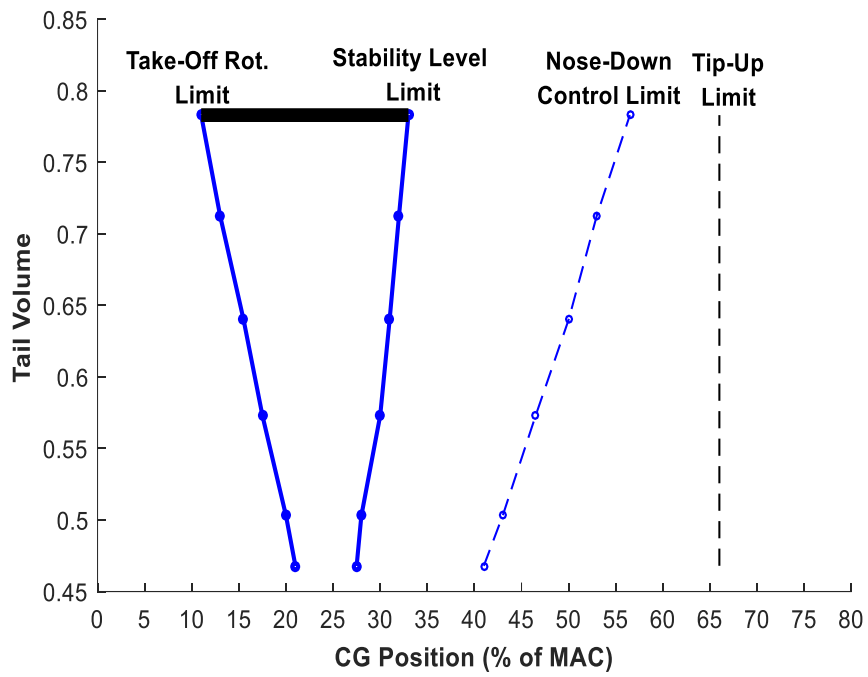


Figure 3.53: Tail Sizing Diagram of HT#6 for Natural Stability at 0.2 Mach

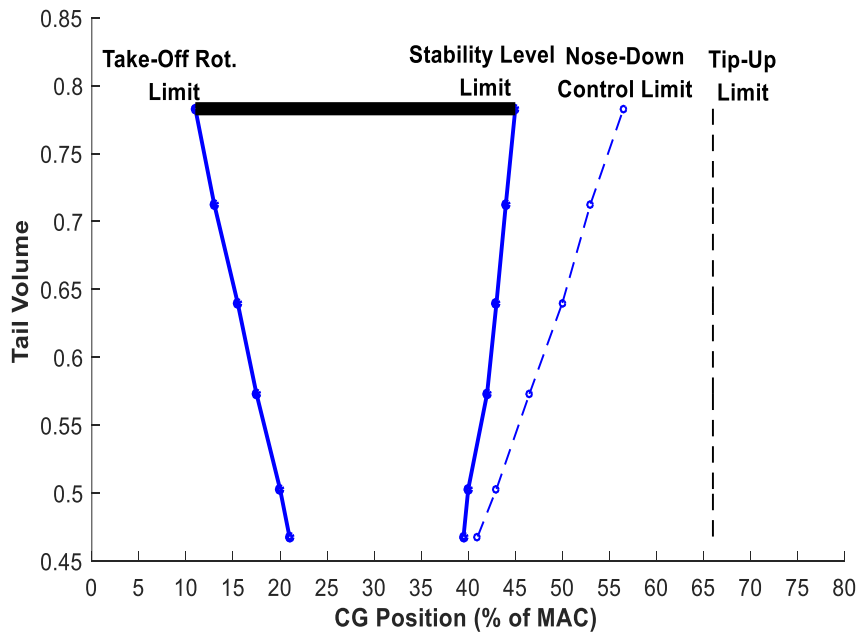


Figure 3.54: Tail Sizing Diagram of HT#6 for Artificial Stability at 0.2 Mach

As seen from tail sizing diagrams, the FWD CG limit is determined from the most FWD CG position required to lift the nose up during the take-off rotation. The limit of FWD CG moves towards front as the tail volume increases.

The aft CG limit is determined from the minimum required level of static stability, nose-down recovery capability at high AoAs or tipback angle requirement. In this study, the limit of aft CG is determined by longitudinal static stability. As tail volume is increased, the limit of aft CG moves rearward. In addition, the aft CG limit goes backward with increase in airspeed from subsonic to supersonic. Therefore, the aft CG limit was determined at 0.2 Mach condition.

As seen from scissor-plots, the limit of aft CG goes significantly rearward with the relaxation of longitudinal static stability. The concept of relaxed static stability increases the allowable operational CG range.

As specified in Table 1.1, the operational CG range of the aircraft is between 35 % and 39% of MAC. The size of the horizontal tail must be determined according to these CG limits. Therefore, the following comments can be done.

For the results based on CFD analyses:

- The limit of FWD CG position can be met with six horizontal tail planforms.
- The limit of aft CG position for natural stability condition cannot be satisfied with any analyzed horizontal tail for 0.9 Mach airspeed. By applying data extrapolation method to the tail sizing diagram of 0.9 Mach (Figure 3.29), the minimum required area of horizontal tail was calculated as approximately 13

m² to be able to provide sufficient level of longitudinal stability up to aft CG limit.

- The aft CG limit for artificial stability condition can be satisfied with HT # 3, HT # 4, HT # 5 and HT # 6. Besides, by utilizing from interpolation method to the tail sizing diagram of 0.2 Mach (Figure 3.10), minimum required horizontal tail area was computed as 8.2 m² which is between the areas of HT # 2 and HT # 3.

For the results based on Datcom analyses:

- The limit of FWD CG position can be satisfied with six horizontal tail planforms.
- The limit of aft CG position cannot be fulfilled with any horizontal tail planform for natural stability condition. By applying data extrapolation method to the tail sizing diagram of 0.2 Mach (Figure 3.53), the minimum required area of horizontal tail was computed as approximately 17.6 m².
- The aft CG limit for relaxed stability condition can be met with six horizontal tail planforms. Minimum required horizontal tail area must be approximately 7.3 m² (HT # 1).

CHAPTER 4

METHODOLOGY

4.1. Computational Fluid Dynamics Method

CFD is a widely used tool in aviation in order to perform analyses during preliminary design phase. Many complex aircraft configurations can be analyzed by utilizing from CFD. CFD has a sufficient capability to perform analyses rapidly and cheaply with a little number of simulations necessary for design [14]. Therefore, the analyses of this study were carried out with use of CFD,

ANSYS Fluent 17.1 was used during CFD analyses as a solver. Fluent uses Reynolds Averaged Navier-Stokes (RANS) method [15].

Fluent supplies different turbulence models such as Spalart-Allmaras, k-epsilon, k-omega, Reynolds stress model. The turbulence model is selected by considering some requirements such as the time available for the simulation, the required level of accuracy, etc. Spalart-Allmaras was chosen as turbulence model during analyses. It is used for modeling viscous flow. The Spalart-Allmaras model is a simple one-equation model. The Spalart-Allmaras model was developed specifically for aerospace applications. Therefore, this model is commonly used in aerospace.

Grid-independence are essential during CFD analyses. Grid-independence means that grid used on the analyses does not have effect the on the results. This provides accuracy on the solutions obtained from analyses. In addition, to prevent time-consuming, unnecessary efforts during the analyses, sufficient number of grid should

be used. Therefore, by considering these two aspects, 6 millions grid elements were used during CFD analyses.

Besides, the order of a scheme is defined in terms of order of error in the Taylor series expansion. This determines the rate of reduction in error with refinement in the grid. 500 numbers of first-order schemes and 3000 numbers of second-order scheme are used to during the analyses.

CFD is valid in principle in all flow regimes [16]. Thus, CFD analyses are performed in subsonic, transonic and supersonic regimes.

The results of CFD analyses are compared with the wind tunnel test results. Figure 4.1 shows the variations of CL with AoA obtained from CFD analyses and wind tunnel tests at subsonic airspeeds. The results of CFD analyses and wind tunnel tests almost coincide with each other up to 20° AOA. However, beyond 20° AOA, difference between two results begins which is an expected situation. At high angles of attack, the nonlinearity is very high and the aerodynamic behavior of aircraft is quite unpredictable.

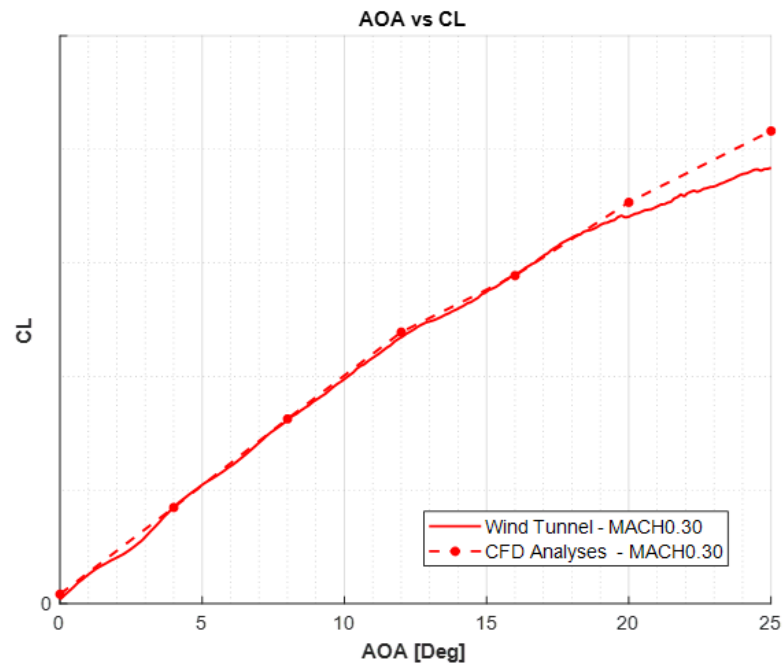


Figure 4.1. The variation of C_L with AoA at 0.3 Mach for results of wind tunnel test and CFD analyses

4.2. DATCOM Method

DATCOM is a rapid design tool to predict aerodynamic stability and control characteristics in preliminary design phase. DATCOM provides a considerable rigorous estimation, especially, at subsonic flight regime [7]. Therefore, DATCOM is used to estimate stability and control derivatives for the subsonic regime during the study.

DATCOM provides different modeling techniques for a configuration such as Body Modeling, Wing-Tail Modeling, Wing-Body-Tail Modeling, etc. A conventional aircraft configuration can be modeled by utilizing from wing, body, vertical tail and horizontal tail technique. Thus, in this study, wing-body-tail modeling technique is used during DATCOM analysis.

In general, DATCOM treats the traditional body-wing-tail geometries including control effectiveness for a variety of high-lift /control devices. High-lift/control output is generally in terms of the incremental effects due to deflection.

Experimental data can be embedded on the DATCOM program which enables more accurate results of the analyses. Wing-body experimental data is used during DATCOM analyses.

Contribution of control devices on aerodynamic coefficients can be obtained from DATCOM analyses. Therefore, analyses of take-off rotation and nose-down recovery were performed for the condition of horizontal tail deflection.

In addition, the deflection of trailing-edge flap can also be treated by DATCOM program. The incremental effects of trailing-edge-flap at zero angle of attack which is the required condition during take-off rotation can be attained during the analyses. The take-off rotation analyses are performed by including the effects of trailing edge flap.

The ground effect on longitudinal stability can be also obtained from DATCOM analysis. The analyses of take-off rotation are performed by including ground effect.

CHAPTER 5

CONCLUSION AND FUTURE WORK

5.1. Conclusion

In this study, the size of horizontal tail for a conventional trainer is determined by considering some requirements, which define the limits of FWD and aft CG position. The tail sizing diagrams are created for each horizontal tail planforms. The minimum size of horizontal tail is determined which satisfies the defined requirements over the operational flight CG range.

The limit of FWD CG is determined from control authority during the take-off rotation. The horizontal tail must have necessary control capability at most FWD CG position. The most FWD CG position is calculated from Eq. 2.50 by utilizing from some major aircraft specifications listed in Table 1.1. The studies on take-off rotation are done with both results obtained from DATCOM and CFD analyses. DATCOM analyses are done with and without ground effect. There is no difference observed between the results. Therefore, take-off rotation calculations are done without ground effect. The results of take-off rotation analyses indicate that the limit of FWD CG moves forward as the size of horizontal tail increases.

The aft CG limit is determined from the minimum required level of static stability, nose-down recovery capability at high AoAs or tipback angle requirement.

The level of static stability is determined from the static margin. The static margin must be at least +5 percent for natural stability condition [8]. When the static stability is relaxed, the static margin can be decreased up to -7 percent [12]. The values of static

margin are calculated for both natural and artificial stability conditions for six horizontal tails. The aft CG position goes rearward with the relaxation of longitudinal stability. Besides, as the size of horizontal tail increases, the aft CG limit moves towards back.

The aft CG limit is also determined from the minimum required nose-down capability at high AoA. The most aft CG positions for minimum nose-down pitch control capability are computed by utilizing from the guideline mentioned in Section 4.2 [5] for each horizontal tail. It can be observed that the aft CG goes backward with increase in the size of horizontal tail.

In addition, the aft CG limit regarding tipback angle requirement is calculated. The tipback angle depends on some aircraft geometric parameters. Therefore, the aft CG limit regarding tipback angle is same for aircraft configurations having different horizontal tail planforms.

The results of the analyses indicate that the necessary level of stability is more critical than the minimum nose-down capability for the determination of the aft CG limit. Therefore, the level of static stability of the aircraft determines the aft CG limit.

The sensitivities of DATCOM and CFD programs are compared with each other. The results of the analyses show that the sensitivity of CFD program on change in the size of the horizontal tail is much higher than the sensitivity of DATCOM program.

The tail sizing diagrams are generated for each horizontal tail from the results based on both CFD and DATCOM analyses in case of both natural and artificial stability conditions. Each calculated CG limits are located on the tail sizing diagrams. The allowable CG range is defined between these CG limits.

The allowable CG range is defined in Table 1.1 as between 35 and 39 % of MAC. Therefore, the minimum size of horizontal tail must be determined by considering this CG envelope. The following comments can be done;

- The results of DATCOM analyses show that the limit of aft CG position cannot be met with any horizontal tail planform in case of natural stability condition; however, this limit can be satisfied with all horizontal tail planforms with artificial stability condition. The minimum required area of horizontal tail is computed as approximately 17.6 m² for natural stability condition while it is approximately calculated as 7.3 m² (HT # 1) for artificial stability condition. Besides, the limit of FWD CG position can be satisfied with all horizontal tail planforms.
- The results of CFD analyses indicate that the limit of FWD CG position can be met with all horizontal tails. However, the aft CG position limit for both natural and artificial stability conditions cannot be satisfied with all horizontal tail planforms. Moreover, the aft CG limit cannot be met with any horizontal tail. The minimum required area of horizontal tail was found as approximately 13 m². The aft CG limit for artificial stability condition can be satisfied with HT # 3, HT # 4, HT # 5 and HT # 6. In addition, the minimum required horizontal tail area is computed as 8.2 m² which is between the areas of HT # 2 and HT # 3.

As a result of these studies, it can be seen that the minimum area of horizontal tail planform can be decreased to approximately 8.2 m² by utilizing from the concept of relaxed static stability. As mentioned previously, the relaxed static stability provides reduction in the size of horizontal tail which causes a decrease in aircraft weight, a decrease in trim drag, and thus an increase in maneuverability.

5.2. Future Work

In future work, other criteria such as time to double, approach trim during landing will be also evaluated. These will provide much more precious estimation on the size of the horizontal tail for the critical design phase of aircraft. Some dynamic problems related with the stabilization of unstable configuration can occur. Therefore, a criterion of maximum allowable dynamic instability, “Time to Double Amplitude”, should be investigated [17]. The limit of FWD CG position can be determined with approach trim during landing. The aircraft must be trimmed at an angle-of-attack about its FWD CG position during landing such that the horizontal tail should have extra control authority for pitch control.

In addition, the benefits of relaxed static stability on performance of aircraft will be studied. The concept of relaxed static stability, as mentioned earlier, augments the performance of aircraft. Reduction in trim drag and; thus, increase in maneuverability will be calculated.

REFERENCES

- [1] Babister, A.W., "Aircraft Stability and Control", Pergamon Press, 1961.
- [2] Abzug, M.J. and Larrabee, E.E., "Airplane Stability and Control, A History of Technologies That Made Aviation Possible", Cambridge University Press, 2002.
- [3] Rising, J.J., "Development of a Reduced Area Horizontal Tail for a Wide Body Jet Aircraft", NASA CR-172278, February 1984.
- [4] Whitford, R., "Design for Air Combat", Jane's Publishing, 1987.
- [5] Nguyen, L.N., and Foster, J.V., "Development of a Preliminary High-Angle-of-Attack Nose-Down Pitch Control Requirement for High-Performance Aircraft", NASA TM-101684, February 1990.
- [6] POINTWISE, Pointwise Inc., 2018.
- [7] Finck, R.D., "USAF Stability and Control DATCOM", AFWAL-TR-83-3048, McDonnell Douglas Corporation, 1978.
- [8] Phillips, W. F., "Mechanics of Flight", John Wiley & Sons, Inc, 2010.
- [9] A Cost-Efficient High-Performance Advanced Pilot Training Aircraft. <https://www.scribd.com/document/390851548/A-Cost-efficient-High-performance-Advanced-Pilot-Training-Aircraft>. Accessed: 2019-09-10.

- [10] Roskam, J., "Airplane Flight Dynamics and Automatic Flight Controls", DARcorporation, 2001.
- [11] Burgun, R., S., "The Design, Analysis, Construction and Testing of an Uninhabited Aero Vehicle Platform", North Carolina State University, Raleigh, 2003.
- [12] Aronstein, D.C., Piccirillo, A.C., "The Lightweight Fighter Program: A Successful Approach to Fighter Technology Transition", AIAA Education, 1996.
- [13] Crisafulli, P.J., "Response Surface Approximations for Pitching Moment Including Pitch-Up in the Multidisciplinary Design Optimization of a High-Speed Civil Transport", Virginia Polytechnic Institute & State University, Virginia, June 1996.
- [14] Tinoco, E.N., Piccirillo, A.C., "The Changing Role of Computational Fluid Dynamics in Aircraft Development", AIAA, 1998.
- [15] ANSYS Fluent 17.1 User's Guide, Fluent Inc., 2016.
- [16] Lesoinne, M., Farhat, C., "CFD-Based Aeroelastic Eigensolver for the Subsonic, Transonic, and Supersonic Regimes", Journal of Aircraft, July-August 2001.
- [17] Mangold, P. "Integration of Handling Quality Aspects Into the Aerodynamic Design of Modern Unstable Fighters ", AGARD CP-508, 1991.

APPENDICES

A. Neutral Point Determination

The results of the studies on neutral point determination obtained from CFD analyses are presented below;

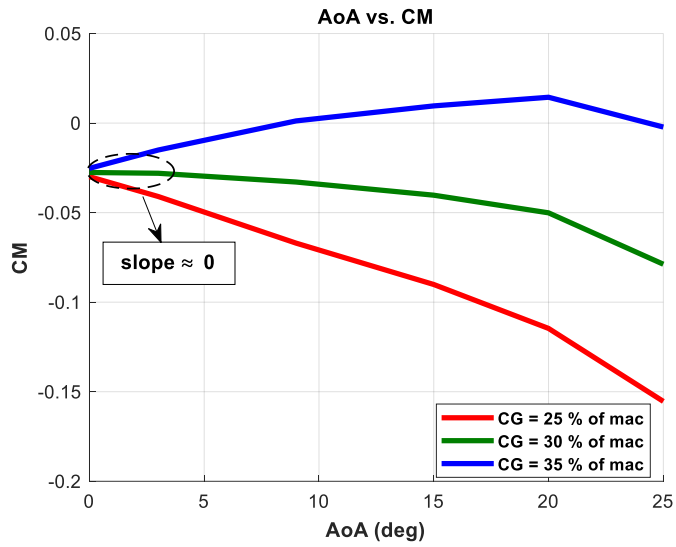


Figure A 1. The variation of. Cm with AoA at 0.2 Mach for HT # 1

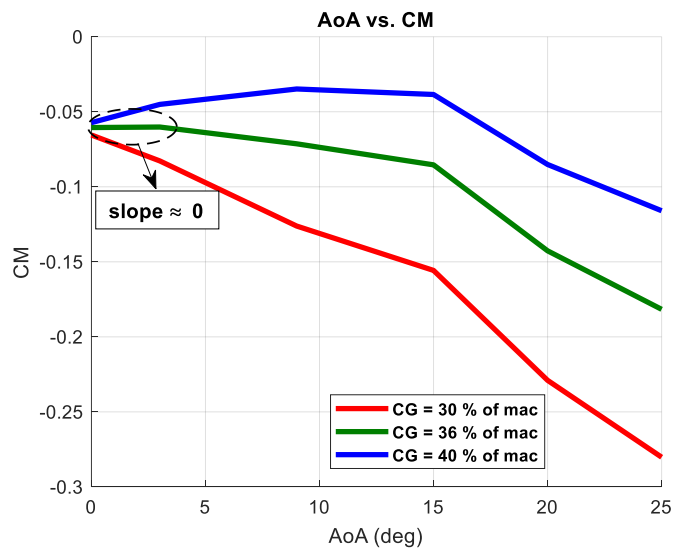


Figure A 2. The variation of. Cm with AoA at 0.9 Mach for HT # 1

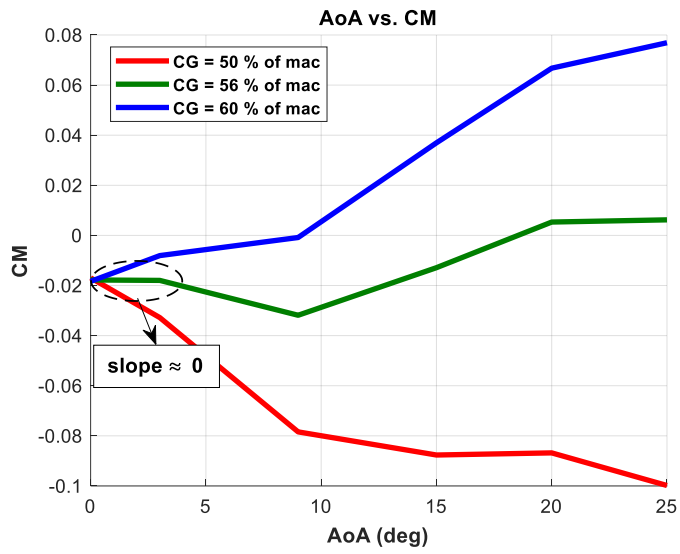


Figure A 3. The variation of. Cm with AoA at 1.2 Mach for HT # 1

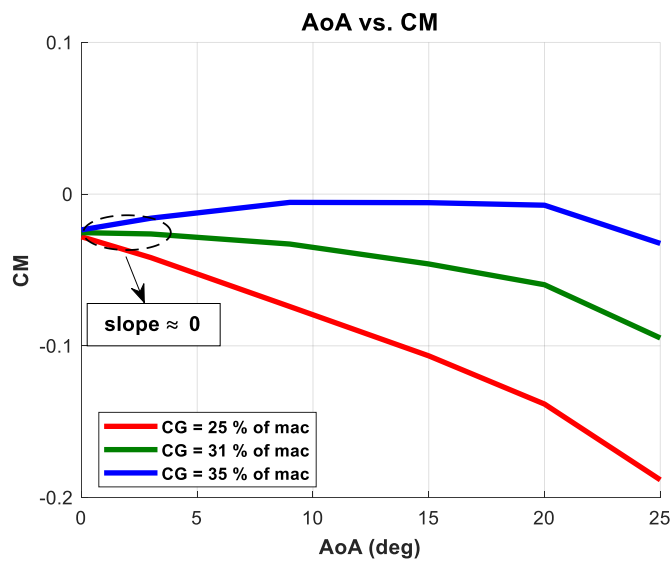


Figure A 4. The variation of. Cm with AoA at 0.2 Mach for HT # 2

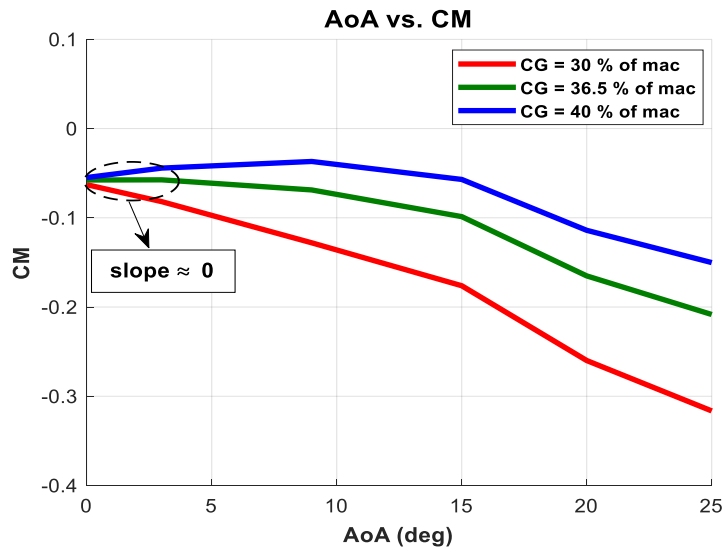


Figure A 5. The variation of. Cm with AoA at 0.9 Mach for HT # 2

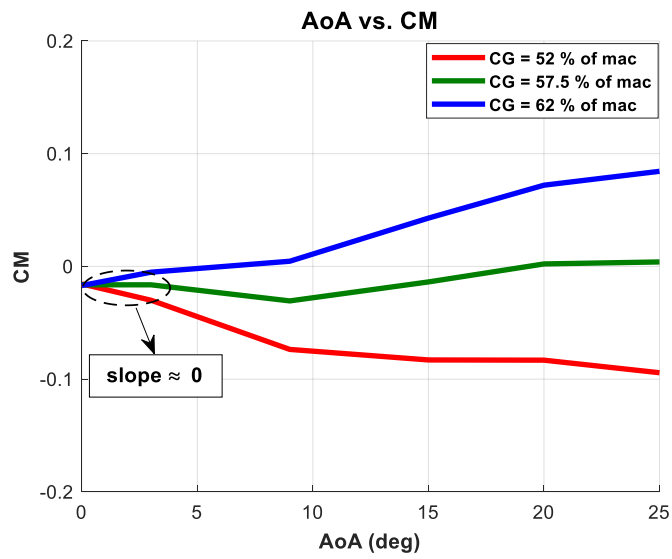


Figure A 6. The variation of. Cm with AoA at 1.2 Mach for HT # 2

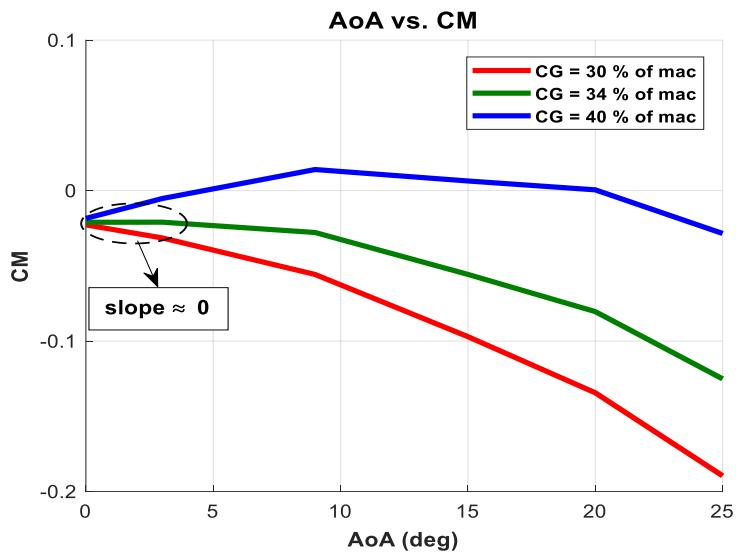


Figure A 7. The variation of. Cm with AoA at 0.2 Mach for HT # 3

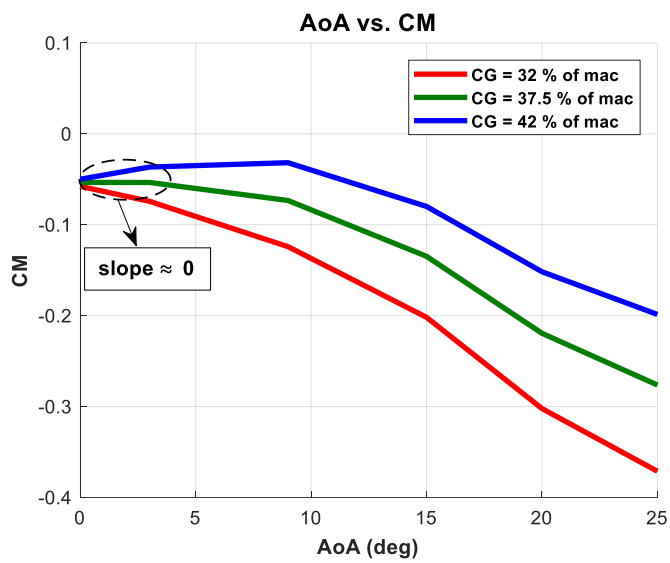


Figure A 8. The variation of. Cm with AoA at 0.9 Mach for HT # 3

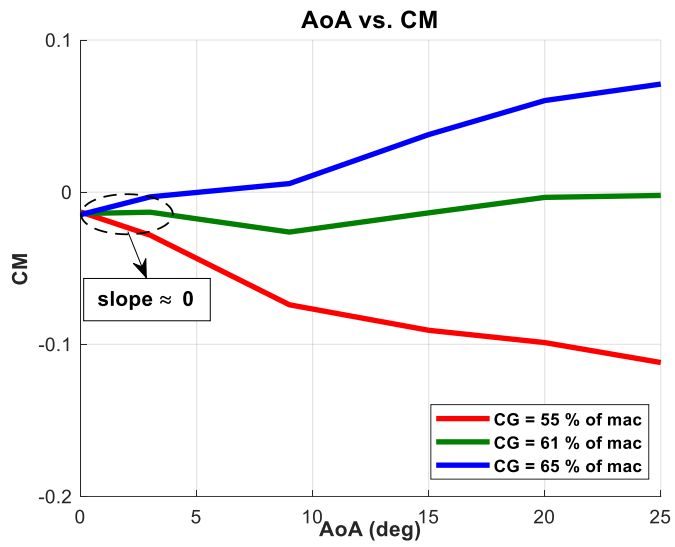


Figure A 9. The variation of. Cm with AoA at 1.2 Mach for HT # 3

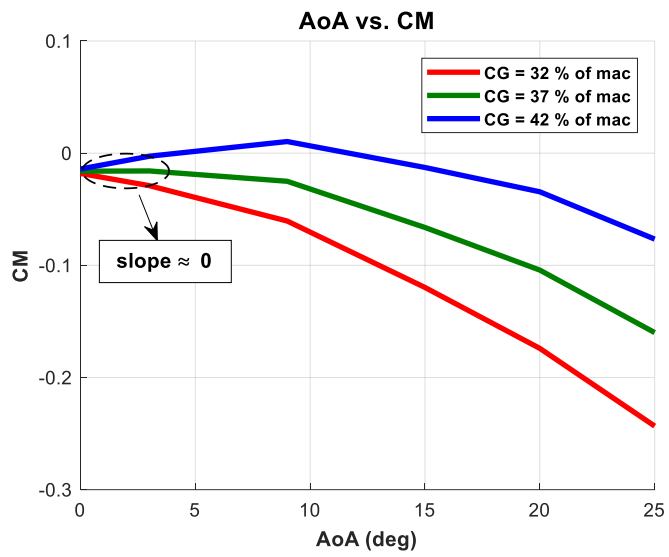


Figure A 10. The variation of. Cm with AoA at 0.2 Mach for HT # 4

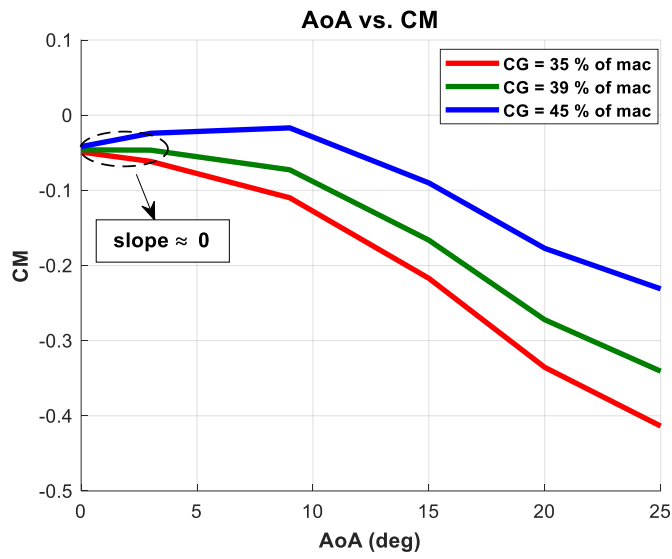


Figure A 11. The variation of. Cm with AoA at 0.9 Mach for HT # 4

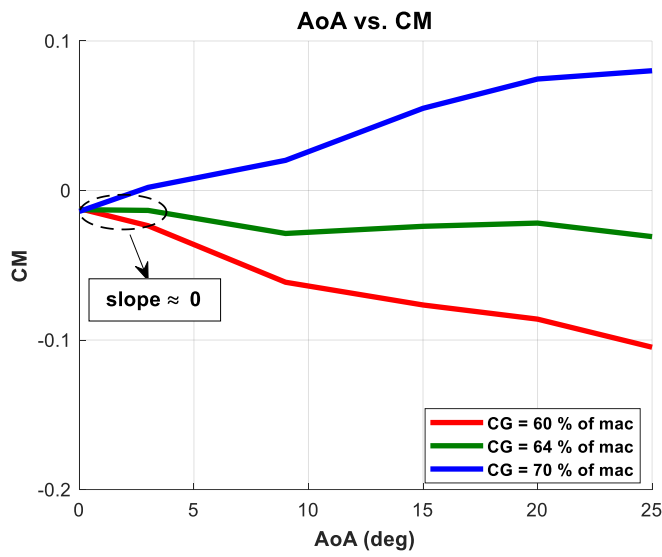


Figure A 12. The variation of. Cm with AoA at 1.2 Mach for HT # 4

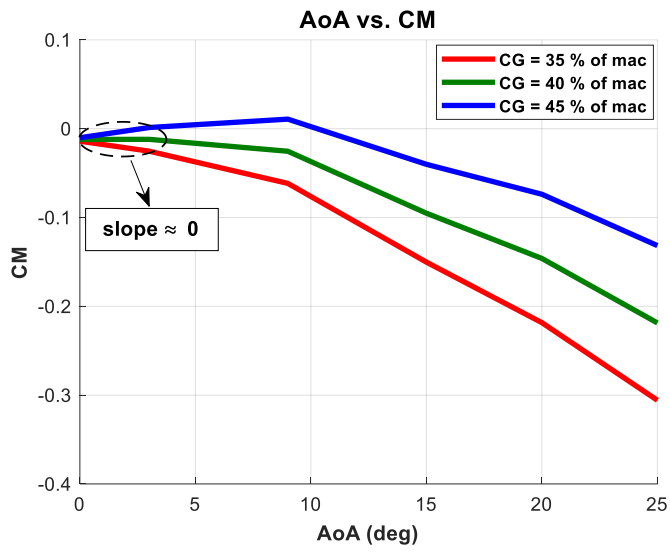


Figure A 13. The variation of. Cm with AoA at 0.2 Mach for HT # 5

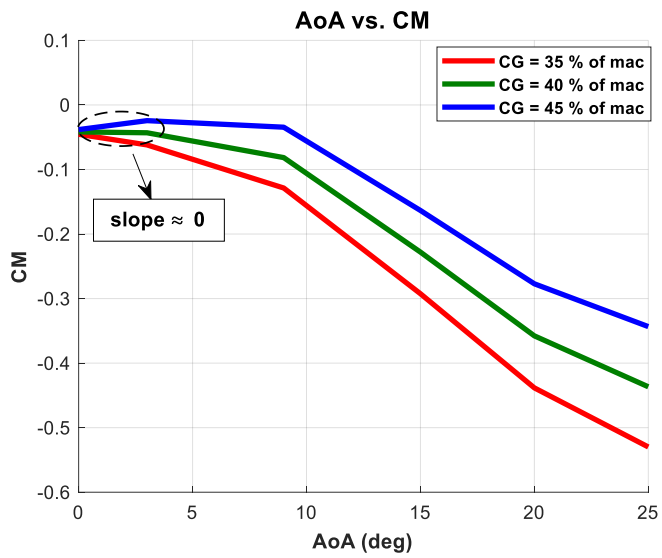


Figure A 14. The variation of. Cm with AoA at 0.9 Mach for HT # 5

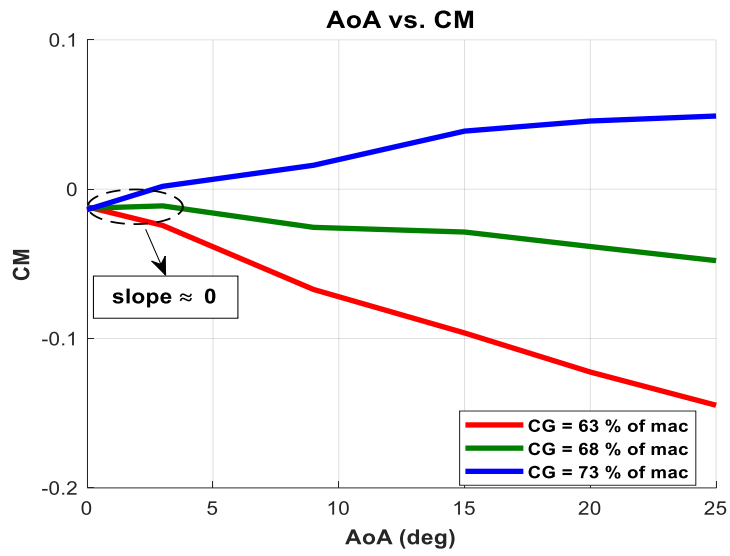


Figure A 15. The variation of. Cm with AoA at 1.2 Mach for HT # 5

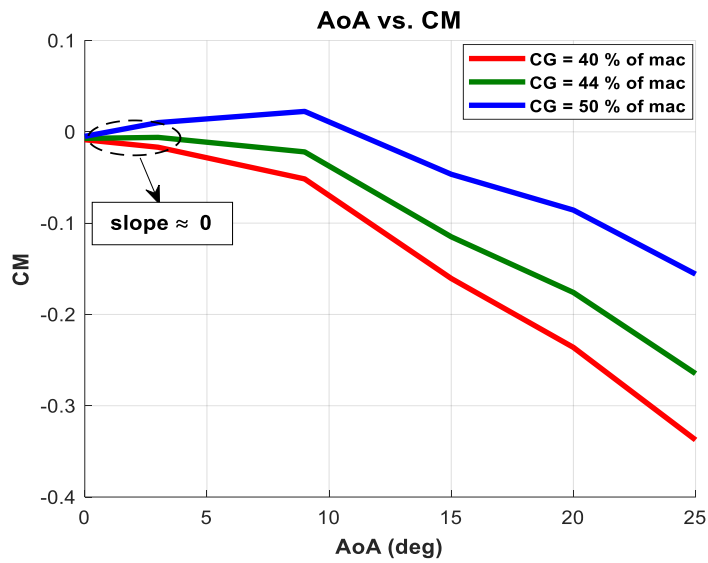


Figure A 16. The variation of. Cm with AoA at 0.2 Mach for HT # 6

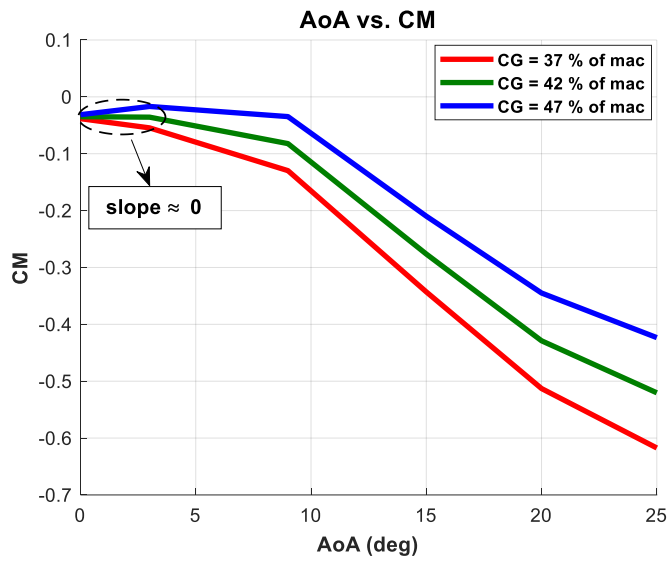


Figure A 17. The variation of. C_m with AoA at 0.9 Mach for HT # 6

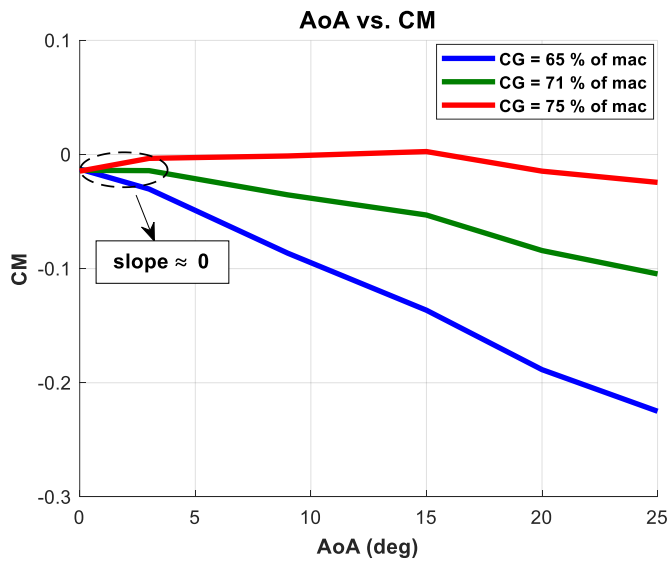


Figure A 18. The variation of. C_m with AoA at 1.2 Mach for HT # 6

The results of the studies on neutral point determination obtained from DATCOM analyses are presented below;

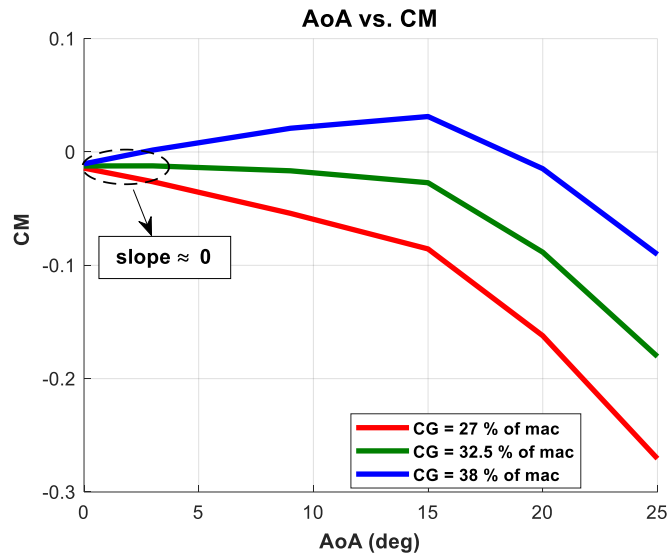


Figure A 19. The variation of. Cm with AoA at 0.2 Mach for HT # 1

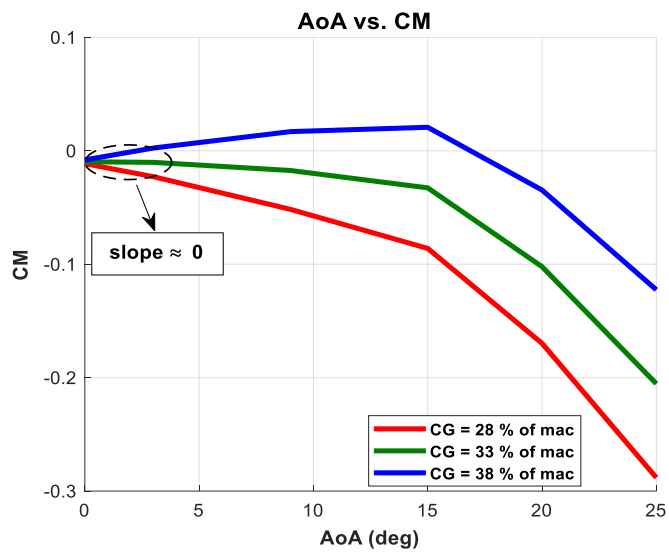


Figure A 20. The variation of. Cm with AoA at 0.2 Mach for HT # 2

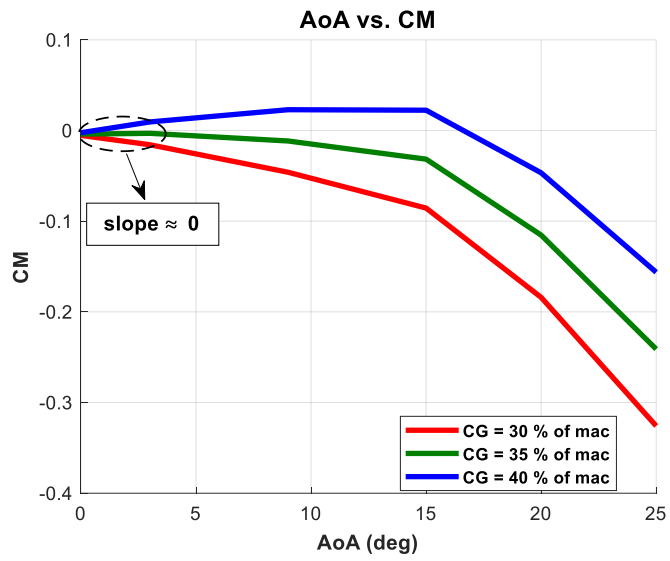


Figure A 21. The variation of. Cm with AoA at 0.2 Mach for HT # 3

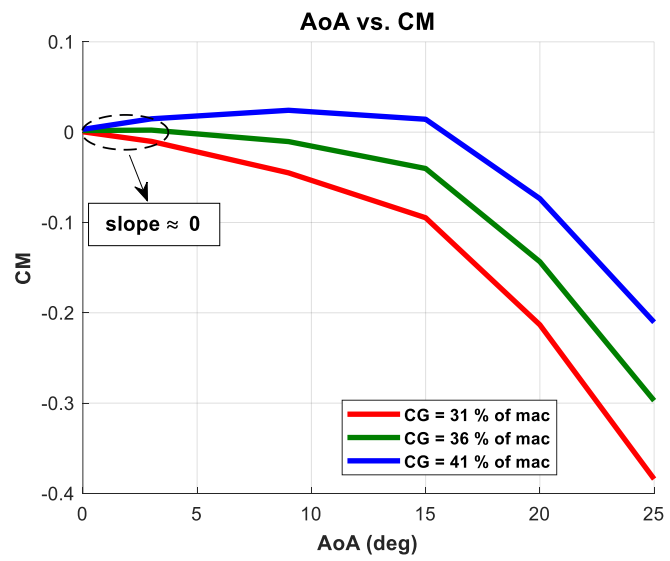


Figure A 22. The variation of. Cm with AoA at 0.2 Mach for HT # 4

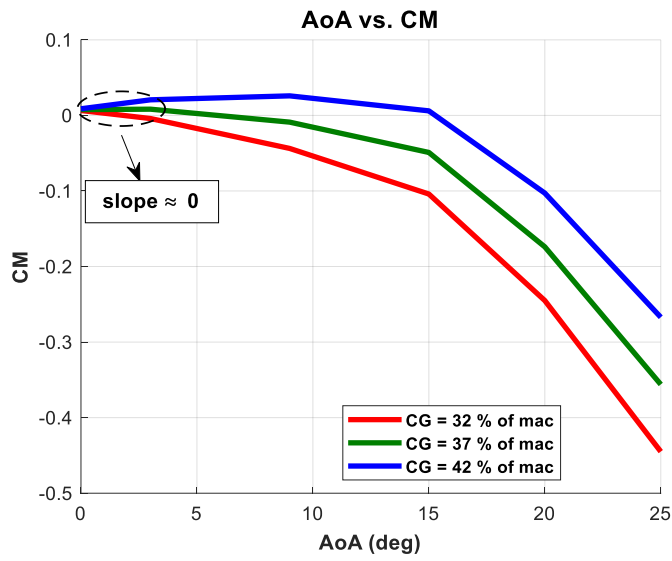


Figure A 23. The variation of. Cm with AoA at 0.2 Mach for HT # 5

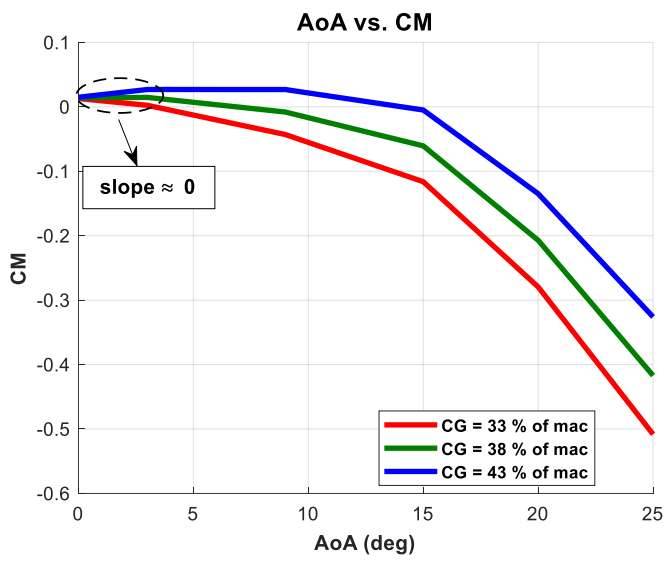


Figure A 24. The variation of. Cm with AoA at 0.2 Mach for HT # 6

B. Minimum Nose-Down Recovery Determination

The results of the studies on the minimum nose-down recovery determination obtained from CFD analyses are presented below;

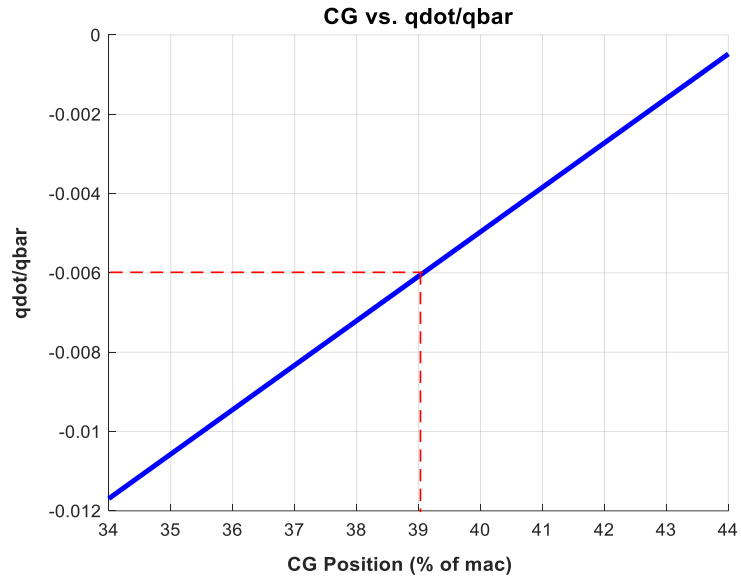


Figure B 1. Nose-Down Recovery Characteristic for HT # 1

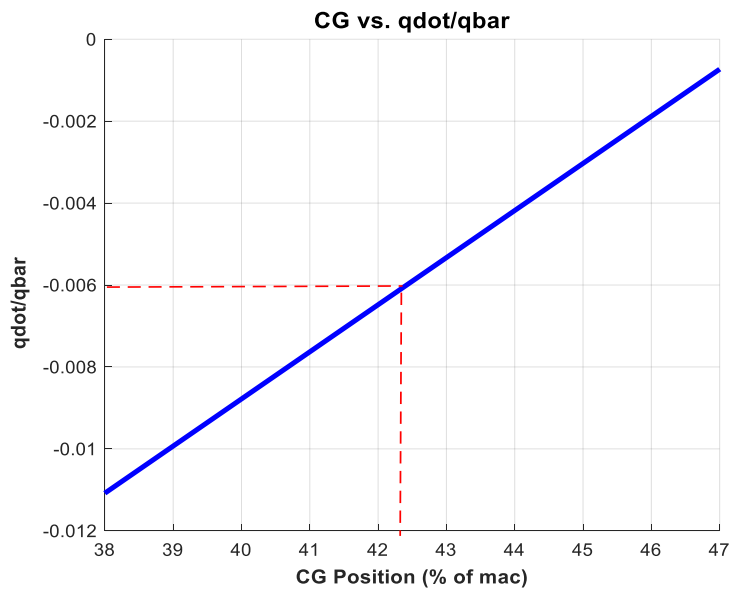


Figure B 2. Nose-Down Recovery Characteristic for HT # 2

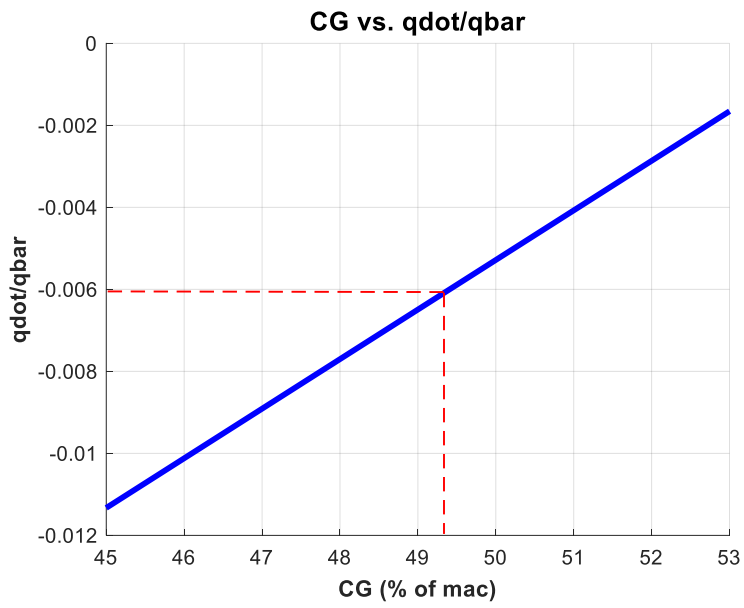


Figure B 3. Nose-Down Recovery Characteristic for HT # 3

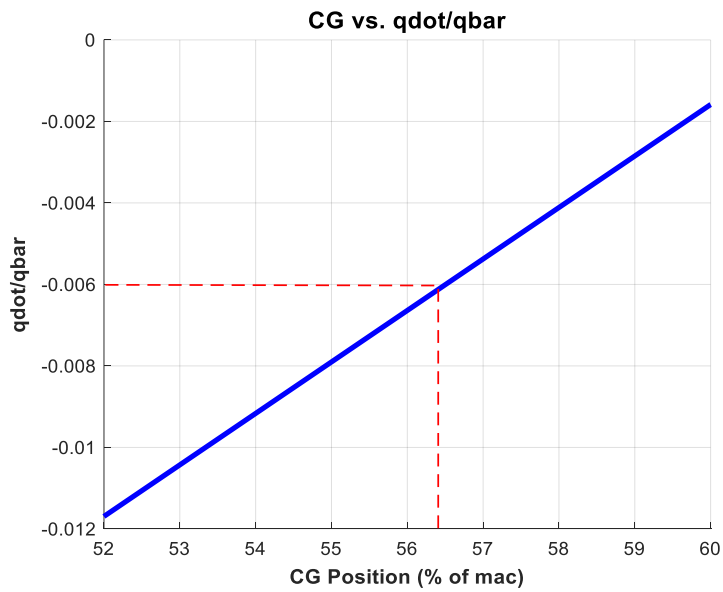


Figure B 4. Nose-Down Recovery Characteristic for HT # 4

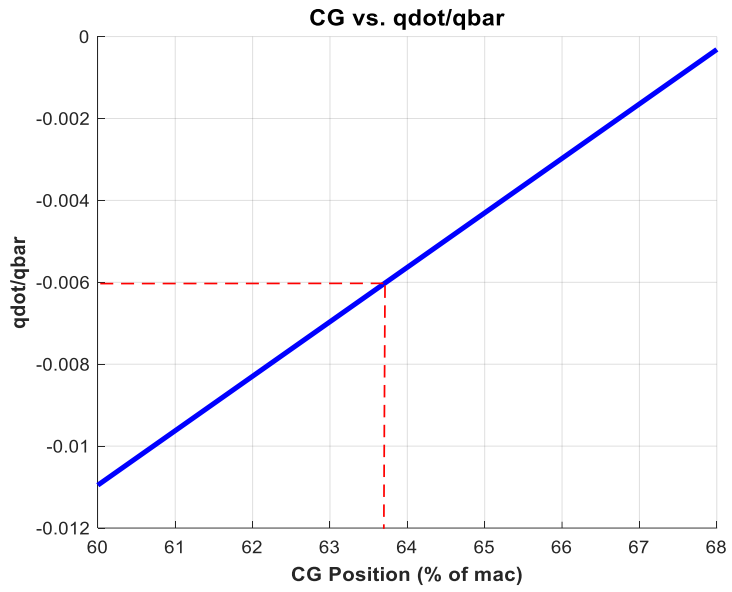


Figure B 5. Nose-Down Recovery Characteristic for HT # 5

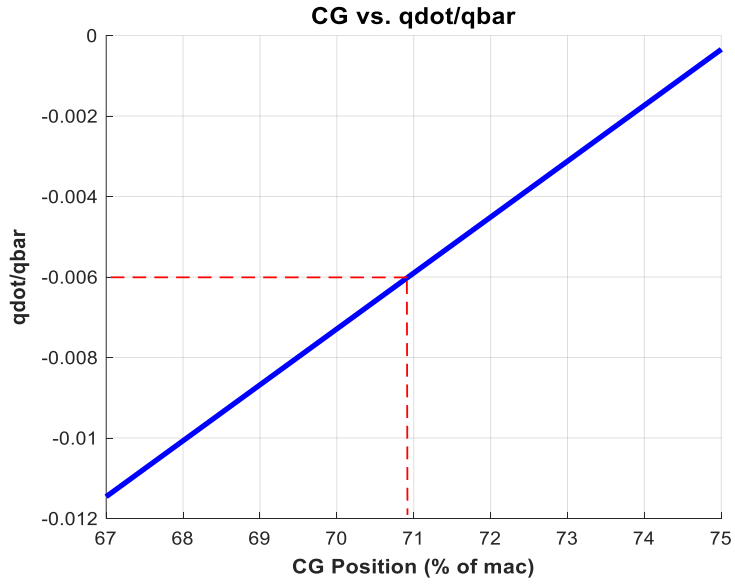


Figure B 6. Nose-Down Recovery Characteristic for HT # 6

The results of the studies on the minimum nose-down recovery determination obtained from DATCOM analyses are presented below;

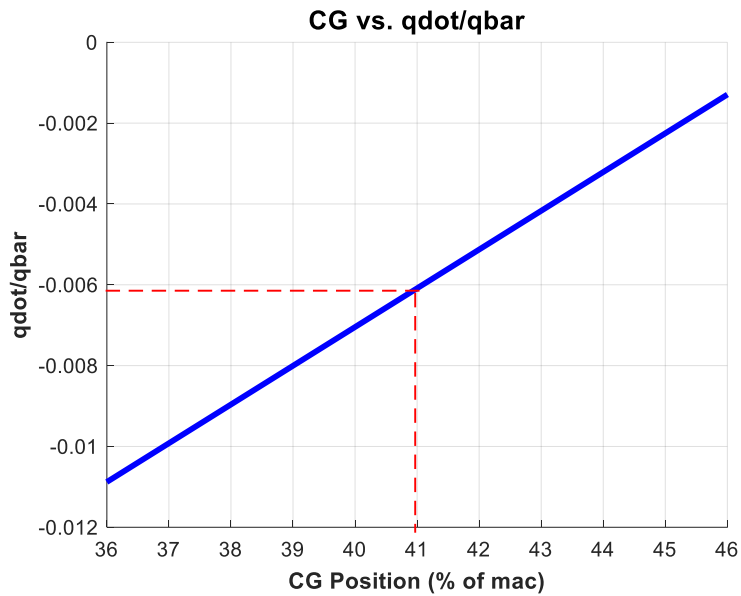


Figure B 7. Nose-Down Recovery Characteristic for HT # 1

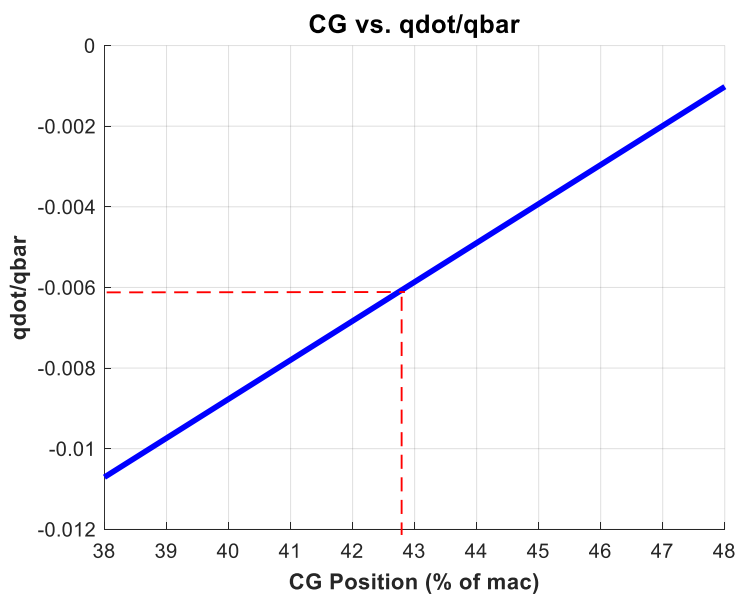


Figure B 8. Nose-Down Recovery Characteristic for HT # 2

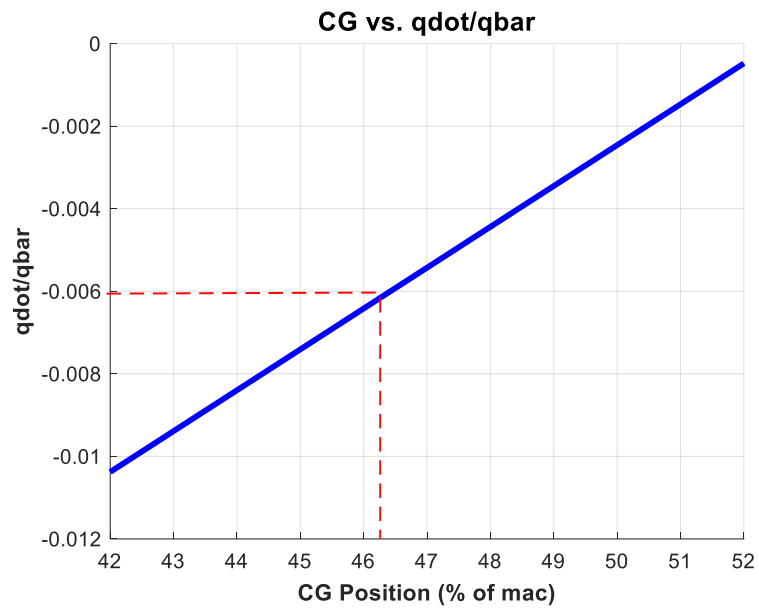


Figure B 9. Nose-Down Recovery Characteristic for HT # 3

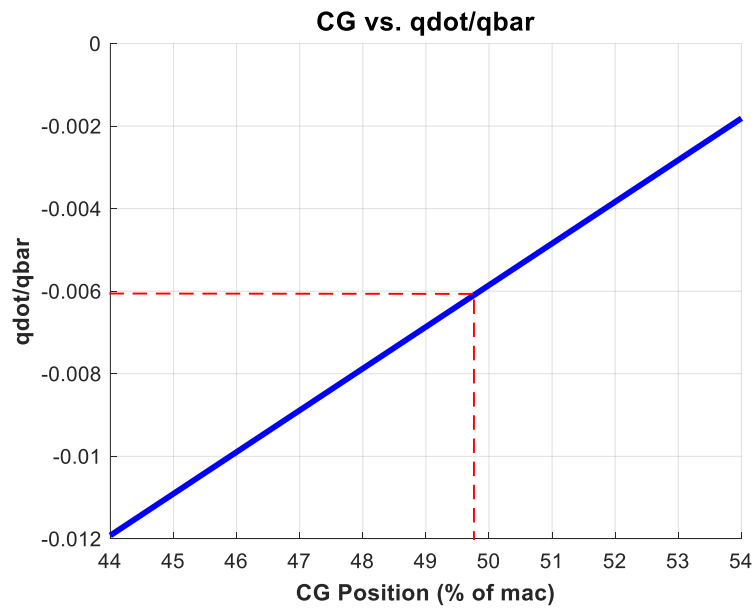


Figure B 10. Nose-Down Recovery Characteristic for HT # 4

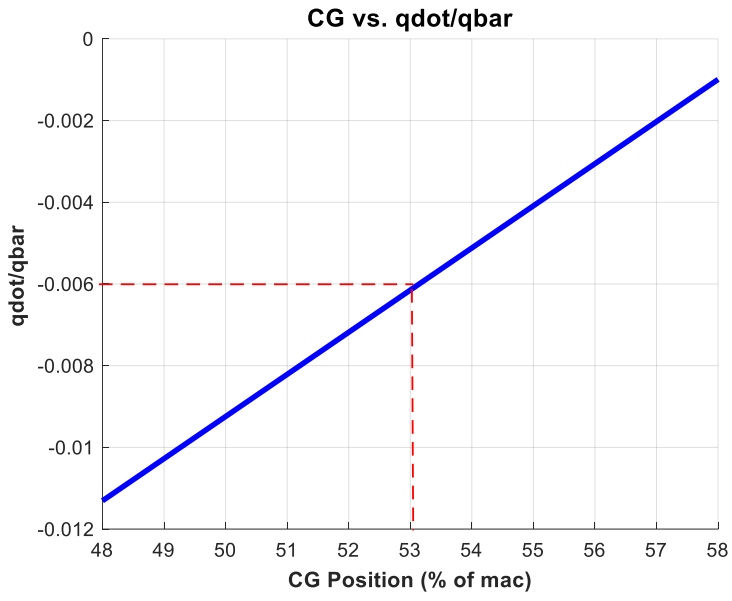


Figure B 11. Nose-Down Recovery Characteristic for HT # 5

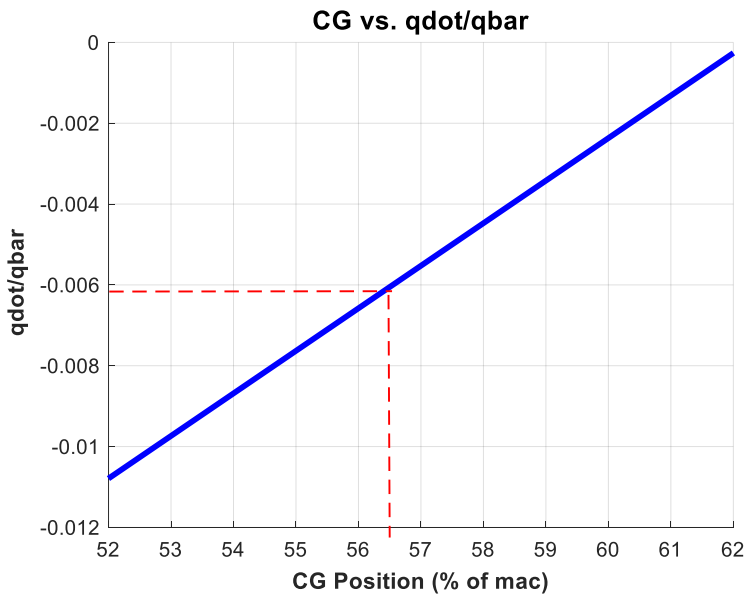


Figure B 12. Nose-Down Recovery Characteristic for HT # 6

